

City Research Online

City St George's, University of London

Citation: Onuchukwu, A. I. (1980). A study of stress corrosion of steel. (Unpublished Doctoral thesis, The City University)

This is the accepted version of the paper.

This version of the publication may differ from the final published version. To cite this item please consult the publisher's version.

Permanent repository link: https://openaccess.city.ac.uk/id/eprint/37096/

Copyright and Reuse: Copyright and Moral Rights remain with the author(s) and/or copyright holders. Copies of full items can be used for personal research or study, educational, or not-for-profit purposes without prior permission or charge, unless otherwise indicated, provided that the authors, title and full bibliographic details are credited, a hyperlink and/or URL is given for the original metadata page and the content is not changed in any way. For full details of reuse please refer to City Research Online policy.

City Research Online: http://openaccess.city.ac.uk/ publications@citystgeorges.ac.uk

A STUDY OF STRESS CORROSION OF STEEL

A THESIS SUBMITTED TO
THE CITY UNIVERSITY, LONDON
FOR THE AWARD OF DEGREE OF
DOCTOR OF PHILOSOPHY

BY

ANTHONY IKEJIOFOR ONUCHUKWU

This work was carried out under the supervision of
Dr. A.C.C. Tseung and Dr. H. C. Chan

JANUARY, 1980

THE CITY UNIVERSITY LIBRARY,
ST. JOHN STREET, LONDON, E.C.1.

ACKNOWLEDGEMENT

The author wishes to express his sincere and grateful thanks to Dr. A. C. C. Tseung, Reader, Director of Chemical Energy Unit, The City University, London and Dr. H. C. Chan, Reader, Faculty of Engineering, Middlesex Polytechnic, Enfield, whose knowledge and immense interest have greatly assisted this investigation.

He is also greatly indebted to his colleagues in the Electrochemical Technology and Material Science research group for their friendly discussion. He appreciates the assistance of [redacted] and the technical staff of metallurgy and fatigue laboratories of the Mechanical Engineering Department of the University, the technical staff of Middlesex Polytechnic and the good job of the typist [redacted].

Finally, the author wishes to thank the Government of [redacted], NIGERIA for the sponsorship during this research programme.

A. I. Onuchukwu

[redacted]

SUMMARY

The joint action of corrosion and tensile stress that gives rise to Stress Corrosion Cracking (SCC) has produced serious premature failure of structural material in several environments. The traditional methods of assessment of the susceptibility of material to SCC have proved time consuming and, in one particular case, it is very cumbersome and unattractive for potential users. An electrochemical technique and adoption of fracture mechanics principles have been used to introduce a simple and rapid technique for the determination of the threshold value of stress intensity of stress corrosion cracking, K_{ISCC}, which is known to coincide with the formation of stretch zone at the crack tip.

Another major problem in environments where metallic structures are deployed, is their susceptibility to hydrogen embrittlement. The isolation of hydrogen evolution from a corroding metallic structure by the introduction of the use of active hydrogen evolution electrocatalysts has been found effective. The significance of the use of more efficient and active hydrogen evolution electrocatalyst is that these electrocatalysts have lower hydrogen overpotential and can operate in both 'sweet' and 'sour' corrosive environments. These electrocatalysts could be connected and/or coated to the steel whilst protected in an hydrogen environment.

Thus, the techniques proposed in this work provide a better assessment of component susceptibility to SCC, prior to the fabrication of the component and possibly the prevention of hydrogen embrittlement could be realized.

CONTENTS

		Page
CHAPTER ONE		
	INTRODUCTION	
1.1.	CORROSION	1
1.2.	STRESS CORROSION CRACKING (SCC)	3
1.3.	POSSIBLE MECHANISM OF SCC	5
1.4.	THE THRESHOLD VALUE OF STRESS INTENSITY OF SCC, K_{ISCC}	7
1.5.	THE PROBLEM	9
1.5.1.	Hydrogen Embrittlement	11
1.5.2.	Hydrogen Permeation in Metals	12
1.5.3.	Effect of Hydrogen Embrittlement on Off-Shore Structures	16
1.6.	HYDROGEN EVOLUTION ELECTROCATALYST	18
1.7.	SUMMARY OF THE PROBLEM	20
1.8.	THE PRESENT WORK	20
CHAPTER TWO		
	AN ELECTROCHEMICAL METHOD FOR DETECTING THE THRESHOLD STRESS INTENSITY IN STRESS CORROSION	
2.1.	INTRODUCTION	
2.1.1.	Literature Survey	22
2.1.2.	Present Work	24
2.2.	EXPERIMENTAL	
2.2.1.	Corrodents	26
2.2.2.	Material Preparation	27
2.2.3.	Mechano - Electrochemical Tests	32

2.2.3a.	Steady State Load - Current Measurements	32
2.2.3b.	Potentiostatic Pulse for Load - Current Measurements	34
2.3.	RESULTS	
2.3.1.	Steady State Measurements	38
2.3.2.	Transient Measurements	39
2.4.	DISCUSSION	43

CHAPTER THREE

HYDROGEN PERMEATION INTO STEEL

3.1.	INTRODUCTION	59
3.1.1.	Hydrogen In Metals	59
3.1.2.	Hydrogen Diffusion Parameters	60
3.2.	EXPERIMENTAL TECHNIQUE	62
3.2.1.	Choice of Material and Preparation	62
3.2.2.	Cell Design	64
3.2.3.	Electrochemical Tests	66
3.2.4.	Potentiostatic and Galvanostatic Polarisation of Bielectrodes	67
3.3.	RESULTS	72
3.3.1.	Hydrogen Permeation Current-Time Profile	72
3.3.2.	Diffusion Parameters of H Permeation in Steel	74
3.4.	DISCUSSION	81

CHAPTER FOUR

HYDROGEN PERMEATION INTO STEEL UNDER APPLIED TENSILE STRESS

4.1.	INTRODUCTION	90
4.2.	EXPERIMENTAL TECHNIQUE	90
4.2.1.	Mechanical Properties of Steel Specimen	90

4.2.2.	Mechano-Electrochemical Test: Hydrogen Permeation Into Steel Under Appleid Stress	92
4.3.	RESULTS	95
4.4.	DISCUSSION	99

CHAPTER FIVE

THE ELECTROCATALYSTS FOR HYDROGEN EVOLUTION REACTION, (h.e.r.)

5.1.	INTRODUCTION	106
5.1.1.	A Survey of h.e.r. Electrocatalyst	106
5.2.	EXPERIMENTAL TECHNIQUE	109
5.2.1.	Preparation and Characterisation of Electrocatalyst for h.e.r.	109
5.2.1a.	Nickel-Cobalt-Sulphide, $NiCo_2S_4$	109
5.2.1b.	Iron Sulphide	110
5.2.1c.	X-ray Analysis	111
5.2.2.	Half Cell Electrochemical Testing	113
5.2.2a.	Electrode Fabrication	113
5.2.2b.	Electrochemical Test	113
5.3.	RESULT	116
5.4.	DISCUSSION	120

CHAPTER SIX

HYDROGEN EMBRITTLEMENT IN STEEL

6.1.	INTRODUCTION	131
6.1.1.	Possible Mechanism and Prevention	133
6.2.	EXPERIMENTAL TECHNIQUE	137
6.2.1.	Methods of Protection of Steel from Hydrogen Embrittlement	137
6.2.1A.	Electrically Connected Steel To An Electro-catalyst	137
6.2.1A.a.	$NiCo_2S_4$ Catalyst Used To Protect Steel From Hydrogen Embrittlement in 0.1M KOH and H_2S	139

6.2.1A.b. $NiCo_2S_4$ Catalyst Used to Protect Steel in 3.5% Nacl Solution and H_2S 141

6.2.1A.c. Iron Sulphide Catalyst Used to Protect Steel From Hydrogen Embrittlement 142

6.2.1A.d. Protection of Steel Under Stress From Hydrogen Embrittlement 144

6.2.1B. Formation of Adherent Catalyst On The Steel As A Method of Protection From Hydrogen Embrittlement 145

6.2.1B.a. Protection Of Steel By The Formation Of Electrocatalyst Conducting Coating 145

6.2.1B.b. The Formation Of Iron Sulphide Coating On Steel In Situ 146

6.3. RESULTS 147

6.3.1. Electrical Connection Of Steel To The Active Catalyst 147

6.3.2. Steel Is Coated With Active Catalyst Against Hydrogen Embrittlement 150

6.4. DISCUSSION 151

CHAPTER SEVEN

7.1. CONCLUSIONS AND SUGGESTION FOR FURTHER WORK 161

7.1.1. Conclusions 161

7.1.2. Suggestions for Further Work 163

REFERENCES 166

APPENDIX 175

INDEX OF TABLES

		Page
2.1.	Chemical composition and heat treatment of steel used.	30
2.2.	The threshold values of stress intensity of stress corrosion cracking K_{ISCC} determined under steady state measurements.	41
2.3.	The threshold values of stress intensity of stress corrosion cracking K_{ISCC}, determined by pulse measurements.	42
3.1.	Diffusion coefficients, limiting current densities at $t = 0.83\ t_\infty$ and $t = t_\infty$ for varying membrane thickness @ 25°C.	76
3.2.	The variation of diffusion coefficient with temperature.	76
3.3.	The effect of temperature on (i) the diffusion coefficient and (ii) the H permeation current density of steel in cyanide catholyte @ 10mA/cm^2 H_2 discharge current density.	77
3.4.	The effect of temperature on (i) diffusion coefficient and (ii) H permeation current density for membrane thickness of 0.254 mm in H_2S with 10mA/cm^2 H_2 discharge current density.	77
3.5.	The effect of temperature on (i) diffusion coefficient and (ii) H permeation current density for membrane thickness 0.254 mm in H_2S.	78
3.6.	The comparison of the amount of H permeation into steel in H_2S, CN^-, and NO_2^- environments.	79
3.7.	The activation energy determined in various catholyte environment and the diffusion coefficient.	80
4.1.	The effects of (i) applied stress (N/mm^2) and (ii) strain (μstrain) on the H permeation current @ 25°C	98
5.1.	Sulphur content (W/W percent) in iron sulphide grade and $NiCo_2S_4$ prepared in a stream of H_2S for 8 hours.	118
5.2.	Kinetic parameters for h.e.r on $NiCo_2S_4$ and FeSx prepared from iron rust.	119

INDEX OF FIGURES

		Page
I.	Schematic SCC data from smooth specimen.	22
II.	Effect of stress intensity or SCC kinetics.	23
1.	Compact Tensile Specimen.	31
2.	Schematic Diagram of Test Assembly.	37
3.	Steady state i-v polarisation curves at 20°C for supporting electrolyte and quinone-hydroquinone electrolyte.	48
4.	RupturedEn30B steel specimen after use in quinone-hydroquinone electrolyte.	49
5.	Typical load-current curve for specimen held at a steady state of -400 mV Vs SCE in sea water.	50
6.	Typical load-current curve for specimen held at a steady state of -1000mV Vs SCE in sea water.	51
7.	Typical load-current plot for specimen of varying fatigue crack lengths in FeII/FeIII cyanide electrolyte at a steady state of -510 mV Vs SCE.	52
8.	Typical load-current relation for millimotar quinone-hydroquinone at a steady state of -610 mV Vs SCE for specimen of varying crack lengths.	53
9.	Load-current plot for specimens of fatigue crack lengths obtained by pulse technique in sea water.	54
10.	Load-current plots for specimens of fatigue crack lengths obtained by pulse technique in quinone-hydroquinone electrolyte.	55
11.	Load-current plots for specimens of varying fatigue crack lengths obtained by pulse technique in quinone-hydroquinone electrolyte.	56
12.	The i-v pulse polarisation for complete rupture En30B steel specimen in quinone-hydroquinone electrolyte (iR corrected).	57
13.	The i-v pulse polarisation curve for complete ruptured En30B steel specimen in synthetic sea water (iR corrected).	58

3.1. The bi-electrode diffusion cell assembly showing the anode and cathode compartments. 65

3.2. Galvanostatic circuit illustration. 68

3.3. Potentiostatic circuit illustration. 68

3.4. Circuit arrangement for the bi-electrode potentiostatic H-oxidation polarisation and cathodic galvanostatic H_2 discharge. 70

3.5. Cydic voltammogram of hydrogen evolution on steel in deaerated 0.1M KOH @ 50 rpm scan rate at 20°C. 85

3.6. Hydrogen permeation current/time profile at 20°C in CN^- catholyte @ (i) 15mA/cm^2 and (ii) 10mA/cm^2 H_2 discharge current density. 86

3.7. Plot of L^2 Vs t for (a) $t = 0.83\ t_\infty$ and (b) $t = t_\infty$ 87

3.8. Plot of reciprocal of the permeation current against membrane thickness. 88

3.9. Plot of log diffusion coefficient / $\frac{1}{T}$ for H permeation on steel En42 in various environment. 89

4.1. Short length tensile strip test piece of En42. 91

4.2. Front view of the mounted Monsant type tensometer with the steel membrane under an applied tensile stress. 94

4.3. The side view of the two compartment cell as mounted on the tensometer. 94

4.4. Stress/strain relation for En42 steel. 102

4.5. Effect of applied tensile stress on hydrogen permeation current for 0.0274 cm membrane thickness. 103

4.6. Hydrogen permeation current (μA) against applied tensile stress (N/mm^2). 104

4.7. Hydrogen permeation current (μA) against strain in the member. 105

4.8. Three compartment cells assembly for i-v performance studies of the sulphide electrodes on h.e.r

5.1. Three compartment cell assembly for i-v performance studies. 115

6.8. Effect of H_2S dissociation on (a) unprotected and (b) protected steel @ 25°C and 75°C in 3.5% Nacl solution. 159

6.9. Effect of cathodic hydrogen polarisation @ 10mA/cm^2 on (i) unprotected steel and (ii) protected steel in 3.5% Nacl and presence of H_2S. 160

CHAPTER ONE

INTRODUCTION

INTRODUCTION

1.1. Corrosion

Corrosion has been a major problem confronting the use of metallic material for construction in most environment. The cost of replacement and maintainance of corrosion damage continues to increase in magnitude and it is of great concern to construction , chemical and oil industries[1-3]. The present chapter is the outcome of the constant search for the pertinent findings and conclusions derived by research workers on the various aspects of the corrosion problem. A critical study of the literature revealed that much has been done and much more research is being carried out in search of a competent and reliable means of protecting mettalic material from corrosion damage. Thus, it is long been recognised that corrosion is the wastage of structural material by chemical or electrochemical action of the material with its environment. This interaction and deterioration of the material, particularly steel, reaches peak activity in certain environments such as water with dissolved salts[4]. Basically, all metals are thermodynamically unstable and tend to react with their environment to produce compounds such as oxides or rust. This is a corrosion process[5-7]. Hence, bare metals particularly iron and steel are prone to corrode in most environments, but the extend of the corrosion attack depends upon a number of factors: the most important of which are the composition and surface conditions of the metal; the corrosion medium itself and the local conditions of the environment. Many years of study on the behaviour of

metals with their environments have shown that, in pure dry air at ambient temperature, a thin oxide film forms on the surface mirror of polished mild steel[8]. Unlike that formed on stainless steel or aluminium, it is not protective in the presence of electrolyte and usually breaks down in air, water and soil. Since, the corrosion product of mild steel is loose, non-adherent and therefore unprotective, corrosion continues until such a material is completely destroyed[8]. It has been established that the deterioration of iron in any environment is represented by the anodic reaction:

$$Fe_{(s)} - 2e \longrightarrow Fe^{+2}(aq) \qquad (1)$$

The conjugate electronation reaction could be hydrogen evolution and/or oxygen reduction given by:

$$H_3O^{+}(aq) + 2e \longrightarrow H_2(g) \qquad (2)$$

$$O_2(g) + 2H_2O(\ell) \longrightarrow 4\ O\bar{H}(aq) \qquad (3)$$

other cathode reactions are possible, but the most feasible reaction depends on the corrosion medium, the pH and the local conditions of the environment[9]. The anode corrosion product of ferrous ions is naturally converted to ferric ion which constitutes the simple form of rust. Wagner et al[10] have shown that the final product is the familiar reddish-brown rust, $Fe_2O_3 . 2H_2O$.

Experience has shown that although the presence of oxygen is usually essential, severe corrosion attack may occur

under anaerobic environment (ie. in the presence of sulphate reducing bacteria present in soil and water)[11]. The anodic reaction is the same, but the cathodic reaction is complex, which results in the reduction of inorganic sulphates to sulphide and the eventual formation of rust and ferrous sulphide[12].

The rate of corrosion attack is obviously the most important parameter, and will determine the life span of a given metal structure[13]. Pourbaix's pH-potential diagram for metal water system is often used to predict the corrosion of iron[14]. But, the presence of H_2S, cyanide, nitrate or chloride in the environments makes the use of Pourbaix diagram very unreliable[15]. These deleterious compounds are known to induce high corrosion rate characterised by non-passivity, pitting and exhibit other forms of localised corrosion attack which in suitable condition would lead to stress corrosion damage of the structure[16-17].

1.2. Stress Corrosion Cracking (SCC)

A corroding metal could be assisted by tensile stress to bring about the rapid failure of the mettalic material in the corrosive environment. Such a failure of a mettalic structure arising from the combining action of corrosion attack and tensile stress is termed stress corrosion cracking, SCC[18-23]. This catastrophe makes the use of mechanical properties of alloys determined in an air environment in material selection and design of components continue to prove unrealiable in other environment where such materials are deployed[23]. Thus, it is well known that

fracture of metallic structures can occur in various chemical environment at static stresses which are considerably below the predicted stress required to cause fracture in air[24]. Although compressive stresses have not been reported to cause SCC, residual and/or applied tensile stresses are known to produce SCC in most environment[24]. It is apparent, therefore, that for SCC to occur there are certain requirements. These are:-

(i) a susceptible metallic material

(ii) chemical species in the environment which are specific to the material and

(iii) the presence of mechanical tensile stress.

The aggresiveness of the corrodent required to cause SCC varies with different material, and failure can occur under only mild conditions which produce no visible corrosion attack in the absence of stress. Even in the presence of stress which may be due to applied service load, heat treatment, cold work or mismatch in fit-up etc., failure can occur with no visible indication of corrosion[25,26]. Hence, fine intercrystalline or transcrystalline cracks can penetrate the member, leading to eventual break up. Stress corrosion failure are thus, a particularly insiduous form of failure often occuring without visible sign of corrosive damage or mechanical strain at stresses considered to be safe when judged by the performance in air[23]. SCC has been the subject of a number of extensive research which has shown that some material may be highly susceptible in environment to which other materials are immune[7].

1.3. Possible Mechanism of Stress Corrosion Cracking

The behaviour and mode of failure of materials depend on the condition of structural material and the environment. Since there are many varying conditions of environment, a common explanation of this phenomenon is improbable. A considerable number of investigations which are summarised in several reviews[27,28] have shown that no single or generalized mechanism is involved in SCC[29]. In some systems, corrosion aspects are of major importance, in others plastic strains and stresses are dominant features. Sometimes, cracks are intergrannular and sometimes transgrannular on the same material. Thus, the same alloy in the same metallurgical condition can be made to crack in an intergranular or transgranular simply by changing the environment. Nevertheless, it is worth while outlining some of the principal conclusions reached in the various investigation into mechanism.

In a simple assessment SCC seems to proceed by three main stages: (a) there is the initiation stage which consists of slow corrosion attack which produces pits or other forms of stress concentration points that can develop into a recognisable crack; (b) there is a stage of slow crack growth, during which is the combined effects of stress and corrosion promote propagation with a corresponding rise in the stress intensity at the crack tip and (c) there is the stage which is reached when the stress intensity to such a level that rapid failure occurs under the action of stress alone. However, in some material stage (c) is not reached as the second stage may produce cracks of sufficient

length in some components to cause leakage and consequent reduction in stress[30].

Hoar and Hines[31] put forward similar views. They suggest that there are three stages involved during SCC., V_{1z}: (1) an induction period; (ii) the initiation of cracks from corrosion damage produced during induction period, and (iii) the propagation of these cracks until complete failure occurs or the stresses responsible for cracking are relieved. Although this suggestion does not elucidate what is responsible for the induction period, however this view is similar to the simple concept that cracks are as a result of the pit associated with stress concentration points[30]. In another work, Hoar et al[32] however pointed out that under the influence of stress preferential metal dissolution occurs in depth at certain regions of disarray on the metal exposed. This, they conclude could be responsible for the induction period and that cracks are produced from the sharp notches initiated. The suggestion that yielding at the advancing edge of the crack increased the local dissolution rate of the metal is supported by the views of many workers[33-35].

Tysack[36] pointed out that it is possible to combine the Hoar and Hines proposal with mechanical model to the development of fracture mechanics concept. He pictures crack propagation as a preferential dissolution of the material at the crack tip which is in the act of fracturing, this is a combinedprocess resulting in a lowering of the effective fracture energy. This line of thought looks attractive in that it offers the possibility that

divergent views can be combined into a coherent concept and ultimately may well lead to a model that is acceptable to all concerned ie. the introduction of fracture mechanics to quantify the mechanism of SCC.

1.4. The Threshold Value of Stress Intensity of Stress Corrosion Cracking, K_{ISCC}

Fracture mechanics provides a way to normalise out the affects of the mechanical conditions perculiar to variations in crack size and shape and the stress which this material discontinuity refuses to support[37].

In order to utilise the fracture mechanics concepts for SCC studies, precracked specimen must be employed and this principle has several advantages in SCC studies[38]. This include (i) the elimination of the undefined localized corrosion attack, which is highly varying and often not representative of material behaviour in service (ii) it avoids the variations in the metal surface in which pitting is very sensitive and (iii) it facilitates the measurements of the slow crack growth rate [39]. Specimen configuration suitable for studying the fracture mechanics of SCC are recommended by Fracture Committee [40]. The adoption of fracture mechanics technique for SCC studies have been found useful because the design information that they provide to potential users and it throws an insight to a better understanding of SCC mechanism. In a review, Scully[38] noted the immense advantages the potential users of material derive from the

application of fracture mechanics. These, among other things are the desired information about the SCC susceptibility that is obtained rapidly, and most significantly comparison between materials can readily be made. Although the generalisation of SCC problem is improbable, predictive capabilities from one environment to another is unreliable, the concept and technique of fracture mechanics has given those in the field the predictive capability, within limit, from one geometry to another.

The fracture mechanics parameter that has been of most help in treating the SCC is the stress intensity factor K. A lot of reviews, proceedings of symposium, handbook and monographs in this field contain fundamental imformation on this fracture mechanics parameter. It is acknowledged that a plate of metal under sustained uniform tensile stress, subject only to the presence of short crack, the elastic stress field at the edge of the crack can be quantified by this single parameter K, which is proportional to the norminal stress and the square root of the crack size[29,41]. From fracture mechanics studies, the parameter K, is a quantitative measurement of the stress intensification at the most vulnerable part of the engineering member ie. at the crack tip. Thus, the stress intensity factor K, classifies the crack extension process into mode ie. the stress intensity opening mode K_1; the stress intensity shearing mode K_{11}; and the stress intensity tearing mode K_{111}. It follows then, that the failure of a component consists of these three modes acting jointly as the stress intensity K, or the fracture toughness K_{1C} is the most significant and tends to dominate the promotion of structural failure[42].

In some environment in which there is a slow crack extension in the member at K_1 values less than K_{1C}, then this subcritical crack growth which is stress corrosion causes a steady increase in K_1 until K_{1C} is reached and unstable fracture occurs[43]. This initial minimum K value corresponding to K_1 value at which environmental failure occurs and below which failure does not occur is termed : THE THRESHOLD VALUE OF STRESS INTENSITY OF STRESS CORROSION CRACKING, K_{ISCC}[41,43,44]. This parameter K_{ISCC}, is usually expressed in unit $MNm^{-3/2}$ and defines the stress level below which SCC does not occur,but above this value becomes catastrophe. K_{ISCC} value is independent of the environment and it has a specific value for each metal alloy.

1.5. The Problem

The problem that has confronted competent hands in this field has been determination of the exact value of K_{ISCC} for metallic material used in the fabrication of components. The search for a technique for the determination of K_{ISCC} that commands the confidence of designers of components and corrosion experts has motivated the present work. Traditionally, smooth specimen is used to determine the threshold value of norminal stress from which the susceptibility of the material to SCC is assessed. This involves the exposure of the material in a corrodent under sustained tensile stress. The time-to-failure parameter when plotted as a function of initial stress level shows a horizontal

assymptote which is designated as the threshold value of norminal stress intensity. The problems involved in the use of smooth test specimen could be summarised as follows: (i) since this technique relies solely on pitting process for its crack initiation and consequent stress intensification leading to crack propagation, the parameter determined will unavoidably depend on the nature of the environment and surface condition of the material, (ii) the time-to-failure will depend on the material size and configuration, and (iii) the time-to-failure will depend on the period of incubation. These variables accompanying this technique make the assessment of threshold value of norminal stress intensity very suspect.

Another method often used involves the use of precracked specimen to determine the K_{ISCC} value. This technique which adopts the fracture mechanics principles ie. eliminates the long period time required for pit growth and accelerated test could be realised. Thus, this technique involved the use of notches and precracked specimen sustained a stress in such a way as to open and extend the crack, hence the norminal stress is intensified near the crack tip. A measure of SCC growth rate as a function of K, shows there is lower levels of K in which crack growth rate becomes very sensitive to K value[45]. In this region, at sufficiently low value of K, there appears to be a threshold which is designated K_{ISCC}. Irwin[29] observed that the K_{ISCC} obtained from this technique depends on ones ability to predict the norminal stress and size of crack like surface flaw. This method does depend on

chance rather than skill, therefore measured value of K_{ISCC} obtained by it throws a cloud of doubt.

However, the use of precracked specimen makes it possible to assess SCC susceptibility of non pitting alloys. But, all the above techniques which are currently being used for the assessment of SCC for the susceptibility of materials are time consuming particularly the use of smooth specimen that depends on pit formation for its crack initiation and propagation.

McIntyre[46], on the other hand, has shown that in an H_2S environment steel test piece failed within several seconds of the crack tip stress intensity reaching K_{ISCC}, and suggests that this environment provided an accelerated method of testing. The problem of this method is that H_2S being toxic requires elaborate safety precautions. As designers and experienced hands in the field do realize the significance of K_{ISCC}, the problem of the determination of the parameter using the available means appear very unattractive due to their time consuming and safety requirements.

1.5.1. Hydrogen Embrittlement

Another major problem that confronts corroding mettalic structures used in service is their susceptibility to hydrogen embrittlement.[7,32] Although the majority of the H_2 produced on the cathodic areas during the corrosion of a material is evolved as gas and assists the removal of corrosion products, some of it

diffuses into the steel and can render it brittle. Peisl[47] has pointed out that these adsorbed hydrogen Hads get dissolved in the metal and occupy interstitial sites in the host lattice. Thus, in all known metal-hydrogen alloy, the dissolved hydrogen expands the crystal lattice of the host metal. And, each hydrogen interstitial causes displacement of the metal atoms from their regular sites and the resulting crystal lattice distortion which effect the physical properties of the metal. This formation of M-H solid solution is a phenomenon which is common among the d-block elements particularly among the elements in the centre of the transition series. Iron, steel, Palladium and its alloys are among these technological material of immense importance that dissolve hydrogen. Hence, relative volume expansion of the metal lattice, due to the solution of one hydrogen atom per metal atom could be responsible for the severe construction problems for such metals used in a hydrogen environment, owing to the drastic change in the dimension of the construction material[47].

1.5.2. Hydrogen Permeation in Metals

The absorption of large volumes of hydrogen by palladium has long been established and continues to be of immense interest in M-H studies. Ubbelohde[48] and Isenberg[49] formulated the metallic theory of hydrogen in hydrides which has been used in the interpretation of a number of recent palladium-hydrogen studies.

Unlike Pd, iron does not form hydrides, instead it has the tendency to dissolve a little hydrogen. And, iron-hydrogen solubility increases with increase in temperature. Hydrogen solubility in iron is not large enough to be of storage interest, although the phenomenon is of great metallurgical importance[50]. Since the entry of hydrogen into iron does not go through hydride formation, it is quite possible that the palladium hydride concept could not be applicable to explain the dissolution of hydrogen in iron and steel. Quite recently, an electrochemical technique has been used to evolve hydrogen on one face of an iron/steel membrane in an electrolyte, the Habs is de-electronated on the second face of the same steel membrane. This de-electronation current is a manifestation of H atom, thus the hydride formation in iron or steel is suspect[51-53].

It is however known that in a corroding steel in an aqueous environment in which H_2 evolution is the electronation reaction. Bokris, Mcbreen and Navis[54] and DaVanethan and Stachurski[52] considered the formation of hydrogen atoms Hads on the metal surface as an essential intermediate step in the electro-kinetic of hydrogen evolution. They postulated various steps which include the desorption of the hydrogen by the formation of the hydrogen gas, H_2 and diffuse into solution. During this desorption process, there is still some adsorbed hydrogen atom which dissolve into the metal constituting absorbed (Habs) hydrogen. This absorbed hydrogen within the bulk metal lattice sets up a hydrogen concentration gradient between the M-Hads entry

face and the bulk of the metal, thus, this concentration gradient becomes the driving force which makes the adsorbed hydrogen diffuse into the metal.

Recently Davanathan and Stachurski[52] introduced a two compartment cell technique to measure H diffusivity in metal using an electrochemical method and the Fick's non steady state diffusion law. Bockris et al[54] used similar technique to determine the diffusion coefficient and activation energy of H permeation into Steel.Glass, Taylor and Beck[55] investigated the effect of H_2S, CN^-, NO_2^- and alkali on the hydrogen permeation in steel. They showed that H dissolution and consequent diffusion increased in the order $H_2S > CN^- > NO_2^- > OH$ (Alkali) in steel. On the basis of this result, Kabozev and Montblannova[56,57] considered the rate - controlling step in H evolution on iron as the recombination. They suggested that the increase in adsorption of anions (ie. CN^-, H_2S, NO_2^- etc.) is due to a lowering of the M-Hads bond. Since there is no significant change in activation energy for M-Hads in these environment, Bockris et al and Taylor et al hold the view that the chemisorbed anion (ie. H_2S, CN^-, NO_2^- etc.) on the iron surface decreases the recombination step of hydrogen during the process of H_2 evolution on the steel substrate. Thus, it follows that it is this decrease in recombination that increases more Hads consequently more H permeation current. This view is realistic and it is acceptable to explain the increase in Hads by the presence of chemisorbed anions.

Also, the rate of hydrogen dissolution in iron and steel

is known to depend on the composition, the structural defects such as interstitial sites, grain boundaries, dislocation etc. in the steel which provide H diffusion paths. Phalen and Vaughen[58] have shown that H dissolution and consequent diffusion in steel is through structural defects paths which are enlarged in size or number of the presence of residual or applied tensile stresses[59]. As the effect of surface stress on hydrogen absorption by steel has not been established, the relationship between surface tensile stress and H permeation is considered an important investigation to be carried out later.

It has been shown recently that the electrochemical conditions (ie. solution pH and electrode potential) at the tip of an advancing stress corrosion crack in steel exposed to 3.5 per cent Nacl solution are favourable for hydrogen evolution regardless of the externally applied potential or the pH of the bulk solution[60]. At the same token, Brown[61] found that the solution inside a fissure on the surface of a specimen becomes very acidic (from pH 6.5 to pH 3.5) and that metallic ions are present. He emphasised his point by plotting the combination of pH and potential observed during cracking on a Pourbaix diagram, he found that the points always fall in that region where hydrogen evolution is possible. He states that "there does not appear to be any valid reason to require a mechanism other than hydrogen embrittlement to account for the cracking of high strength steels in salt water". Also, for low alloy steels, without applied potential, SNAPE[61] attributed failure mainly to

hydrogen embrittlement. Thus, the failure of a metallic structure could be the responsibility of stress corrosion cracking and/or the hydrogen embrittlement where the specific cause cèlébre in any environment is not clear.

1.5.3. Effect of Hydrogen Embrittlement on Off-Shore Structures

One of the major problems in off-shore gas and oil pipe lines is their susceptibility to stress corrosion cracking due to hydrogen embrittlement. The problem is particularly serious in riser pipes which carry the hot crade oil or gas from the ocean bed to the under water pipes which transport the fuel to the shore. The riser pipes are subjected to considereable stress caused by oil or gas pressure as well as the pounding action of the waves. The presence of H_2S or moist CO_2 which is strongly adsorbed and dissociates very easily on the steel structure. The action of H_2S is generally assumed to be due to the poisoning of the H atom recombination sites by strongly adsorbed $S^{=}$, thereby forcing the H atoms to diffuse into the metal lattice. Hence, this phenomenon could be responsible for the internal corrosion of pipelines and equipment which are encountered in most oil and gas production units. However, the degree of internal corrosion attack will vary with the production site and this will change during the production life of the well and also as operating procedures and the production rate change. This is because the rate and type of corrosion is dependent on various parameters, such as the amount of water co-produced with the gas and/or crude,

the presence and concentration of Co_2, and/or H_2S, the pH, the salt content and ingress of oxygen. This type of corrosion can be classified into two basic types, namely "Sweet" corrosion due to presence of Co_2 and water and "Sour" corrosion due to the presence of H_2S. In both cases, the rate of the cathodic H_2 evolution is increased, leading to Hads and dissolution into the metal lattices, consequently more hydrogen embrittlement and premature failure. Moreover, in the presence of carbonic acid, the localized corrosion attack on the steel is increased; the presence of pits would enhance the possibility of stress corrosion. The evolution of hydrogen can be written as:-

$$H_3O^+(aq) + e \longrightarrow H_2O(\ell) + Hads \qquad (1)$$

$$Hads + Hads \longrightarrow H_2(g) \qquad (2)$$

In sour pipes, H_2S reacts with steel to form iron sulphides. On such surfaces, reaction (2) is the rate determining step and the possibility of adsorbed H atom (Hads) diffusing into the steel would be greatly increased.

$$xHads + Fe \longrightarrow FeHx \qquad (3)$$

This will then result in hydrogen embrittlement, which has been identified as the main cause of stress corrosion cracking of internal steel pipe lines during gas and crude oil production[62].

Present protective measures[62] have been taken to prevent hydrogen embrittlement, including:-

(i) Design : by eliminating abrupt changes in flow direction, the corrosion caused at local sites is minimised.
(ii) Proper choice of materials : this is, however, often constrained by cost and practical considerations. In certain areas chromium steel have been used but mechanical requirements and the possibility of their cracking in high chloride, high temperature environments restricted their large scale use.
(iii) Inhibitors : this is the most favoured method at the moment. Basically, these are organic molecules in corporating active polar groups containing sulphur, nitrogen or phosphorous eg. alkylamines or amides. These compounds adsorb on the metal surface and decrease the rate of electrochemical reaction. However, the inhibitors have to be added either continuously or at weekly intervals. Moreover, it is not certain whether it would be very effective in sour pipes, since the inhibitors cannot stop the reaction between H_2S and steel. Tomashov[63] considered that greater effectiveness of control may be achieved by adopting more than one method of protection that they all effect the same controlling factor.

1.6. Hydrogen Evolution Electro Catalyst

Literature has shown that iron and/or steel is a poor electro catalyst for hydrogen evolution. Platinum is often an alternative choice to steel for H_2 evolution. Thus, the tendency

of H_2 evolution occuring on steel surfaces during corrosion process could be due to pH of the environment.

Bockris et al[64] have recently shown that electronic factors markedly influence the heat of activation in reactions involving chemisorbed species, and Mills[65] results also confirmed the earlier view that electronic properties are a major factor affecting H_2 evolution catalytic activity.

Thus, from the experimental results as well as theoretical considerations it is most probable that an efficient electrocatalyst for H_2 evolution could be achieved by developing a compound which has a fairly moderate M-Hads bond energy, a good electrical conductivity, corrosion resistant and most significantly a low hydrogen overpotential.

By taking the above consideration into account, recent work at The City University on an E.E.C. funded project entitled "OPTIMISATION OF TEFLON BONDED GAS POROUS ELECTRODE", Tseung and Man[66,67] developed what could be described as a novel nickel-cobalt-sulphide, $NiCo_2S_4$, cathode catalyst which gave over 1000 mA/cm^2 at - 170 mV vs RHE in 5 M KOH at 70°C after ohmic correction. Recent life tests in 5M KOH @ 85°C, have confirmed that Teflon bonded $NiCo_2S_4$ cathode catalyst can operate at 1 A/cm^2, -130 mV vs RHE (Ir corrected) for over a test period of 3300 hours without any deterioration in performance. Moreover, $NiCo_2S_4$ is not affected by H_2S from which it is prepared and subsequent exposure to air even at 85°C shows immense corrosion resistance.

1.7. Summary of the Problem

In summarizing the problem, it is evident that the use of smooth specimen for the assessment of SCC susceptibility of metallic materials has proved very suspicious. This is because the results, based on its use depend on the period of incubation, material surface and size, and environmental conditions which all together are known to vary markedly. Also, the use of precracked specimen for K_{1SCC} determination as described above has proved time consuming. However, the recent method of determining K_{ISCC} by the use of precracked specimen in H_2S environment does command the confidence of competent hands in this field, but the elaborate safety requirement because of the toxicity of H_2S handicaps its frequent application. Thus, this makes it cumbersome and unattractive for potential users.

1.8. The Present Work

Therefore, the present work aims at finding a simple, rapid and reliable method to assess the SCC susceptibility of materials before such materials are used. It is intended to achieve this goal by using a precracked specimen and an electrochemical method to determine the threshold value of stress intensity of SCC, K_{ISCC}.

The isolation of H_2 evolution from the corroding material could be a better technique of protecting a metallic structure from hydrogen embrittlement. Thus, the second part of the

present investigation introduces the use of some active H_2 evolution electrocatalysts to isolate the hydrogen evolution from a corroding material.

These techniques proposed in this work for the determination of K_{ISCC} value and the isolation of hydrogen evolution from a corroding metallic structure should throw light in the choice of material in the design of components and possibly eliminates the failure of such components by hydrogen embrittlement.

CHAPTER TWO

AN ELECTROCHEMICAL METHOD FOR DETECTING THE THRESHOLD STRESS INTENSITY IN STRESS CORROSION

CHAPTER II

AN ELECTROCHEMICAL METHOD FOR DETECTING THE THRESHOLD STRESS INTENSITY IN STRESS CORROSION.

2.1. INTRODUCTION

2.1.1. Literature Survey

The search for a simple technique to be used for the assessment of the stress corrosion susceptibility of material has been the problem confronting designers and competent hands in this field. Traditionally, smooth specimen is used to determine the threshold value of norminal stress from which the susceptibility of the material to SCC is assessed. A typical investigation of this type is shown in Fig. 1 below, which plots applied stress against time to failure for a magnesium alloy exposed to a 3.5 per cent Nacl solution[20]. As the magnitude of the stress decreases, the time for failure increases. Such plots have been obtained

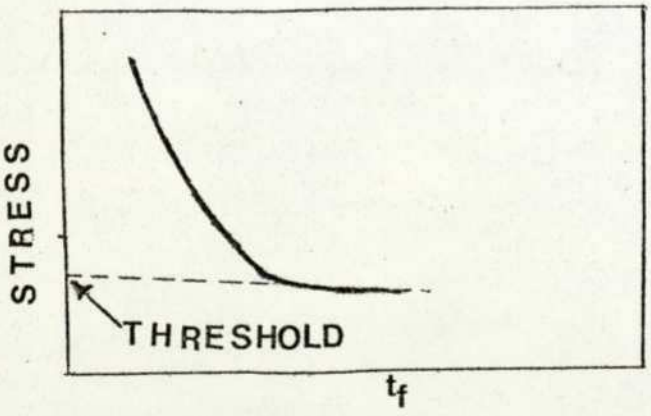


Fig.I Schematic SCC data from smooth specimen

for various material/environment combinations and can be seen that stress threshold are not always obtained in short-term testing. Time to failure, even at high stresses, can be very long in this type of experiment, as some initiation process, usually the

formation and enlargement of a corrosion pit, is required before cracks will propagate. Such an initiation process may occupy a high proportion of the failure time.

Another method often adopted to measure the threshold value of stress intensity of stress corrosion cracking involves the adoption of fracture mechanics[37,41]. When a precracked metal is stressed in such a way as to tend to open and extend the crack, the norminal stress is intensified near the crack tip. The fracture mechanics parameter, ie. stress intensity K is used to quantify the stress field at this point as shown in figure II.

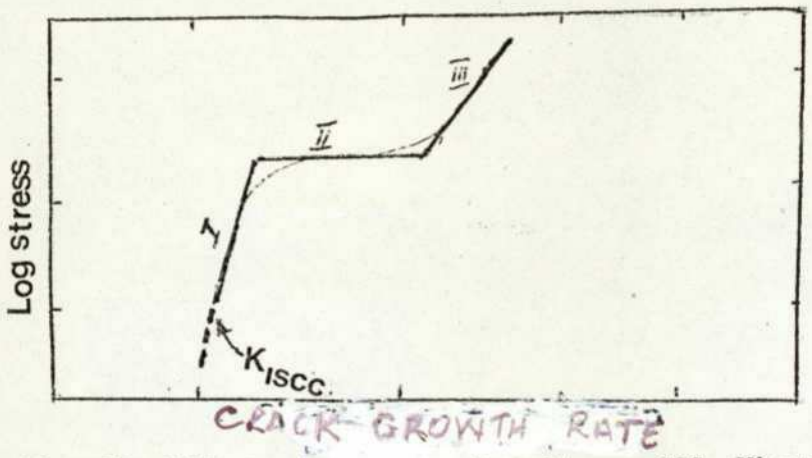


Fig. II Effect of stress intensity or SCC Kinetics

The SCC growth rate is measured as a function of K as shown in Fig. II. Here, the ones marked II, the crack growth rate is high and is insensitive to K. At a lower levels of K ie. region I, the crack growth rate becomes very sensitive to K. At sufficiently low value of K there appears to be a threshold which has been designated K_{ISCC}, that such a genuine threshold K exists has been clearly proved for titanium alloys in salt water, and it appears probable in steel, but its existence is in

question in some aluminium alloys[21]. The value of such a parameter of K_{ISCC}, where such a genuine threshold exists depends on ones ability to predict the combination of remote (nominal) stress and size of crack-like surface flaw through the use of Irwin relation[29]. Thus, the value of K_{ISCC} determined by this method will undoubtedly depend on the skill of the worker and possibly will not command the confidence of all concerned.

McIntyre[46], on the other hand, has shown that in an H_2S environment using the precracked steel test specimen failed within seconds of the crack tip stress intensity reaching K_{ISCC}. He suggests that this environment provided an accelerated method of testing. Although this method is reliable, the only problem that it poses is that H_2S is toxic, thus elaborate safety precautions are required and this makes it unattractive to potential users.

2.1.2. Present Work

The present chapter is devoted to the introduction of a simple and rapid method for the determination of the threshold value of stress intensity for stress corrosion cracking designated K_{ISCC}[41,43,44]. It has been shown by McIntyre that K_{ISCC} coincides with the formation of the stretch zone, thus the problem of determination of K_{ISCC} can be also the detection of the stretch zone[46]. This investigation proposes to adopt the fracture mechanics[37,41] principle and an electro-chemical approach based on the simple fact that as the stretch zone forms a greater area will be exposed

to the corrodent and thus the corrosion current will increase significantly, irrespective of whether the system is polarized anodically or cathodically. In order to achieve this goal, a compact tension notched and precracked specimen insulated with tensol cement except at the crack tip as the test specimen will be used for the investigation. By subjecting this specimen to an impressed voltage during application of tensile load, the detection of the formation of the stretch zone by a sharp increase in current due to the sudden increase in exposed area was realised. The load level corresponding to this sharp increase in the current was used through the application of fracture mechanics[38,40] to determine the threshold value of stress intensity of stress corrosion cracking, K_{ISCC}.

It is however observed that by using sea water as corrodent for this investigation, the reaction corrosion products impeded the magnitude of this sharp increase in current at the threshold. It became desirable to change to reversible electrolyte system, and improved on the technique by using the potentiostatic pulse method. However, the same K_{ISCC} value was obtained by this improved method for the same steel specimen, but the magnitude of the sharp increase in current was of much higher value. And, most remarkable is that the values of K_{ISCC} and exposed surface at the stretch zone obtained in this work compared very favourably with the result of McIntyre[46] for the same steel specimen.

2.2. EXPERIMENTAL TECHNIQUE

2.2.1. Corrodents

The corrodent used by several workers in stress corrosion tests is an aqueous solution of 3.5 per cent sodium chloride buffered at a pH 3.8 by the addition of 1.02 per cent potassium bi-phthalate. This pH level is chosen because it has been found to be the pH at the tip of a stress corrosion crack in several high strength steel in the absence of an applied potential, regardless of the pH of the bulk solution outside the crack. Marine environment is known to contain chemical species which have aggresive corrosive attack to a broad spectrum of metals and alloys especially the entire family of steel. Natural sources of sea water are not often used for laboratory tests due to the presence of microbiological impurities[68]. Synthetic sea-water is known to be free of organic impurities and has been considered useful for this work. Its chemical constituent is known[69] by BDH Analar grade samples used. This synthetic sea-water has pH 8.5, specific gravity 1.03 and resistivity 25 Ohm-cm at 25°C. Corrosion polarisation studies show that synthetic sea-water is corrosive and -400 mV Vs SCE is sufficient to induce corrosion of steel while -1000mV Vs SCE could give rise hydrogen evolution on steel[13,70].

Another corrodent used in this work was 4×10^{-2} equimolar ferricyannide and ferrocyanide in tenth molar KCl as the supporting electrolyte. This concentration has pH 9.10

and resistivity 84 Ohm cm at 20°C. The i-V polarisation curve was determined for this concentration which was observed to show appreciable current with less corrosion affect on the surface of steel used as working electrode.

A reversible hydroquinone-quinone system was also considered very useful for the investigation and estimation of the surface exposed on the bare metal at the stretch zone during SCC. The electrolyte was prepared by the dissolution in tenth molar potassium nitrate as supporting electrolyte, a known weight quinhydrone which in solution dissociates to set up quinone-hydroquinone equilibrium[71]:-

$$\underset{\text{(Quinone)}}{C_6H_4O_2} + 2e + \underset{\text{(Hydronium ion)}}{2H_3O^+} \rightleftharpoons \underset{\text{(Hydroquine)}}{C_6H_4(OH)_2}$$

This millimolar of quinone-hydroquinone in tenth molar kNO_3 as supporting electrolyte gave a reproducibility result on steel working electrode. This concentration has pH 5.67, resistivity 100 Ohm cm and open circuit voltage (OCV) was about -480 mV Vs SCE. Cylic voltametric studies of this system have shown reversibility characterised by two electron transfer peaks. A steady state potentiostatic i-V polarisation curves were determined within the first electron transfer region in both aerated and deaerated solution for this concentration Fig. (3).

2.2.2. Material Preparation

An En30B (ie. 835 M 30) steel brand of chemical composition in Table2-I was chosen because the results obtained

in this work could be compared with results of earlier workers[46]. The steel was machined in the longitudinal direction to produce specimen dimension 30 mm x 20 mm x 13 mm, which has a V - notch end with a root radius not exceeding more than 0.013 mm and from which a fatigue crack not greater than 2.54 mm would be developed Fig.(1). This specimen satisfied the conditions as recommended by material testing institutes[40]. These test specimens were heat treated to a temperature of 830°C in an argon environment in the furnace for one hour. This was followed by oil quenching at room temperature and tempered at 200°C and cooled at room temperature. These specimens were polisehd with very fine grade emery paper in a direction that could not interfere with the observation of the fatigue crack to be initiated at V - notch tip.

A fatigue crack α, was developed from the starter notch end by the application of dynamic load levels. This was achieved by subjecting the test piece to a dynamic loading in air. The Servo Fatigue Test Machine, model 181R/CY which was maintained at 8.0 kilo Newton (kN) and 0.4 kN of maximum and minimum tension loads respectively at the frequency of 10 Hz. An amplitude of 3.8 kN load was realized for this fatigue cycle[72]. A hand lense, magnification X20, was used to observe the initial crack at the tip of the starter V - notch. Once the crack was initiated, it was observed to propagate by the help of the hand lense and at the same time, the maximum load was gradually reduced to 2.0 kN. Thus, the maximum load

now at 2.0 kN, amplitude of 0.8 kN, the frequency was still maintained at 10 Hz while the crack was closely watched to grow ´. An average of about 1.5×10^5 cycles was required to initiate and grow a fatigue crack length exceeding about 1.25 mm. The exact fatigue crack lengths on each specimen were measured using the matellurgical Vicker Projection microscope at magnification X 100. The fatigue crack lengths used in this investigation were between 1.25 mm and 1.95 mm.[40] These precracked specimen were protected from the environment with glue tapes placed on the cracks and stored in a desicator until required for the tests.

The precracked specimen was to be used as the working electrode in the corrodents. Thus, Tensol cement, an I.C.I. grade 6 polymer product was used to insulate the specimen except the V - notch end which was the entry of the corrodent into the cracks was sliced open with a knife edge before the electrochemical test. The coating of the specimen was repeated until the precracked specimen and its attachment were adequately insulated.

The effectiveness of the coating was tested by subjecting an insulated specimen to similar stress-anodic and stress-cathodic potentiostatic polarisations in the corrodents and determined the corrosion reactions currents. The corrosion current values obtained in these trial tests were negligible which indicated that the insulation was effective as far as both the coated specimen and attachments were handled with dexterity.

TABLE 2·1

CHEMICAL COMPOSITION AND HEAT TREATMENT OF STEEL USED

ELEMENTS (wt %), IRON BALANCE

STEEL	C	Si	Mn	S	P	Ni	Cr	Mo	V	HEAT TREATMENT
En30B (837 M 30)	0.31	0.21	0.49	0.024	0.012	4.11	1.21	0.24	-	A830 OQ T200
En24	0.34	0.23	0.55	0.045	0.030	1.60	1.13	0.30	-	A830 OQ T600
En42J A_1S_1 1080	0.85	0.35	0.75	0.05	0.05	-	-	-	-	As Rolled
En42 A_1S_1 1070	0.75	0.30	0.65	0.05	0.05	-	-	-	-	As Rolled

* Austenitisation Temperature (°C)

** Oil Quenching

*** Tempering Temperature (°C)

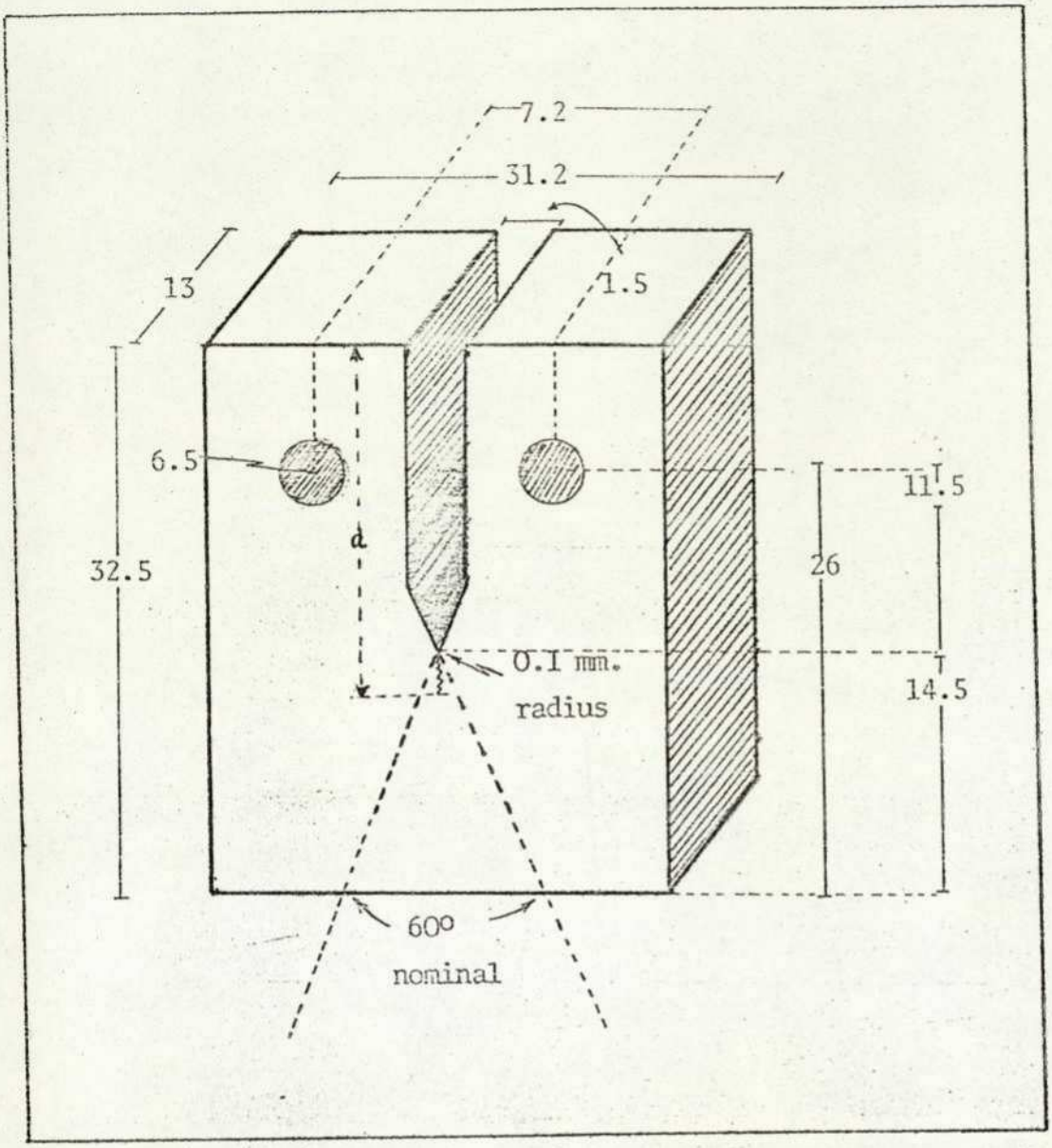


Fig. 1.- Compact Tensile Specimen, Dimension in mm
(a = total notch and fatigue crack lengths)

2.2.3. Mechano - Electrochemical Tests

The joint action of applied mechanical stress and corrosion on a material in an aqueous corrodent constitute stress corrosion. This concept was employed for this investigation.

a. Steady State Load - Current Measurements

Within the starter V-notch of the insulated test specimen, the surface leading into the fatigue crack which was covered with coatings was carefully scratched open with a knife edge. This specimen was the working electrode (W.E.) in synthetic sea-water as corrodent. Platinium screen was the counter electrode (C.E.). The W.E. was subjected to static loading in the Monsanto Type Tensometer Machine and at the same time held at a chosen potential of -400 mV Vs Saturated Calomel Electrode (SCE) housed in a luggin capillary as the reference electrode (RE) as in Fig.(2). The initial load applied to the W.E. was kept at zero kN, and its steady state current was recorded. Then, the load was increased in steps of 0.25 kN or 0.50 kN at a regular interval of about 60 seconds. A maximum load of 6.5 kN or 7.00 kN was attained in each test and throughout each run, the W.E. was maintained at anodic potential of -400 mV Vs SCE by an electronic potentiostat and the current was recorded by a digital voltmeter at each loading step. The anode current recorded was plotted against the corresponding applied load levels.

In the second test in sea-water, a fresh coated pre-cracked specimen was used in the same test assembly Fig. (2). This time, the specimen was maintained at -1000 mV Vs SCE in which hydrogen evolution was the dominant reaction on the test specimen. The current at zero load was measured. The current was recorded at subsequent load increases applied in the usual manner. Thus, the cathodic current recorded was plotted against the corresponding applied load level. It could be necessary to limit the time between the loading to about 20 seconds in order to minimize the effect of too much hydrogen evolution within the fissure.

For the same test in ferri-ferro cyanide corrodent, the W.E. was held at -510 mV Vs SCE cathodic potential. The load was increased from 0.00 kN in steps of 0.25 kN to a maximum heed level of 8.00 kN. A digital voltmeter (D.V.M.) connected across a known electrical resistor was used to monitor the current at each loading step. It was however observed that the current recorded was a steady state current ie. when the potentiostat which was preset at -510 mV (SCE) was switched on, a much higher current recorded was observed to decay from about 120 μA to the steady state of 25 μA in about 55 seconds. Therefore, all current measurements were made at this steady state value. The load-current plot was obtained in the same manner for this system.

In quinone-hydroquinone systems, oxygen inhibits the initial reduction reaction rate, but the limiting current density is independent of oxygen coverage[73]. It became desirable to

hold the W.E. at -600 mV Vs SCE which was within the limiting potential range as shown in Fig.(3). This was achieved by presetting the electronic potentiostat at -600 mV Vs SCE, and the system was allowed enough time to attain its open circuit voltage (O.C.V.) of -480 mV SCE before the potentiostat was switched on. Again, the current was observed to decay from 75 μA to steady value of 40 μA in 90 seconds. Thus, at this steady state current, the load was increased in the same manner (ie. from 0.00 kN in steps of 0.75 kN to a maximum of 8.00 kN). The current was recorded by the DVM and the typical load-current plot was obtained for this system.

b. Potentiostatic Pulse for Load - Current Measurements

The application of potentiostatic pulse technique in this investigation was to eliminate the mass transfer control[75] which was responsible for the small value of current in the steady state measurements. Thus, this procedure was observed to increase the recorded current in this electrochemical test.

The determination of the double layer charging time for the corrodents used was concluded by applying a 50 mV Vs SCE below the O.C.V. for synthetic sea-water and quinone-hydroquinone system respectively. A typical current-time responses of the double layer charging were obtained on the storage oscilloscope[75,76]. The sharp spike was due in each case to the charging of the double layer, and the continuous trace at longer time could be attributed to pseudo-capacity effect. The charging times obtained were

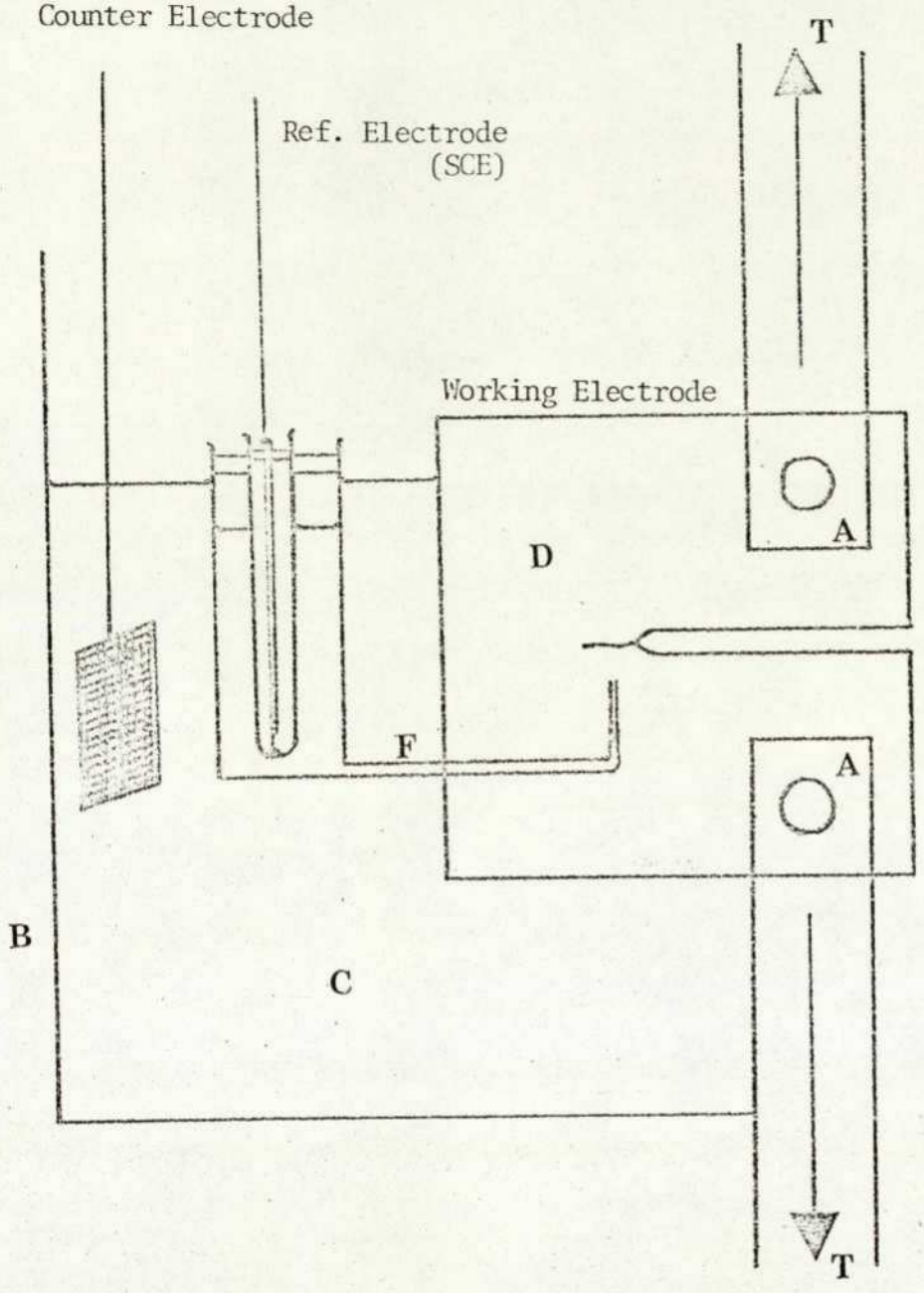
600 μ-second and 400 μ-second for hydroquinone-quinone and sea water respectively.

The same precracked steel specimen was insulated in the same manner and immersed in the quinone-hydroquinone redox system. This was the working electrode W.E. which was held at its open circuit potential (-480 mV Vs SCE) by an electronic potentiostat while at the same time maintained under applied load in the Monsanto type tensometer as illustrated in the test assembly Fig.(2). By using a pulse generator, the O.C.V. was rapidly changed to the limiting current voltage region (ie. -610 mV Vs SCE) which was within the first electron transfer region for 10 milli-second. The oscilloscope was used to obtain the current-time response. The pulse application was repeated on the same electrode at each applied load level and the pulse time in each case was kept at 10 m sec. The plot of applied load against the peak current responses was obtained for this system. Also, an i-V pulse polarisation curve was obtained on a fatigue surface which was prepared by a complete rupture of the precracked specimen Fig.12 . Basically, this was accomplished by rupturing the precracked specimen of known crack length in air at about 15 kN, then the entire half of the test piece except the fatigue crack which was distinguishable from the notch and the rapid rupture surfaces on the specimen similar to Fig.(4). In the same manner as above, the potentiostatic pulse at 10 m second was applied between the O.C.V. and Ep (where Ep was the applied pulse potential decreased from

-450 mV Vs SCE in steps of 10 mV Vs SCE to a minimum of -800 mV Vs SCE).

Similarly, the second half of the ruptured specimen was used to determine identical i-V pulse polarisation curve in systhetic sea water Fig.(13).

Again, the same insulated specimen of known crack length was immersed in synthetic sea water as the working electrode (W.E.). The W.E. was held at its O.C.V. by an electronic potentiostat and as usual maintained under applied load. At each increasing load level, the O.C.V. was rapidly changed to pulse potential Ep (ie. -1000 mV Vs SCE) in 8 milli-second while the current time response was traced on the oscilloscope. The peak of the current responses was plotted against the corresponding applied load level.



A : Metal Attachments for load application

B : Plastic Reservoir for sea water

C : Sea Water

D : Coated Metal test piece

F : Luggin Capillary

T : Tensioning Force

Fig. 2 Schematic Diagram of Test Assembly.

2.3. RESULTS

2.3.1. Steady State Measurements

The load - current plot obtained for the steady state polatisation in sea water are displayed in Figs.(5 and 6). It is interesting to examine these figures. First, the anodic mode Fig.(5), there is a gradual increase in current corresponding to a similar increase in applied load expressed in kilo Newton. This simultaneous increase in both current and applied load is observed to be more pronounced particularly the current which shows a sharp increase at specific applied load level. Secondly, in the cathodic mode Fig.(6), the current is insensitive to the increase in load, but at a particular load level, there is a sudden increase in current which is short lived as the magnitude of the current recedes to its original value after few seconds. Thus, unlike the cathodic current which is predominantly H_2 evolution current, the anodic current is stress corrosion current which is observed to increase with applied load.

In the steady state polarisation of the same specimen under sustained loading in ferricyanide - ferrocyanide medium as a corrodent, the load current plot is in Fig.(7). The current is observed to increase gradually with increase in applied load. But at particular load level the current increased sharply and recedes with the same gradual increase in load. Thus, this sensitive increase in corrosion current with applied load observed in this medium is an evidence that ferri - ferrocyanide medium is corrosive to iron and steel. Thus, the dark bluish colouration observed

during the tests could be the corrosion products.

The steady state polarisation measurement for the same specimen under sustained load in quinone - hydroquinone redox system shows yet another interesting result. A close observation of the load - current plot Fig.(8), shows that the current is independent of the applied heed, until at the critical load level where the current shows a sharp increase with the applied load.

2.3.2. Pulse Measurement

The potentiostatic pulse application to these investigations is observed to increase the values of the recorded current because the mass transfer difficulty has been eliminated. The absence of the problem is well reflected in the current measured by this technique compare with the above results.

In sea-water, the pulse method applied on the specimen under sustained load in the cathodic mode, the current measured improved by more than a hundred fold. Again, the current is independent of the applied load except at the critical load level in which a sudden increase in current is observed. Unlike in the steady state tests, the current does not recede to its original value above the critical load levels Fig.(9).

For quinone - hydroquinone redox system, the current is observed to be insensitive to the increase in applied load as indicated above, but at the critical load level, there is a sudden and tremendous increase in current which quickly attains a limiting

value at higher load levels figs. 10 and 11.

These sudden increases in currents observed in these investigations are due to the attainment of the critical load which is responsible for the formation of stretch zone at the crack tip of the steel specimen. Thus, the critical load level responsible for each observed sudden increase in current in the each medium considered is used for the calculation of the threshold value of stress intensity of stress corrosion cracking K_{ISCC}, as shown in Tables 2.2 and 2.3. By considering the dimensions, initial fatigue crack length and load at which a sudden change in current occurs, the K_{ISCC} value for the steel specimen could be calculated using the fracture mechanics relation[36,39,40] :-

$$K_{ISCC} = \frac{P \cdot \beta}{B \cdot W^{1/2}}$$

where β = a/w, and often provided in literature[40]. Otherwise it would be estimated by using the following relation[38,39].

$$\beta = \left\{ 29{\cdot}6 \left(\frac{a}{w}\right)^{1/2} - 185{\cdot}5 \left(\frac{a}{w}\right)^{3/2} + 655{\cdot}7 \left(\frac{a}{w}\right)^{5/2} - 101{\cdot}7 \left(\frac{a}{w}\right)^{7/2} + 638{\cdot}9 \left(\frac{a}{w}\right)^{9/2} \right\}$$

where P = Load at which current increased sharply

B = Breadth of the specimen

W = Width " " "

a/w = Ratio of total flaw length (ie. notch and fatigue crack lengths) to width of specimen, fig.1.

The K_{ISCC} calculated for the steel specimen in the steady state measurements in synthetic sea-water, ferricyanide-ferrocyanide

and quinone - hydroquinone are given in table 2.2 While table 2.3 shows K_{ISCC} values obtained in synthetic sea-water and quinone-hydroquinone from the pulse technique.

TABLE2.2

The threshold values of stress intensity of stress corrosion cracking K_{ISCC}, for En 30B steel determined by Steady State Load current measurements in (i) Synthetic sea-water, (ii) Ferricyanide-ferrocyanide and (iii) quinone-hydroquinone environments.

Environments	Fatigue Crack Length α (cm)	Critical Load k_1 (kN)	Threshold Value K_{ISCC}, (MN $m^{-3/2}$)
Sea water (Anode Mode)	0.1338 0.1523	3.00 2.75	11.86 10.94
Sea water (Cathode Mode)	0.1355 0.1470 0.1723	3.25 2.75 2.50	12.68 10.94 9.95
Ferri-ferrocyanide	0.1350 0.1460	3.00 2.75	12.25 11.24
Quinone-hydro-quinone	0.1385 0.1465	3.00 3.00	12.17 12.27

TABLE 2·3

The threshold values of stress intensity of stress corrosion cracking K_{ISCC} , and the determined lengths of the surface exposed on the bare En 30B steel at the stretch zone by the transient load current measurement in sea water and quinone-hydroquinone environments.

Environments	Fatigue Crack α (cm)	Critical Load k_1 (kN)	Threshold Value K_{ISCC}, MN $m^{-3/2}$	Crack Opened $\Delta\ell$ (mm)
Sea water	0.1755 0.1785	3.00 2.75	12.68 11.88	0.0277 0.0117
Quinono-hydro quinone	0.1637 0.1647 0.1287 0.1268	2.50 2.50 3.25 3.25	10.42 10.40 12.98 13.04	0.0318 0.0420 0.0210 0.0160

2.4. DISCUSSION

Another examination of the load - current profile for the specimen in synthetic sea water in the anodic mode fig.5, shows a responsive increase in current to the corresponding increase in applied load. This current increase becomes pronounced at the critical load at which supposedly a stretch zone is formed. The simultaneous increase in corrosion current with supplied load is the out come of stress corrosion. Again, in the cathodic mode, load-current in sea water fig.6, shows that the H_2 evolution current is independent of the applied load until at the critical load which shows a sharp increase in current possibly due to formation of the stretch zone. But, the increased current quickly receded to its original value. This sharp decrease even at much higher load above the critical load has been caused by the hydrogen gas bubbles blocking the reaction surface in the fissure. This phenomenon was investigated by switching off the applied voltage on the potentiostat while continued to maintain the constant applied load just above the critical load for 15 minutes to allow the hydrogen gas occluded within fissure to diffuse into the bulk solution. Then, the applied potential was restored by switching on the potentiostat, the magnitude of the current was found to have returned to the higher value (50 μA). Thus, within about 15 minutes hydrogen accummulation again caused the fall back to the lower value.

The average K_{ISCC} calculated based on specific fatigue

crack lengths and the critical loads for both anode and cathode modes for the specimen in sea water were 11.40 MN $m^{-3/2}$ and 11.20 MN $m^{-3/2}$ respectively as shown in Table 2. In the same corrodent (ie. Sea water), the load current profile obtained by the pulse technique displayed indentical insensitivity of the current with increased applied load except at the critical load level. At this critical load, the current increased sharply in the same manner but did not decrease Fig.9 as observed above. The absence of this decrease even at load well above the critical load could be attributed to the short time (10 m sec.) which is not enough for more hydrogen gas bubble to accummulate within the micro crack. Similarly, the average K_{ISCC} obtained by this pulse technique in sea water from Table2.2 is 12.28 MN $M^{-3/2}$ which is comparable to the average 11.30 MN $m^{-3/2}$ as obtained for the same specimen in sea water by the steady state method. Hence, it could be considered that K_{ISCC} average for the material using the two techniques is 11.79 MN $m^{-3/2}$.

The load - current relation for the same specimen in ferricyanide-ferrocyanide corrodent shows that the current increase depends on the increase in applied load which depicts stress corrosion process Fig. 7. The average K_{ISCC} obtained for the same steel specimen is 11.70 MN $m^{-3/2}$ in this medium, Table 2.2. This value of K_{ISCC} is very close to the average value of 11.79 MN $m^{-3/2}$ obtained for the same steel in sea water.

For the quinone-hydroquinone system, the load current profile is basically the same but the current value is highly

increased in the potentiostatic pulse technique more than in the steady state. The ratio of the sharp increases in current at the formation of the stretch zone in both techniques shows that steady state current is 100 times less than the pulse technique. However, the load - current relations in the two techniques in quinone-hydroquinone medium repeated the insensitivity of the current to the increase of the applied load except at the stretch zone, but the current in each case attains a limiting value at higher load, Figs. 10 & 11. The K_{ISCC} obtained from the two techniques are displayed in tables 2 & 3, from which the average K_{ISCC} are 11.80 MN $m^{-3/2}$ and 11.96 MN $m^{-3/2}$ for the steady state and pulse techniques respectively. The average of these two is 11.79 MN $m^{-3/2}$ for the steel specimen.

Summarising therefore, the K_{ISCC} for the En 30B steel in sea water, ferricyanide-ferrocyanide, and quinone-hydroquinone media are 11.79 MN $m^{-3/2}$, 11.70 MN $m^{-3/2}$ and 11.88 MN $m^{-3/2}$ respectively. It is very remarkable that within the experimental and environmental differences particularly with the wide variations of the prepared fatigue crack lenghts the same magnitude of K_{ISCC} are obtained. And, most remarkably, these K_{ISCC} values compare favourable with that reported by McIntyre[46] of 12.09 $\pm$ 1.10 MN $m^{-3/2}$ for the same steel specimen in H_2S environment. Thus, these values of K_{ISCC} from this investigation[77] as well as my preliminary work[78] and that of McIntyre, have supported the view that an alloy has a specific value of K_{ISCC} which is independent of environment[41,46].

The degree of the surface exposed at the stretch zone could not be corrolated to the recorded current obtained by the steady state measurements because of mass transfer control effect which makes such corrolation very suspicious. However, the peak current obtained by the potentiostatic pulse technique and the predetermined i-v curves Fig. 12 & 13 are used to estimate the length of surface exposed at the stretch zone in synthetic sea water and quinone-hydroguinone media. For the varying crack lenghts and environment ie. sea water and quinone-hydroquinone, the average stretch zone in both environment are 0.0161 mm and 0.0277 mm respectively as shown in Table3. An average of these two values for the same steel specimen is 0.0219 mm which compares favourably with the result obtained by direct electron microscopic examination of 0.009 mm by earlier worker[46].

The steel specimen used to determine the stretch zone in quinone-hydroquinone environment for 45 minutes test period at the maximum applied load of 8.00 kN is dried in an oven at 75°C, then ruptured at 15 kN in air. A visual inspection of the two halves of the specimen shows four distinctive surfaces Fig.4. These include the notch, fatigue, stretch zone and rapid rupture surfaces. The stretch zone is relatively very small compared with the fatigue surfaces and surprisingly seems not to propagate further as the load is increased even at higher load levels well above the critical load level.

Summarising therefore, the steady state and potentiostat pulse methods have been used to determine the same value of K_{ISCC}

of the steel specimen considered in various environments. The results obtained by the technique proposed in this work[79] compare very favourable with McIntyre's results for the same specimen in H_2S environment. Thus, the simplicity and the rapid result obtained by using this technique could save a lot of time for the potential users and possibly restores the confidence of experts in the field.

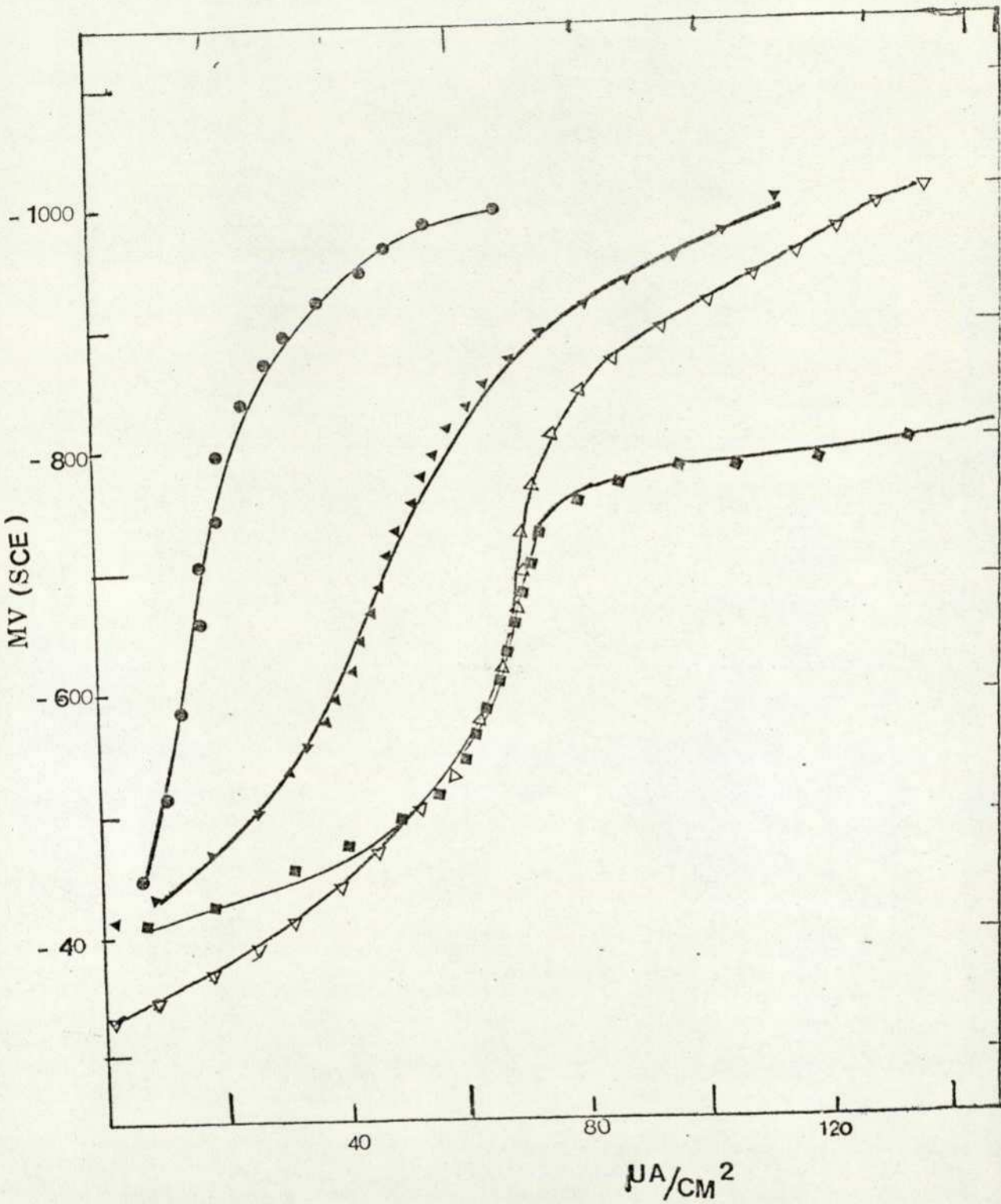
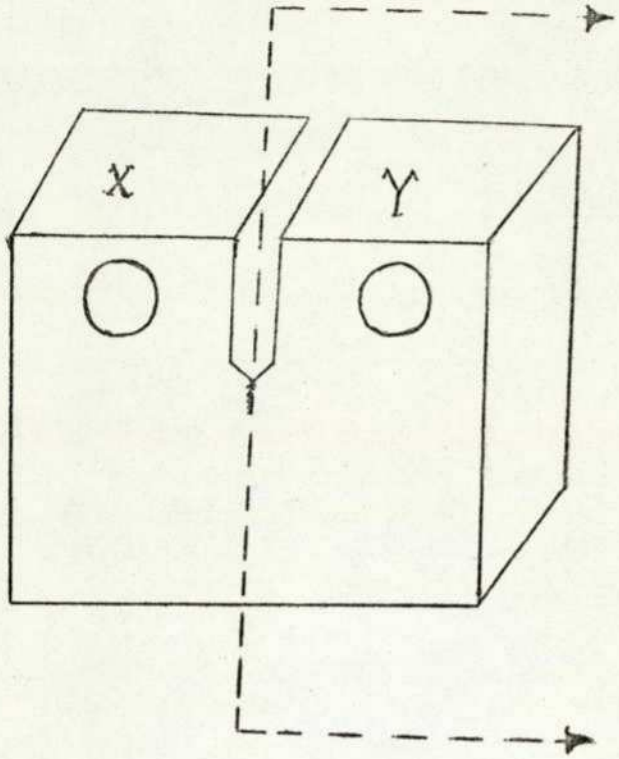
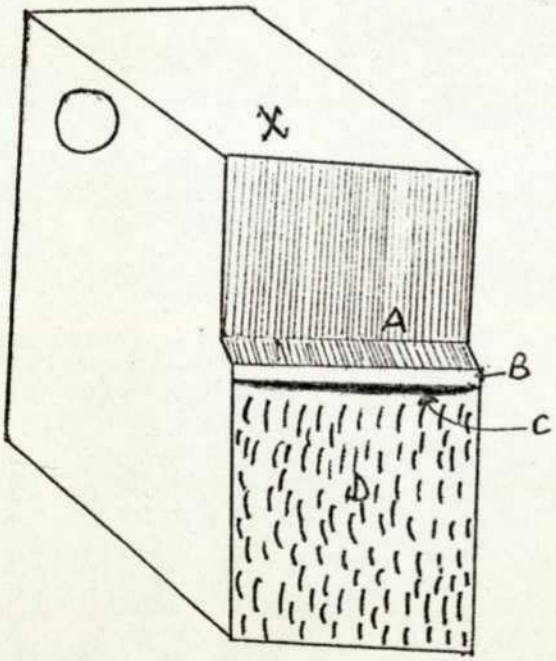


Fig. 3. Steady state i-v polarisation curves @ 20°C for
(a) ●—● deaerated 0.1M kNO_3 supporting electrolyte
(b) ▲—▲ supporting electrolyte in air
(c) ▲—▲ quinone-hydroquinone in supporting electrolyte in air, and
(d) ■—■ deaerated quinone-hydroquinone in supporting electrolyte.



(i) Compact En30B steel dried after use in quinone-hydroquinone environment. X and Y indicates two halves of the component after fracture in air



(ii) X-half of the component under visual inspection. Four distinctive surfaces:

A : Notch
B : Pre fatigue crack
C : Stretch zone
D : Rapid rupture

Fig. 4.

(i) En30B steel used in aqueous environment before rapid rupture in air at 15 kN.

(ii) One half after fracture in air for visual inspection on the effect of electrolyte/stress at stretch zone.

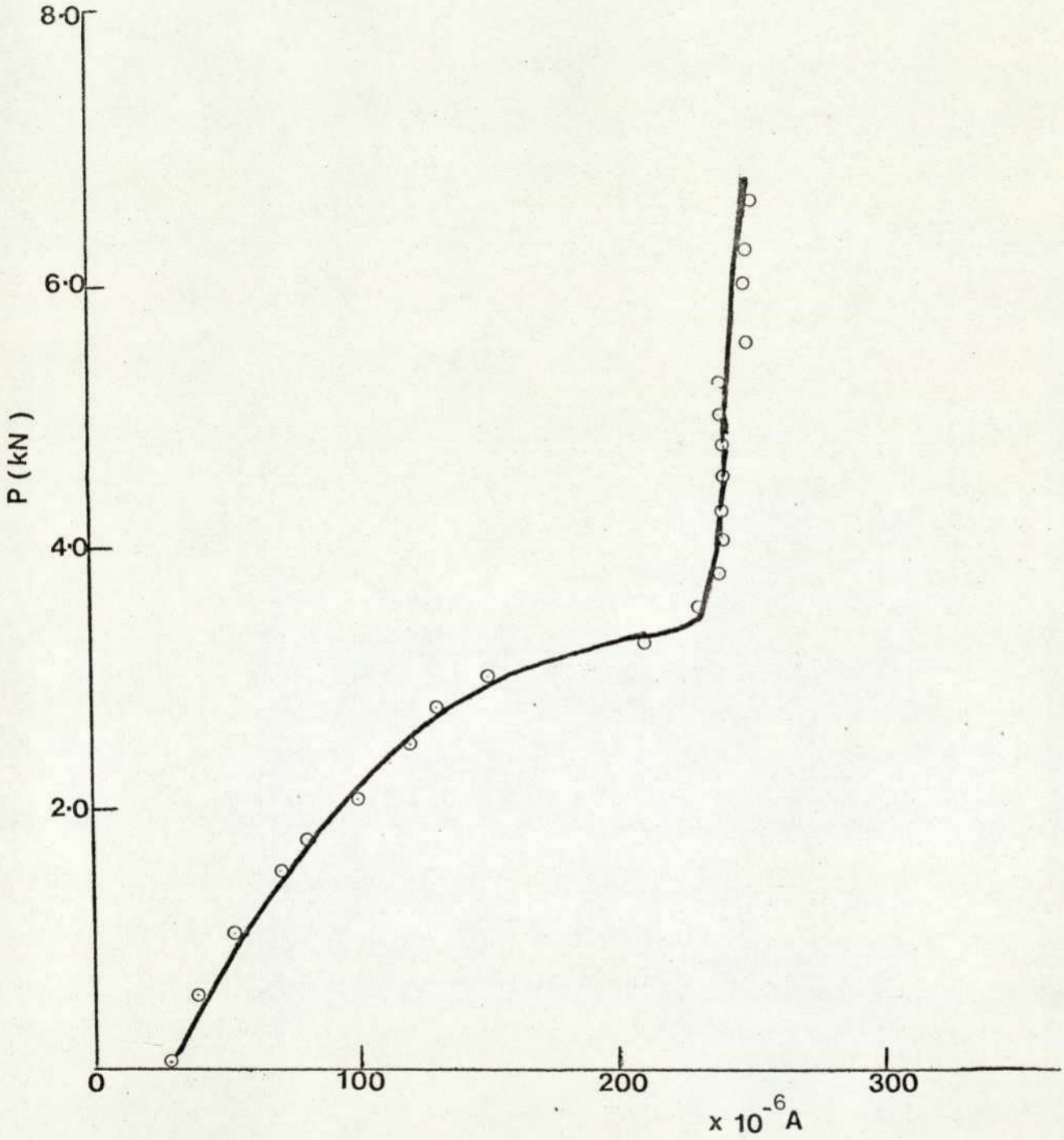


Fig. 5. Typical Load - current curve for specimen held at a steady state of -400 mV vs SCE in sea water.

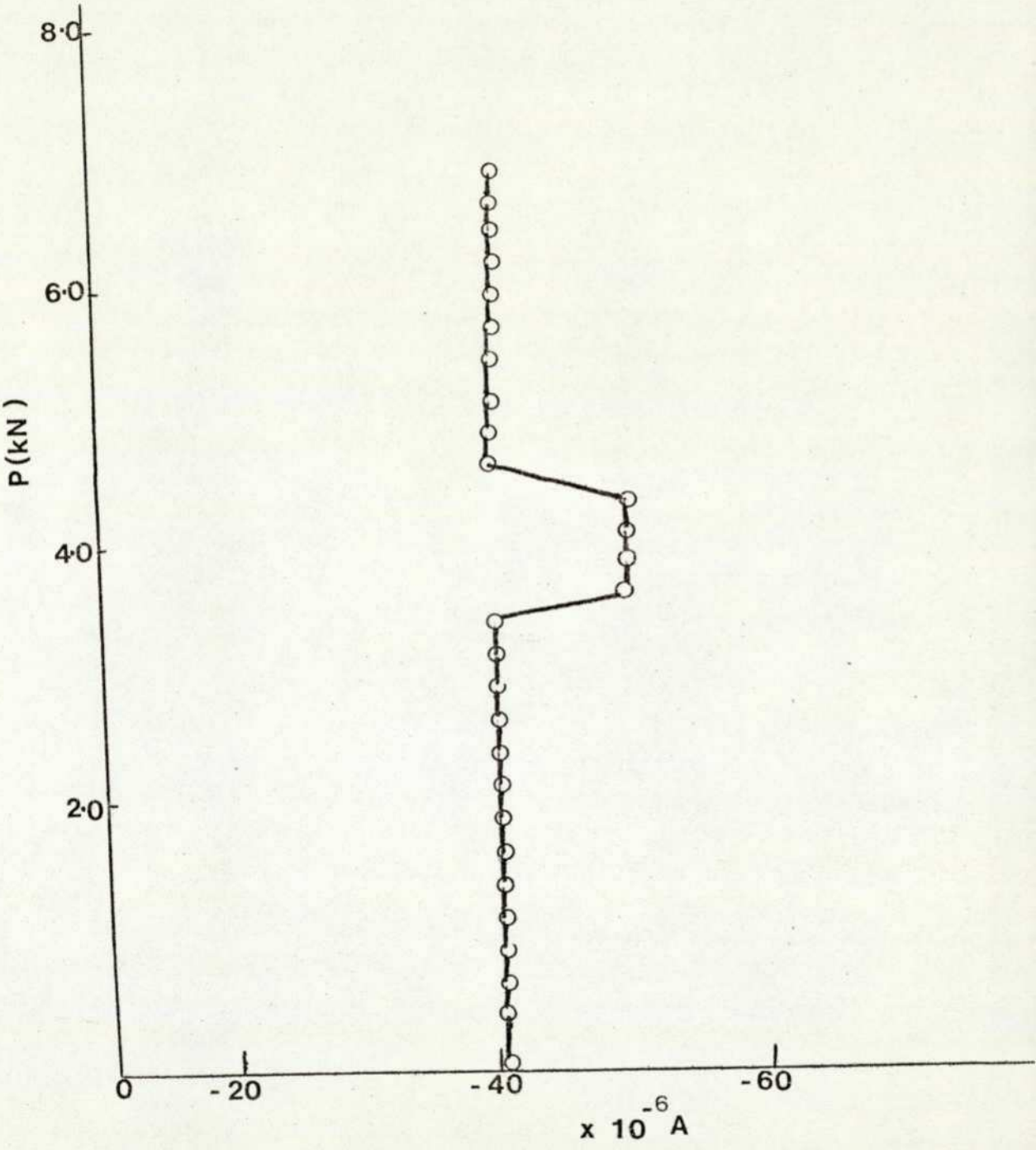


Fig. 6. Typical Load - current curve for specimen held at a steady state of -1000 mV vs SCE, in sea water.

STEADY STATE MEASUREMENTS

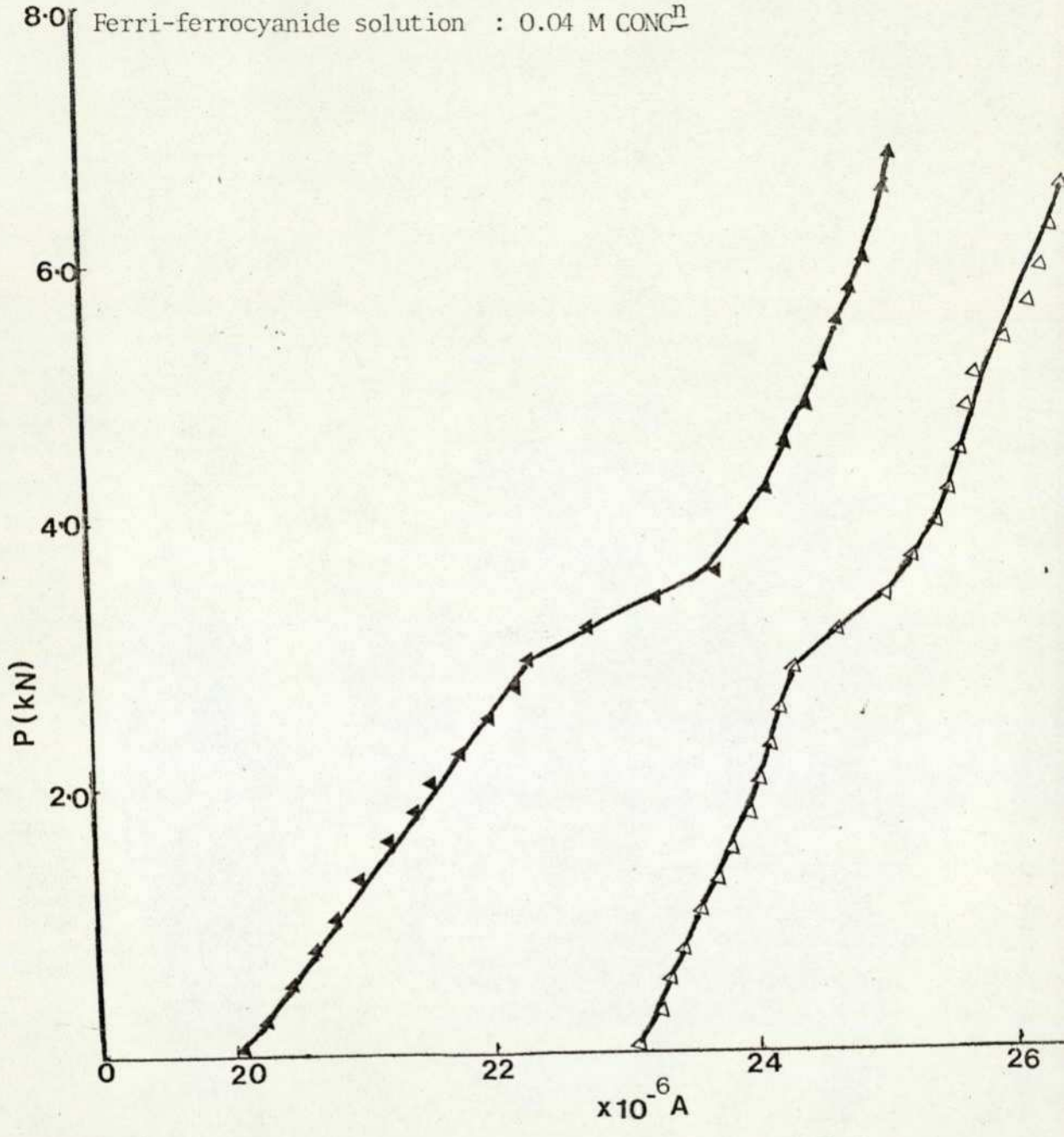


Fig. 7. Typical Load—current plot for the specimens of fatigue crack lengths (a) ▲——▲ 1.3150 mm and (b) Δ——Δ 1.3530 mm held at a steady state of -510 mV SCE in FeII/FeIII cyanide electrolyte.

STEADY STATE MEASUREMENT

Quinone-hydroquinone Conc^{n} 10^{-3}M

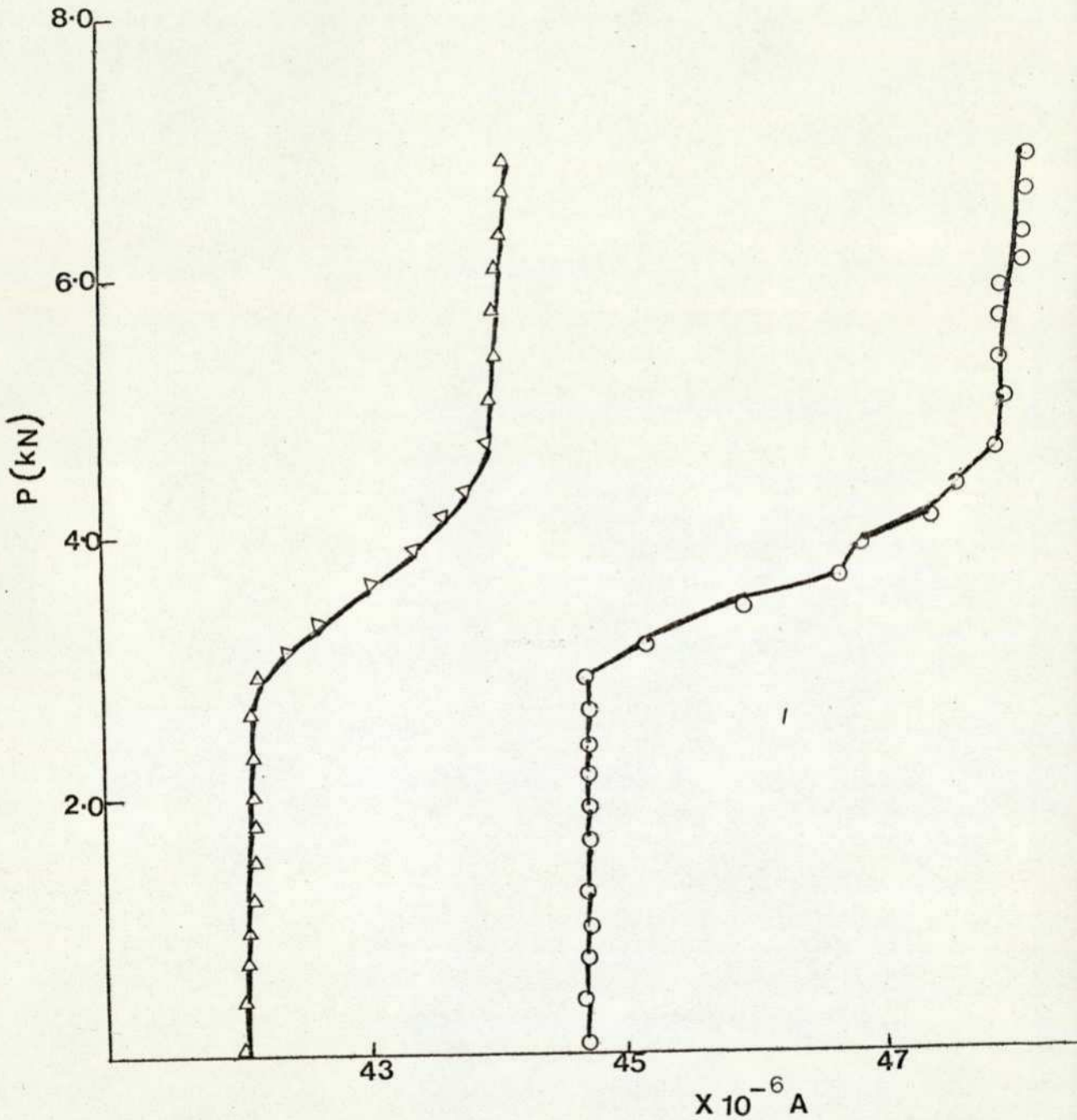


Fig. 8. Typical Load - current relation for millimolar quinone-hydroquinone at a steady state of -600 mV SCE for specimens of crack lengths (a)Δ–Δ 1.4650 mm and
(b)o–o 1.3850 mm

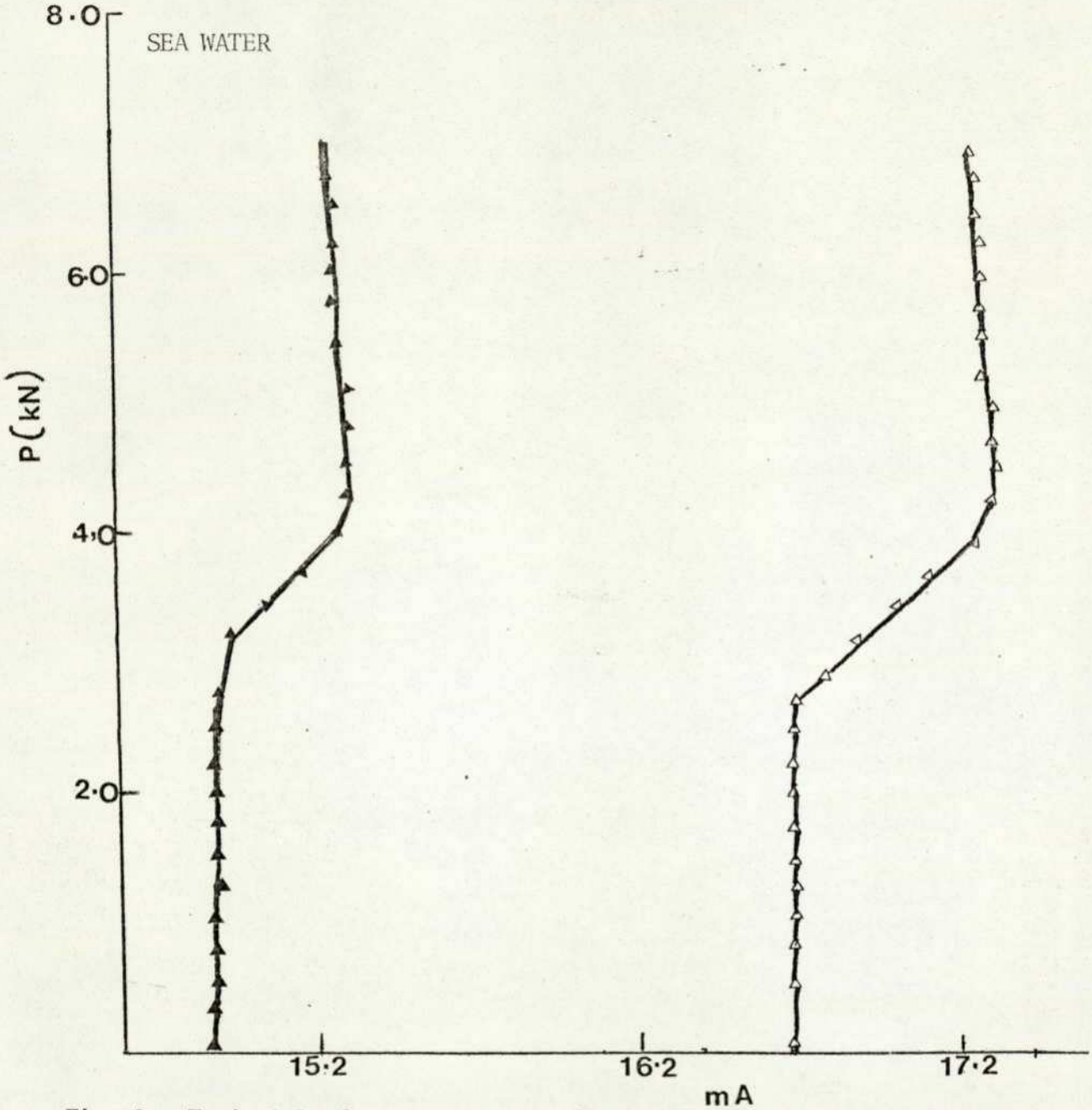


Fig. 9. Typical Load - current plot for specimens of fatigue crack lengths
(a) ▲——▲ 1.7850 mm and
(b) Δ——Δ 1.7550 mm at 8 m sec. potentiostatic pulse in sea water.

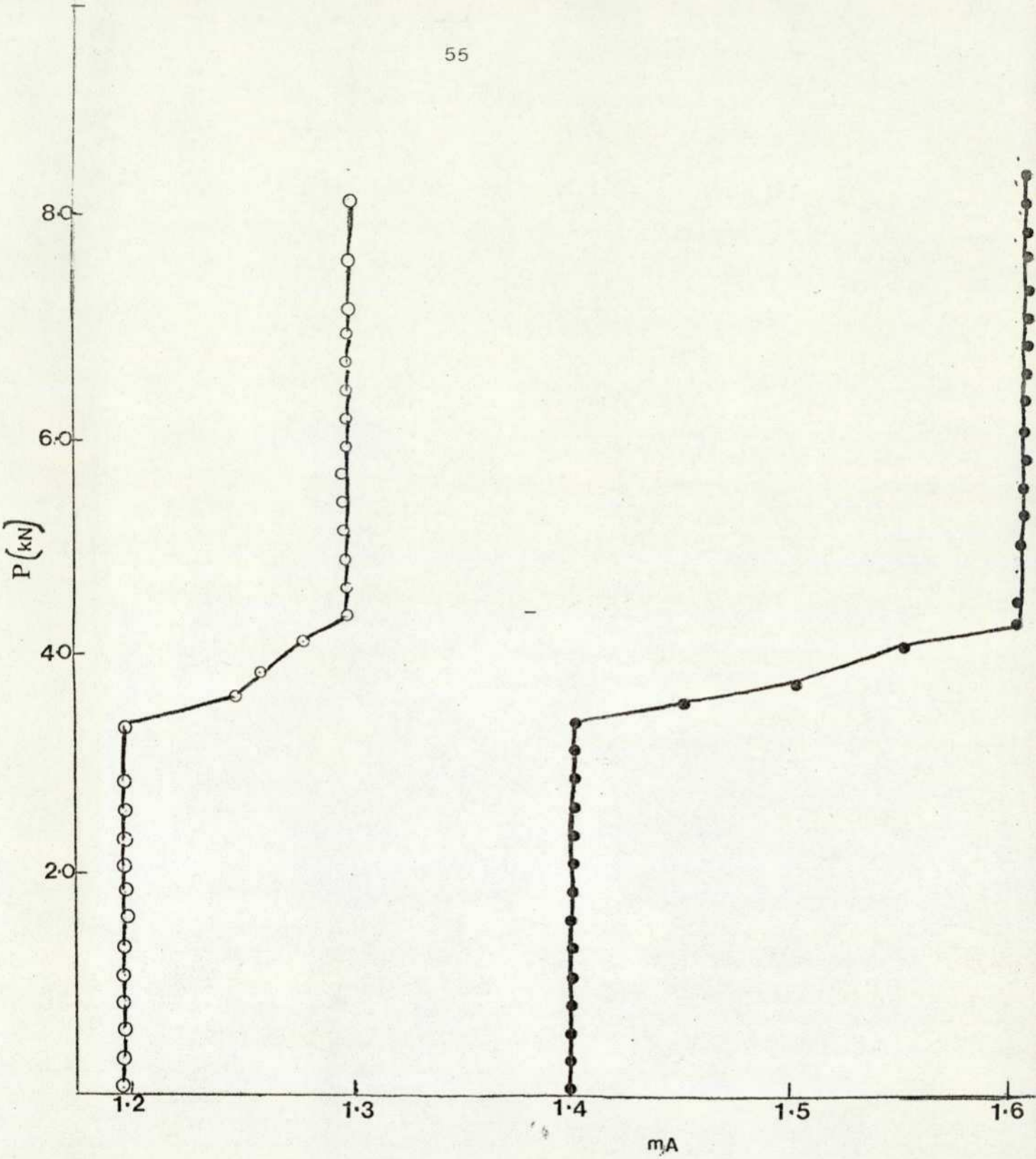


Fig. 10 - Typical load/current plots for specimens of fatigue crack lengths (a) o—o 1.268 mm and (b) ●—● 1.2870 mm @ 10 m sec. potantiostatic pulse in quinone-hydroquinone medium.

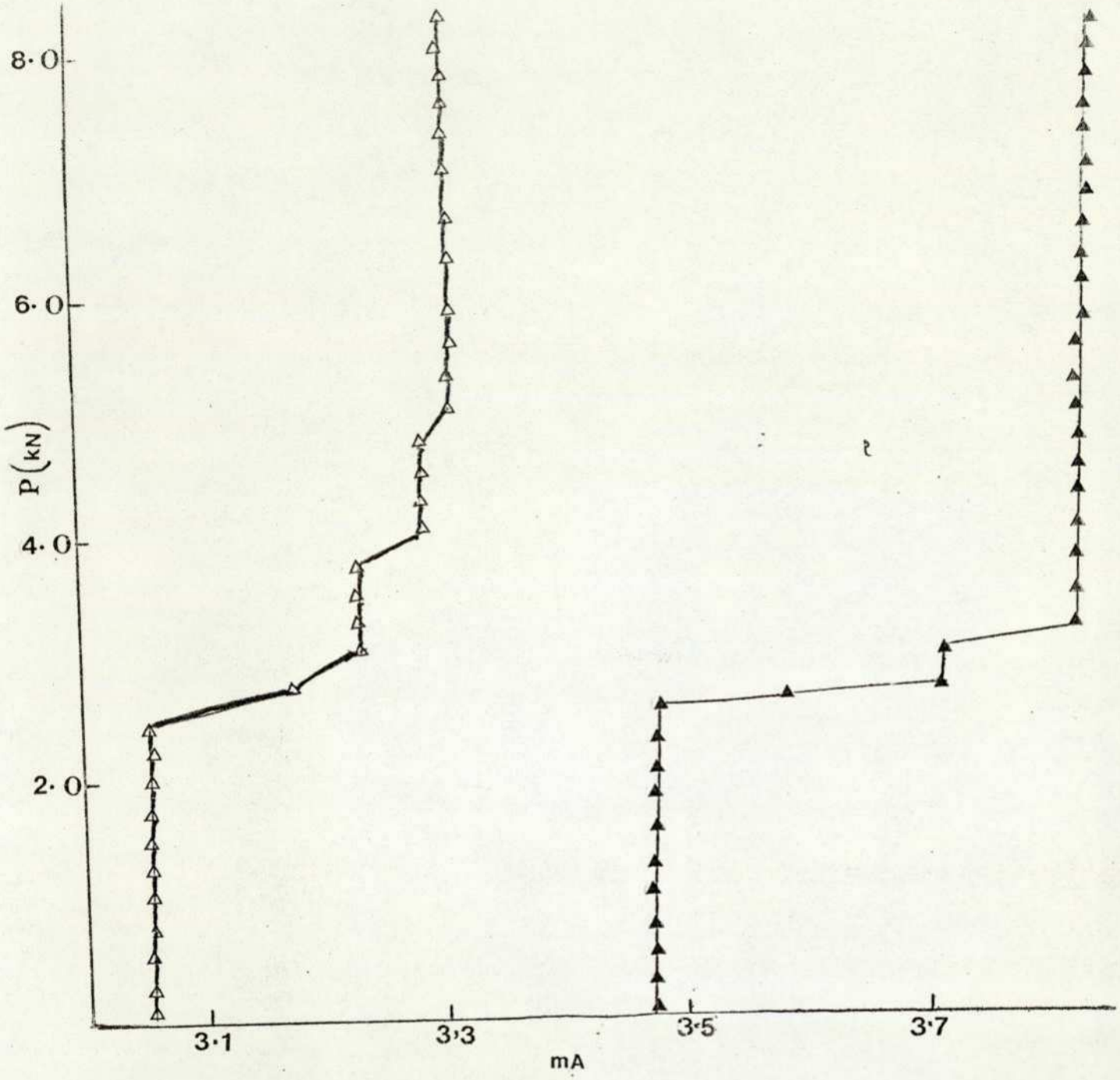


Fig. 11. Load/current plots for specimens of fatigue crack lengths
(a) △——△ 1.6470 mm
(b) ▲——▲ 1.6370 mm @ 10 m sec. potentiostatic pulse in quinone hydroquinone.

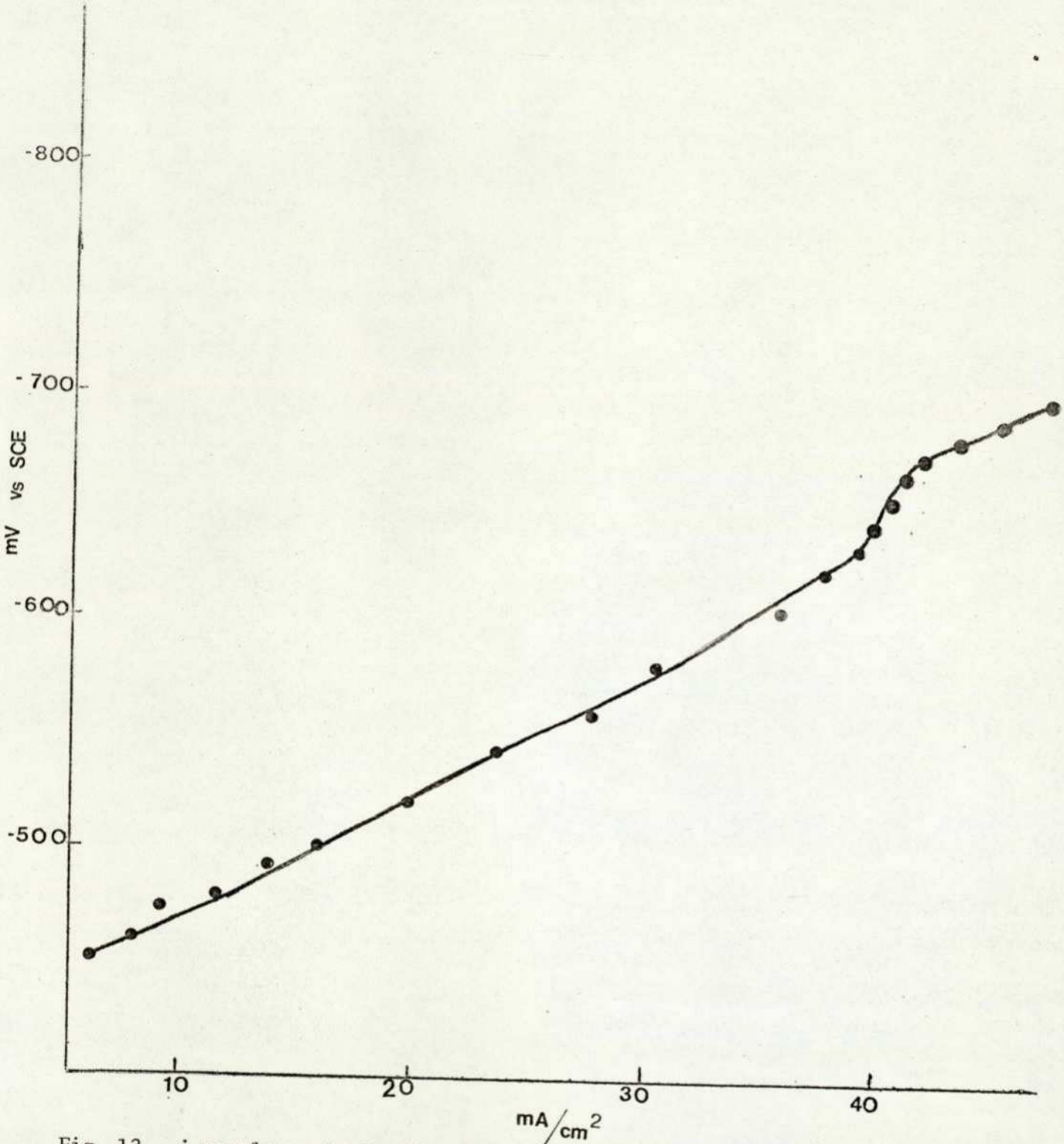


Fig. 12. i-v pulse polarisation for complete ruptured En30B steel specimen (in Fig. 4) in quinone-hydroquinone electrolyte (iR corrected)

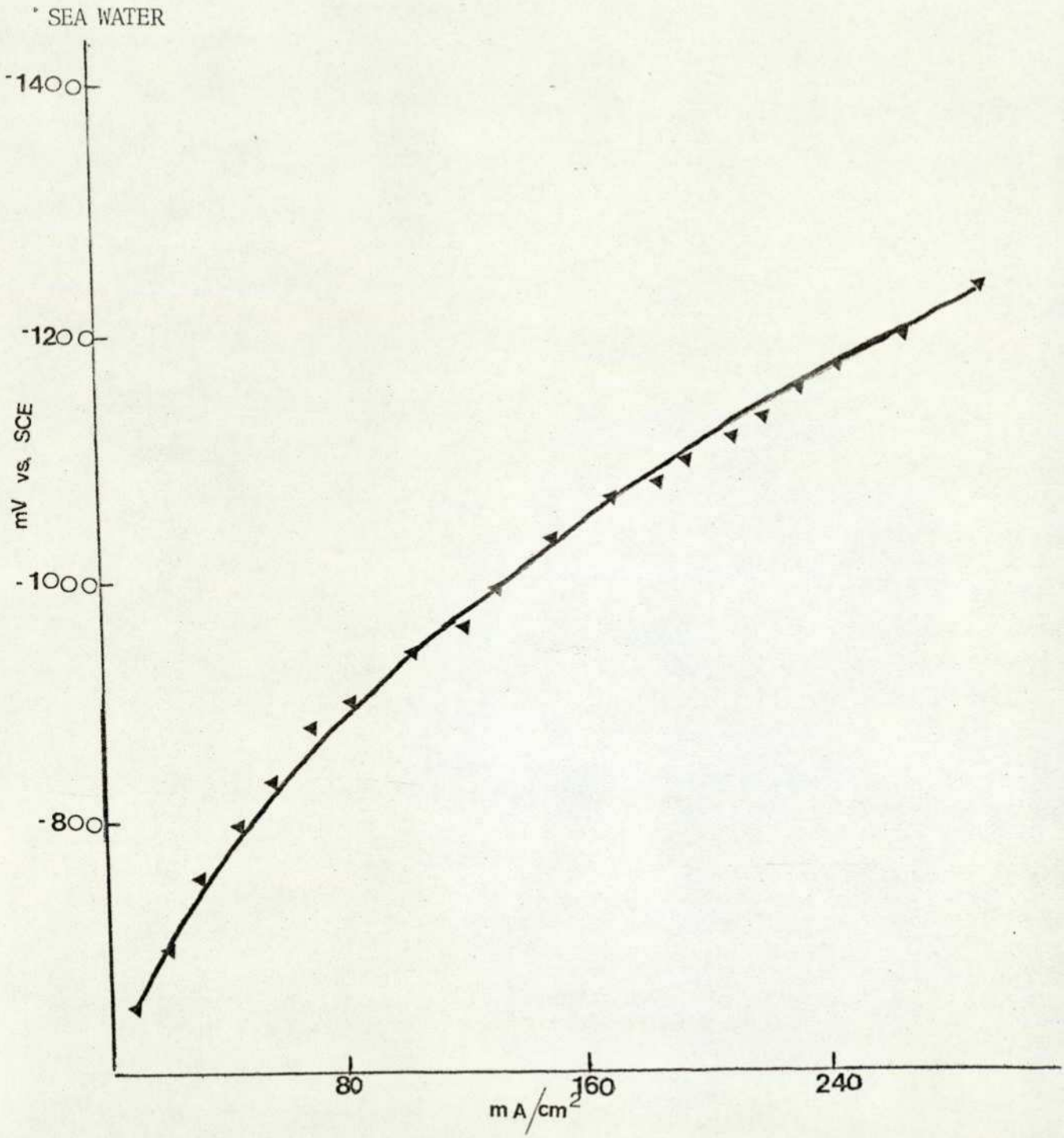


Fig. 13. i-v pulse polarisation curve for complete ruptured En30B steel specimen in synthetic sea water. (iR corrected)

CHAPTER THREE

HYDROGEN PERMEATION INTO STEEL

CHAPTER III

3.1. INTRODUCTION

3.1.1. Hydrogen in metals

This chapter investigates the absorption and consequent dissolution of hydrogen in metals. The hydrogen diffusion parameters in steel are determined and several factors which induce more hydrogen permeation are investigated.

Recent studies of hydrogen permeation in metal have been dominated by palladium and titanium, little is known about hydrogen diffusion in iron and steel.[48,50] It is,however, known that in corroding steel in an aqueous environment in which hydrogen evolution is the electronation reaction, some of the hydrogen evolved are absorbed into the lattice of the steel.[32,50] Bockris, Mcbreen and Nanis[80] and Devanathan and Starchurski[52,81] considered the formation of hydrogen atoms adsorbed Hads on the metal surface as an essential intermediate step in the electrokinetics of hydrogen evolution. They postulated various steps which include the desorption of the hydrogen by the formation of the hydrogen gas H_2, and diffuse into solution. During this desorption process, there is still some adsorbed hydrogen atoms which dissolve into the metal constituting absorbed hydrogen. This absorbed hydrogen within the bulk metal lattice sets up a hydrogen concentration gradient between the hydrogen-metal entry and the bulk of the metal, thus, this concentration gradient becomes the driving force which makes the adsorbed hydrogen diffuse into the metal. Recent work has demonstrated that diffusion of hydrogen (H) in the bulk of the metal is a fairly fast process.[52,80]

3.1.2. Hydrogen Diffusion Parameters in steel

The assessment of H diffusion rate has been demonstrated by different methods. Traditionally, the permeability and diffusion rate of H through steel membrane are determined using the modified form of Troiano, Berth and Steigerwald cell[82]. This technique has been used to measure the hydrogen passing through a steel membrane into an evacuated known volume. Basically, it involves one side of the steel membrane being exposed to an electrolyte while the membrane is held at H_2 evolution potential and the other side is the evacuated volume container. The H permeability is determined from the pressure rise as a function of time, while the comparative diffusivities are determined from the time lag as postulated by Barrer[51].

Recently, Davanathan and Stachurski[83,84] introduced a separate technique to measure diffusivity using electrochemical method. This involves the use of a thin steel membrane which separates two identical cells containing an electrolyte. The H entry face of the membrane is maintained at hydrogen discharge current while the H diffusing through is being oxidized by maintaining a H oxidation potential. The rate at which hydrogen diffuses through the membrane is determined by the current needed to maintain the constant H anodic potential at the second face of the membrane. Thus, the ionization current is the manifestation of the hydrogen permeating through the steel membrane from the surface on which hydrogen is evolved.

The number of H diffusing through the steel membrane per unit time is proportional to the concentration gradient as established by Fick's law. Thus, the changes in H concentration (ie. permeation current density) with time dc/dt could be quantified by Fick's second diffusion law:

$$\frac{\partial c}{\partial t} = D\left(\frac{\partial^2 C}{\partial x^2}\right)_{y,z} \quad \text{.....3.1.}$$

where c = the change in concentration

t = time change for the change in concentration

x = the thickness of the steel membrane

D = Diffusion coefficient (cm^2/sec)

y,z = denote that diffusion is considered only in one direction.

By using Laplace transformation and Error function based on the following assumptions:

(i) $C = Co$ @ $x = o$ and $t = o$

(ii) $C = O$ @ $x = L$ and $t \gtrless o$

McBreen, Nanis and Becks[53] obtained the solution of equation 3.1 as:

$$D = 0.25\ x^2/t \quad \text{.....3.2.}$$

where D in the diffusion coefficient, for membrane thickness x, and t : the time required by the H permeation current to reach $0.83\ I_{\infty}$ (limiting current). Thus, the diffusion coefficient determined in this work is based on equation 3.2.

Diffusion coefficient D is known to vary with the nature of the solute atoms, solid structure and with changes in temperature. For solid structures ie. iron and steel which exhibit surface defects such as lattice imperfections like impurities, dislocations, precipitation, grain boundaries and existance of residual or applied service load, the diffusion coefficient for such material

will depend on these defects[85]. However, diffusion coefficient is related to the temperature using the Arrhenius equation for the electrochemical reaction system as follows:-

$$D_t = D_o \exp -E_A/RT \quad \ldots\ldots\ldots\ldots\ldots\ldots 3.3$$

where D_t : Diffusion coefficient at any temperature

D_o : Experimentally determined factor for the diffusion species

E_A : H - activation energy of permeation

R : Universal gas constant (1.987 Cal/Mol/^oK)

T : Absolute temperature

Thus, since the number of diffusion H with its activation energy varies exponentially with the reciprocal of temperature, equation 3.3. would be useful for the determination of E_A of H permeation through steel in this work. Also, Devanathan et al[83,84] two compartment electrochemical cell technique would be used for the investigation of the effect of steel membrane thickness. and surface impurities in the electrolyte on the H permeation in steel.

3.2. EXPERIMENTAL TECHNIQUE

3.2.1. Choice of material and preparation

The En42 steel membrane or foil, Table 2.1 chapter II, was chosen for this work because this grade of steel is supplied in variable thickness ie. 0.254 mm, 0.381 mm , 0.7112 mm and even 0.9144 mm all of the same width 101.6 mm and for any length. Since comparison of H permeation rate with steel membrane thicknesses is envisaged, this brand of steel was very adequate. The steel membrane was polished with 400 and P600A abrasive of water

proof silicon carbride paper grades until a smooth surface was obtained. This polished smooth surface was degreased with acetone in cotton wool buds. The membrane was cut with mechanical shears into the dimensions required to fit the two flanges of the two compartment cell. A nickel electrical conductor was spot welded onto the prepared tip of this steel membrane. This was once more degreased with acetone and stored in the dessicator until required for use.

For the electrolytes, deionized, distilled water was used to prepare one tenth molar potassium hydroxide. This solution was electrolysed using gold and platinium foil electrodes for about 24 hours under constant magnetic stirring. Thus, the catholyte consits of this electrolysed solution. The anolyte contains one-centimolar potassium nitrite and ten-micromolar palladium chloride both in the electrolysed one tenth molar potassium hydroxide. Hence, both the catholyte and the anolyte are stored in two separate covered volumetric flasks.

Except for the H_2S gas bubble direct into the catholyte of the two compartment cell as H permeation inducing anion agent, other inducing anion agents ie. Centimolar potassium cyanide and centi-molar potassium nitrite were prepared in the electrolysed one tenth molar potassium hydroxide as supporting electrolyte. These two catholytes were stored safely in covered volumetric flasks until required for use. A Corning-EEl, model 109, digital pH meter was used to determine the pH of anolyte (12.68) and catholyte (12.65) and the reagents were of the Analar grade.

3.2.2. Cell Design

The cell design used in this work was a modified cell used by Devanathan et al.[83,84] Basically, it consisted of two identical compartments of glass ware with flanges. These flanges were mirror image of the other and between them was the steel diffusion membrane which has sticky teflon tapes that served dual purposes: (a) it exposed a known specific geometric area on the steel membrane to the electrolyte on both sides of the cell, and (b) provided a cushioning effect as a water-tight gasket between the glass flanges and the metal surfaces. The steel membrane has the same diameter as the flanges, hence the whole joint was covered with silicon set 151 aquasealant, a product of I.C.I. A pyrex and aluminium brackets with long screws were simultaneously used to hold this joint firm and water tight Fig. 3.1. This joint separated the anolyte from the catholyte compartments. The anode compartment has a saturated colomel electrode (SCE) reference electrode housed in a luggin capillary pointing close to the working electrode (ie. A side of the steel membrane), a column containing the platinium counter electrode and a tube that led in nitrogen gas, through a sintered disc into the cell. Similarly, the cathode side has two columns: one for Pt counter electrode, and a nitrogen gas inlet tube. The nitrogen was let out of the cells through bubblers on either side of the two compartment cell assembly in Fig. 3.1.

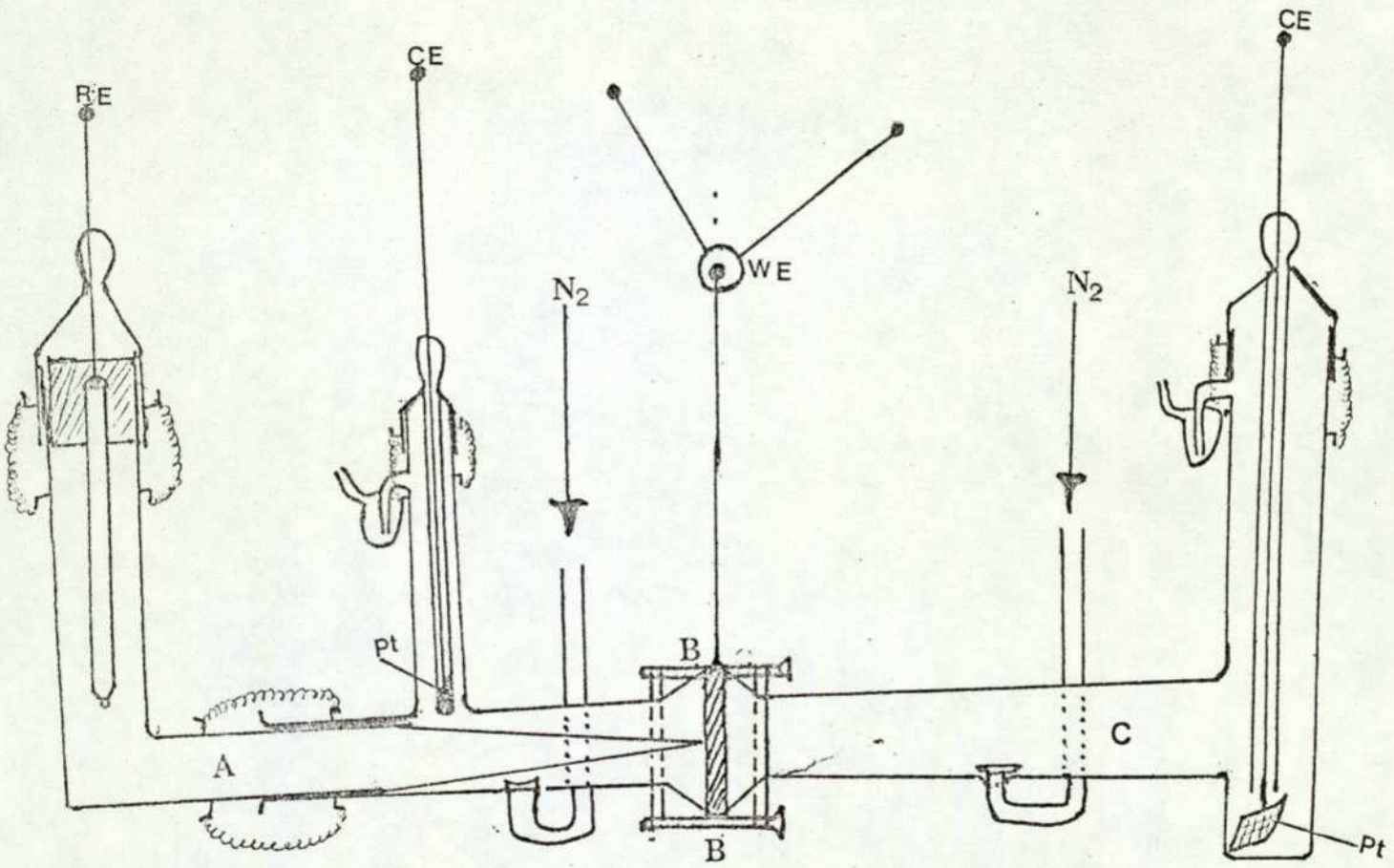


Fig. 3.1. The Bi-electrode Diffusion Cell Assembly showing the Anode (A) and Cathode (C) compartments. (B) Aluminium brackets and steel screws.

3.2.3. Electrochemical Tests

The cyclic voltammogram was determined for H_2 evolution and de-electronation processes using En42 steel membrane as electrocatalyst in deaerated tenth molar potassium hydroxide using Bryan model 29000 A4 X-Y pen recorder, a potentiostat, a wave generator etc. At a sufficiently slow speed rate, the current voltage variation was observed to show two peaks on the H_2-evolution direction. The first peak -750 mV (SCE) was characteristic of the adsorption and protonation process while the second pronounced peak above -950 mV SCE was the H_2 evolution. On the return cycle, a peak was observed about -570 mV Vs SCE which was the de-electronation of hydrogen. The de-electronation was reproduced by recycling the system between O.C.V. and the protonation region which substantiated that the peak at -570 mV Vs SCE was de-electronation of H. Fig. 3.5. But, the electrodeposition of palladium on the steel membrane made the de-electronation peak shift to more positive value, and this palladium plated surface provided more reproducibility.

A galvanostatic steady state polarisation technique involved the use of potentiostat to maintain a fix potential across a fixed electrical resistor from which the current that passed into the cell was recorded. This principle would be used to maintain the cathode side of the membrane in the two compartments at constant H_2 discharge current density for a long period of time. Fig.3.2. shows the circuit arrangement for this principle.

The potentiostatic polarisation which involved maintaining

both the working electrode and the reference electrode at a constant potential by using a potentiostat. The circuit arrangement Fig. 3.3. shows how this principle would be used to maintain the anode side of the steel membrane in the two compartment cell at H de-electronation potential. The H de-electronation current which was a measure of the H permeation process would be recorded by X-t pen recorder.

3.2.4. Potentiostatic and Galvanostatic Polarisation of the bielectrodes

The electrochemical technique for the study of the permeation process of H through steel was realised by the use of bielectrode system. This has been achieved by the use of a modified form of Devanathan and Starchurski cell assembly[52,81]. This involved the use of polished and degreased steel membrane which separated the two electrolytes at the joint as described above and shown in Fig.3.4. The faces of the steel membrane on both sides were exposed to approximately 1.00 cm^2 geometric area to the respective electrolyte by the use of sticky teflon tapes.

Initally, the anolyte surface of the bielectrode membrane was plated with thin layer of palladium. This was accomplished by passing 2 mA/cm^2 for 10 m second using a galvanostatic pulse technique. These current and time were estimated to electrodeposit a thin layer of palladium on the steel membrane at the anolyte side of the two compartment diffusion cell in Fig. 3.1. The H_2 evolution arising during this electrodeposition

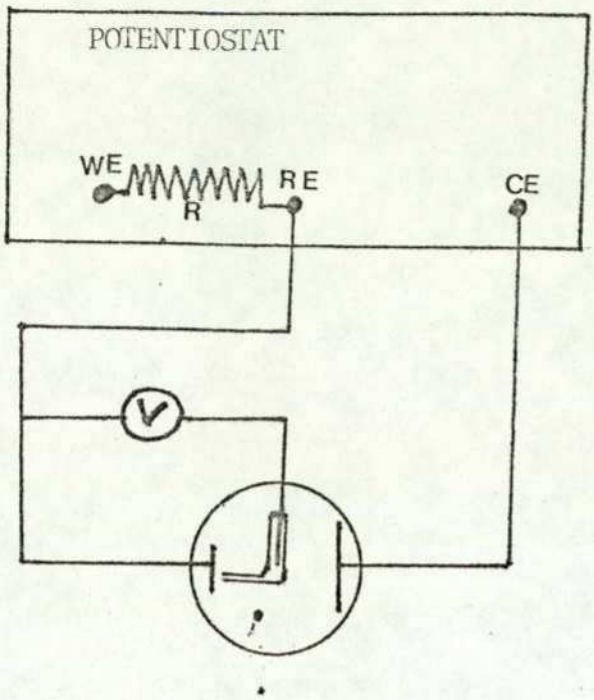


Fig. 3.2. Galvanostatic Circuit Illustration

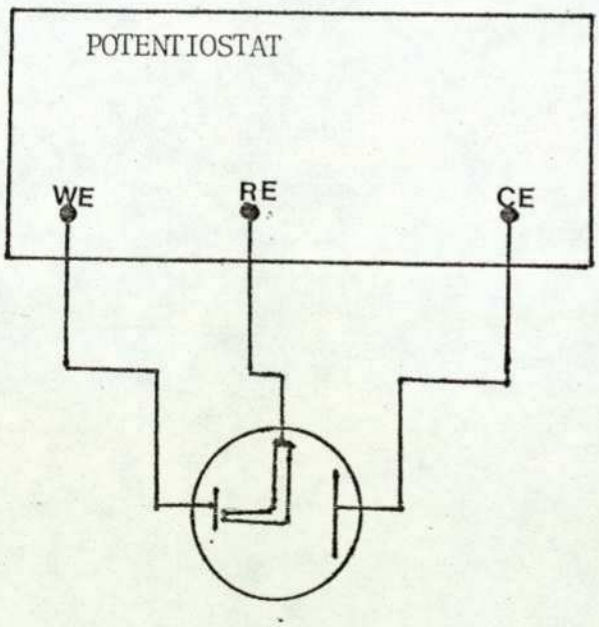
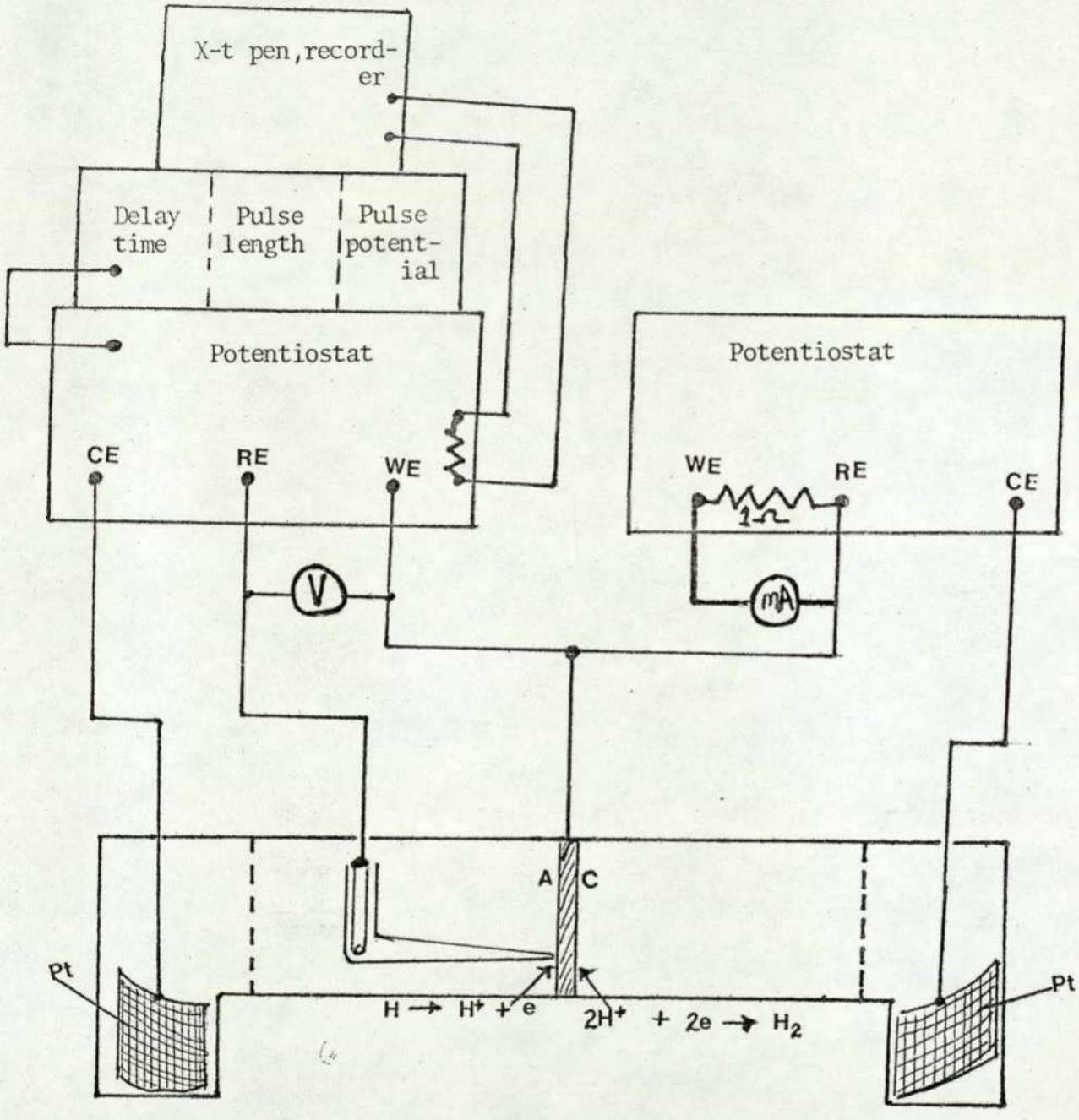


Fig. 3.3. Potentiostatic Circuit Illustration

process was oxidized before the cathodic H_2 charging was commenced by adjusting the anode potential to the H - deelectronate value. An X-t pen recorder was used to monitor the H-oxidation current which decays slowly to about zero. As the X-t recorder traces a constant value of H-oxidation current, the 10 mA/cm^2 H_2 discharge current was commenced on the cathode side of the diffusion membrane by using the second potentiostat. Within minutes, the X-t recorder started to trace an increasing H permeation current. This increase was the manifestation of the arrival of H from the H_2 discharge side at the cathode. The permeation current increased as much as the H continued to arrive for de-electronation until a limiting current was attained.

A stop of the H_2 discharge by switching Off the 10 mA/cm^2 from the potentiostat, has shown that within seconds, a sharp decrease of the H permeation current being monitored by the X-t recorder. As long as the H discharge current density was cut off, the decrease in the H permeation continued until zero H permeation current was realised. The permeation current was restored as soon as the 10 mA/cm^2 H_2 discharge current was maintained by switching On the potentiostat. The circuit arrangement for this process is shown Fig. 3.4. It is, however, important to point out that H_2 gas was bubbled into the anolyte especially during the electroplating process and continued during the de-electronation of permeated hydrogen. Also, the anolyte was electrolysed in situ for about an hour before the permeation test was commenced.



3.4. Circuit arrangement for the bi-electrode potentiostatic H-oxidation polarisation and cathodic galvanostatic H_2 discharge.

The effect of membrane thickness was investigated by changing the diffusion membrane at the joint Fig. 3.1. with 0.254 mm, 0,381 mm, 0.7112 ,, and 0.9114 mm. The H permeation current and diffusion coefficient were determined for each membrane thickness by the same technique as described above. The effects of temperature between 20° and 75°C were investigated using 0.254 mm steel membrane and from this result the activation energy of H permeation in steel was determined.

Various Catholyte environments were used to study the effect of the presence of specific anions in the catholyte would have on the H evolution and permeation on the steel membrane. For this purpose, a steel membrane thickness of 0.254 mm was used and the anions considered were CN^-, NO_2^-, O^-H and the H_2S gas. Basically, the anolyte was maintained as above for all the tests. The millimolar concentrations of potassium cyanide, potassium nitrate and tenth molar of potassium hydroxide were used respectively as the catholyte and in each case a fresh steel membrane was fitted at the joint. Fig. 3.1. In the case of H_2S, the tenth molar potassium hydroxide was the supporting electrolyte which was saturated with H_2S by passing the gas through it. Two techniques were deployed for these tests Viz: (i) The presence of an anion in the catholyte without the application 10 mA/cm^2 H_2 discharge current, and (ii) The presence of an anion in the catholyte followed by a simultaneous application of 10 mA/cm^2 H_2 discharge current density. Thus, from this procedure, the effect of these anions on the H permeation current at temperatures

between 20°C and 75°C as well as the activation energy of H permeation in each anion were determined.

Caution: H_2S being very toxic, elaborate arrangement was made to prevent any harzard. An acidified 0.5 M potassium permanganate was used to oxidize it as soon as it was let out of the catholyte.

3.3. RESULTS

3.3.1. Hydrogen Permeation Current-Time Profile

Initally, the X-t pen recorder was monitoring the de-electronation current arising from hydrogen evolution during the electrodeposition of palladium on the anode side of steel membrane. This de-electronation current being monitored by X-t pen recorder was observed to decrease to a very low constant value which attained to zero at much longer period. As the 10 mA/cm^2 hydrogen discharge was commenced at the cathode side of the diffusion membrane, within minutes, the current being monitored was observed to increase. This increase in X-t pen recorder current was an indication of the arrival of the H from the cathode side through the steel membrane for de-electronation at the anode side. A delayed time or time lag was observed, this was from the time the 10 mA/cm^2 hydrogen discharge current was commenced to the time of the increase in current on the X-t pen recorder. After the time lag (A-B), the current increased fairly gradually to attain a constant current value, as shown in Fig. 3.6. At a prolonged time period, the 10 mA/cm^2 H_2 discharge current was switched off, within seconds, this limiting H

permeation current started to decrease, and decreased very rapidly for the first few seconds and fairly gradual thereafter (C-D). The decrease in H permeation current continued to its zero value at much prolonged period as shown in Fig. 3.6. The reproducibility of the magnitude of the H permeation current on the same diffusion membrane depended on the time of exposure of the membrane to the catholyte. Passivation of the catholyte side of the steel diffusion membrane continued to be possible especially when the 10 mA/cm^2 H_2 discharge current was cut off. In this case, the H permeation profile was realised, but the magnitude of the limiting current could be difficult to attain possibly due to large ohmic drop in the cell.

The same H permeation profiles were obtained by the presence of chemical anions in catholyte for each test. Thus, the H permeation current-time profile was typical of Fig. 3.6, but the magnitudes of the H permeation limiting current measured at 25°C increased in the order $H_2S > CN^- > NO_2^- > KOH$ for the same steel membrane thickness for the presence and absence of the application of 10 mA/cm^2 hydrogen discharge current at the cathode side. The time lag decreased in the order $H_2S < CN^- < NO_2^- < KOH$ Tables 3.2, 3.3, 3.4, 3.5 and 3.6.

For each chemical anion in the catholyte, I observed that increase in temperature increased the H permeation limiting current in the same order ie. $H_2S > CN^- > NO_2^- > KOH$ (Blank) and the time lag decreased in the same order ie. $H_2S < CN^- < NO_2^- < KOH$ as shown in Table 3.6.

3.3.2. Diffusion Parameters of H Permeation in Steel

In order to test the validity of the relation proposed by McBreen et al (ie. equation 3.2 section 3.1.2.), the time t required for the H permeation current I_t, to attain 83 per cent of the H permeation limiting current (I_∞) for various membrane thicknesses were determined as shown in Fig.3.6. and Table 3.1. Thus, a plot of square of the membrane thickness x^2, against time from Table 3.1 confirmed a linear relation from which the diffusion coefficients (ie. the gradients) were calculated, Fig. 3.7. The gradients of the two straight lines in Fig 3.7 for $t = 0.83\ t_\infty$ and $t = t_\infty$ gave diffusion coefficient values: 6.82×10^{-8} cm^2/sec and $5.56 \times 10^{-8} cm^2/sec$ respectively at 25^oC for this steel membrane. The two diffusion coefficients together gave an average of $6.2 \times 10^{-8} cm^2/sec$ which could be compared confidently with $D \underline{\Omega}\ 10^{-9} cm^2/sec$ obtained for Armco iron by McBreen et al[53] at 25^oC using the same technique. Also, a plot of the membrane thickness against the reciprocal of the H permeation current depicted a linear relation as predicted by Fick's Law of diffusion ie. that the diffusion process of H through the steel membrane was bulk diffusion controlled as observed by Beck, Bockris, and McBreen[59] Fig. 3.8.

The diffusion coefficient was observed to vary with temperature, thus the diffusion coefficient was determined for each chemical anion introduced into the catholyte. In the use of each anion, the cathode side of the diffusion membrane was maintained at 10 mA/cm^2 H_2 discharge current. But, in another

use of H_2S gas, the 10 mA/cm^2 H_2 discharge current was cut off, thus the permeation was predominantly due to H_2S dissociation on the steel membrane at the cathode side for all the temperature range considered. In Tables 3.2, 3.3, 3.4, and 3.5, the diffusion coefficient and H permeation limiting current were observed to reflect marked increases in the environments and temperatures investigated. Hence, H permeation current increased tremendously due to combined effect of H_2S and 10 mA/cm^2 H_2 discharged current compared with small effects due to cyanide, nitrite or KOH. Table 3.6.

An Arrhenius plot Fig. 3.9 of the logarithm of diffusion coefficients against the reciprocal of the absolute temperatures was obtained based on the re-arrangement of equation 3.3. section 3.1.2. as shown:-

$$\text{Log}_{10} D_T = \text{Log}_{10} D_o - \frac{E_A^*}{2.303\ R}\left(\frac{1}{T}\right) \ldots\ldots 3.4$$

where the meaning of the symbols remain the same. The above relation was used to compute for the activation energy for H permeation in steel membrane in the environments investigated. Thus, the activation energy obtained are shown in Table 3.7.

TABLE 3.1

Below shows the diffusion coefficients, limiting current densities at $t = 0.83\ t_\infty$ and $t = t_\infty$ for varying membrane thickness in tenth molar potassium nitrite catholyte at 25°C from which L^2 versus t plot is obtained in Fig. 7.

Membrane Thickness (cm)	Diffusion Coefficient D cm^2/sec	Limiting Current Density. I_∞	Time to Attain I	Time to Attain 0.83 I_∞
L $cmx10^2$	$Dx10^8 cm^2/sec$	$\mu A/cm^2$	t_∞(mins)	t (mins)
2.540	5.241	13.28	62.65	52
3.810	5.820	9.85	125.30	104
7.112	7.464	6.38	344.57	286
9.144	6.816	4.67	615.66	511

TABLE 3.2

Shows the variation of diffusion coefficient with temperature for thickness of steel membrane of 0.254 mm in potassium hydroxide as the catholyte.

t^oC	T °K	Diffusion Coeff. D x $10^8 cm^2/sec$	Log_{10} D
24	297	4.41	-7.36
36	309	4.89	-7.31
42.5	315.5	5.10	-7.29
56	329	7.47	-7.13
62.5	335.5	8.40	-7.08
76	349	9.95	-7.00

TABLE 3.3.

Shows the effect of temperature on (i) the diffusion coefficient D, and (ii) the H permeation current density for membrane thickness of 0.254 mm in cyanide catholyte medium @ 10 mA/cm^2 H_2 discharge current density.

t ^oC	T ^oK	Permeation Current density $I_t=0.83I_\infty$	Diffusion Coeff. D x $10^7 cm^2/sec$	$Log_{10}D$
25	298	33.20	1.12	-6.95
30	303	53.95	1.22	-6.91
43	316	58.10	1.58	-6.80
54	327	87.15	2.24	-6.65
66.5	339.5	93.8	2.69	-6.57

TABLE 3.4

Shows the effect of temperature on (i) diffusion coefficient and (ii) H permeation current density for membrane thickness of 0.254 mm in H_2S with 10mA/cm^2 H discharge current density.

t ^oC	T ^oK	Permeation Current density $I_t=0.83I_\infty$	Diffusion Coeff. D x $10^7 cm^2/sec$	$Log_{10}D$
26	299	266	1.34	-6.87
35	308	320	1.58	-6.80
51	324	345	2.24	-6.65
62	335	375	2.56	-6.59
81	354	487	4.27	-6.37

TABLE 3.5

Shows the effect of temperature on (i) diffusion coefficient and (ii) H permeation current density for membrane thickness 0.254 mm in H_2S catholyte medium.

^{o}t	T ^{o}K	Permeation Current density $I_t = 0.83 I_\infty$ $\mu A/cm^2$	Diffusion Coeff. $D \times 10^7 cm^2/sec$	$Log_{10} D$
26	299	52	3.67	-5.44
37	310	91	4.48	-5.39
50	323	156	5.2	-5.28
62	355	286	6.72	-5.17
71	344	420	9.48	-5.10

TABLE 3.6

Shows the comparison of the amount of H permeation into En42 steel in various environments at 10mA/cm^2 H_2 discharge current.

H_2S ENVIRONMENT			
Temp °C	Catholyte Discharge I_c MA/cm^2	Permeation current density I_∞ µA/cm^2	I_∞/I_c x 100
26	10	320	3.2
35	"	385	3.85
51	"	415	4.15
62	"	450	4.50
81	"	517	5.17

(ii)

CN^-	ENVIRONMENT		
Temp °C	Catholyte Discharge density I_c MA/cm^2	Permeation current density I_∞ µA/cm^2	I_∞/I_c x 100
25	10	33.0	0.33
30	"	54.0	0.54
43	"	58.0	0.58
54	"	87.0	0.87
66.5	"	94.0	0.94

(iii)

NO_2^- ENVIRONMENT			
Temp °C	Catholyte Discharge current density I_c MA/cm^2	Permeation current density I_∞µA/cm^2	I_∞/I_c x 100
24	10	5.2	0.05
36	"	8.0	0.08
42	"	10.0	0.10
56	"	25.0	0.25
76	"	37.0	0.37

TABLE 3.7

Shows the activation energy determined in various catholyte environment and the diffusion coefficient D_o.

Catholyte Condition	Activation Energy K Cal / mole /°K	Diffusion Coefficient D_o cm^2 / sec
0.1M KOH + 10 MA/cm^2	3.44	1.30×10^{-9}
0.1M KOH + H_2S + 10 MA/cm^2	4.26	4.17×10^{-7}
0.1M KOH + CN^- + 10 MA/cm^2	4.47	3.47×10^{-7}
0.1M KOH + H_2S only	4.03	8.13×10^{-6}

3.4. DISCUSSION

The H permeation current is realised by applying an H de-electronation potential on the anode site of the bielectrode steel membrane. This H de-electronation site is protected from anodic dissolution and possible passivation of the steel membrane by electroplating a thin layer of palladium. This thin electroplated element did not materially affect the rate of the permeation of atomic hydrogen H, which is rate controlled only in the steel membrane as observed by Devanathan[81]. The H permeation current density is observed to increase with increase in the H discharged current at the cathode site of the steel membrane. And, each increase in H permeation current density time profile is characteristic of sharp increase before setting to constant value which is more pronounced at large H_2 discharge current density, Fig.3.6. It is not clear what is responsible for the sharp increase but from results of ealier workers, a possible lattice defect of the steel membrane is not ruled out.[52,53,81] However, at 10 MA/cm^2 H discharge current density, this sharp increase is not very pronounced, and does not affect the determination of the diffusion parameters based on the steady state limiting current density.

An additive (ie. anion) in the catholyte is observed to increase the H permeation current, Table 3.3,3.4, 3.5,3.6, thus the magnitude of the permeation current depends on the catholyte additive, the steel membrane thickness, the temperature and the H discharge current density. By keeping these variables constant, it was observed that H permeation current increase in the order

$H_2S > CN^- > KOH$ as the catholyte additives are varied. Table 3.6. Beck, Devanathan and Starchurski[52] obtained similar trend for Armco iron membrane and Bockris, McBreen and Nanis[80] confirmed the same behaviour for the Armco iron membrane. I investigated further, the role of CN group on the H permeation current by varying the CN^- concentration which again shows the dependence of H permeation current on the high concentration of CN^- as obtained by Glass, Taylor and Beck[55]. On the basis of these observations, Kabosez and Montblannova[86] in considering the rate-controlling step in H evolution on iron is not H recombination, but suggested that the increase in H permeation is due to a lowering of the M-Hads bond caused by the adsorption of anions (ie. CN^-, H_2S, NO_2^-, etc.). Although the rate determining step assumed by these workers is no longer an acceptable one for iron as postulated by Bockris[87], Devanathan and Starchurski[83], nevertheless, their ideas can be incorporated in the mechanism of hydrogen evolution and entry into the steel as deduced later in this work.

The diffusion coefficients of 1.34×10^{-7} cm^2/sec; 1.12×10^{-7}/sec and $4.41 \times 10^{-8} cm^2/sec$ determined for En42 steel membrane in H_2S, CN^- and KOH catholyte respectively, Table 3.2, 3.3 & 3.4, do not reflect the differences in the catholyte additives particularly for the H_2S and CN^-. This result is in good agreement with 3.8×10^-7 cm^2/sec contained in Palczewske Ratajczyk's work for Armco iron, Devanathan et al obtained 2.0×10^{-7} cm^2/sec for AISI 4340 steel[52] and Wood[88] got 1.25×10 cm^2/sec for SAE 4130 steel, all the results were obtained at

25°C. However, other workers have obtained lower diffusion coefficient (ie. Gellar and Sun calculated 2 x 10^{-5} cm^2/sec for Armco iron which is in fair agreement with the above results. In this work, it is observed that the diffusion coefficient varies markedly with temperature as predicted by Arrhenius relation for the catholyte system investigated, but it is found to be independent of membrane thickness which substantiates the McBreen, Navis and Beck approximate solution of Fick's second law (equation 3.1,section 3.1.2). However, the H permeation current density is shown to be inversely proportional to be membrane thickness Fig. 3.8. as predicted by Fick's law and supported by work of Bockris, Beck and Nanis.

The activation energies determined from this work for En42 in H_2S, CN^- and KOH catholyte additives by the Arrhenius plot are 4.26 Kcal/mole/°K respectively, Table 3.7. Also, the activation energy determined only by the dissociation of H_2S on the catholyte site of the steel membrane without 10 MA/cm^2 H discharge current density is 4.03 Kcal/mole/°K. The activation energy obtained in the KOH catholyte shows a slight difference from that of H_2S, and CN^- but they are of the same order of magnitude. However, the activation energy in KOH is in good agreement with 3.05 $\pm$ 0.10 Kcal/mole/°K for cast iron (0.012 Ni) by Stross and Tompkins[89]. However, Heinrich, Johnson and Crouthamel obtained 10.26 Kcal/g-atom/°K for Armco iron in cyanide environment[90]; Smithels and Rensley work contains activation energy of 11.0 Kcal/g-atom/°K[91] and Benneck et al[90] also obtained activation energy of 9.4 Kcal/g-atom/°K all the values are for

Armco iron in cyanide catholyte. The 4.47 Kcal/mole/^{o}K and 4.26 Kcal/mole/^{o}K obtained in this work for CN^- and H_2S catholyte environments are in good agreement with the above results particularly the recent activation energy of 9.2 Kcal/g-atom/^{o}K for Armco iron polycrystals by Bockris et al[59]. Thus, from these identical activation energy values it is aboundantly evident that these additives could be playing identical role in the H permeation process. Therefore, the lowering of the M-Hads bond energy as proposed by Kabozev and Montblanova could not be considered as a serious factor. Instead, the experimental evidence as well as the theoretical analysis by Beck, Glass, and Taylor[55] have disclosed that CN^-, which is strongly chemisorbed during H-charging of a steel surface, effectively retards the recombination rate of simultaneously adsorbed hydrogen atom. The chemisorption increases rapidly with H-charging time, and this results in a rise in the hydrogen coverage and creation of a steep hydrogen concentration gradient at the steel catholyte surface. This mechanism explains the initial sharp rise of H permeation current in the CN^- and H_2S containing catholyte which is responsible for the high hydrogen coverage at this side of the membrane. Thus, since there is no marked difference in the H permeation activation energy, the additive (ie. anion) must be playing an identical role, ie. decreasing the recombination of the H at the cathode side.

The H dissolution rate in steel seems to be varying with steel and depends on the composition of the steel, the lattice defects and possibly by residual and applied stress. The influence of applied stress to H permeation would be investigated later.

Fig. 3.5. Cyclic voltammogram of hydrogen evolution on steel in deaerated 0.1M KOH @ 50 rpm scan rate at 20°C.

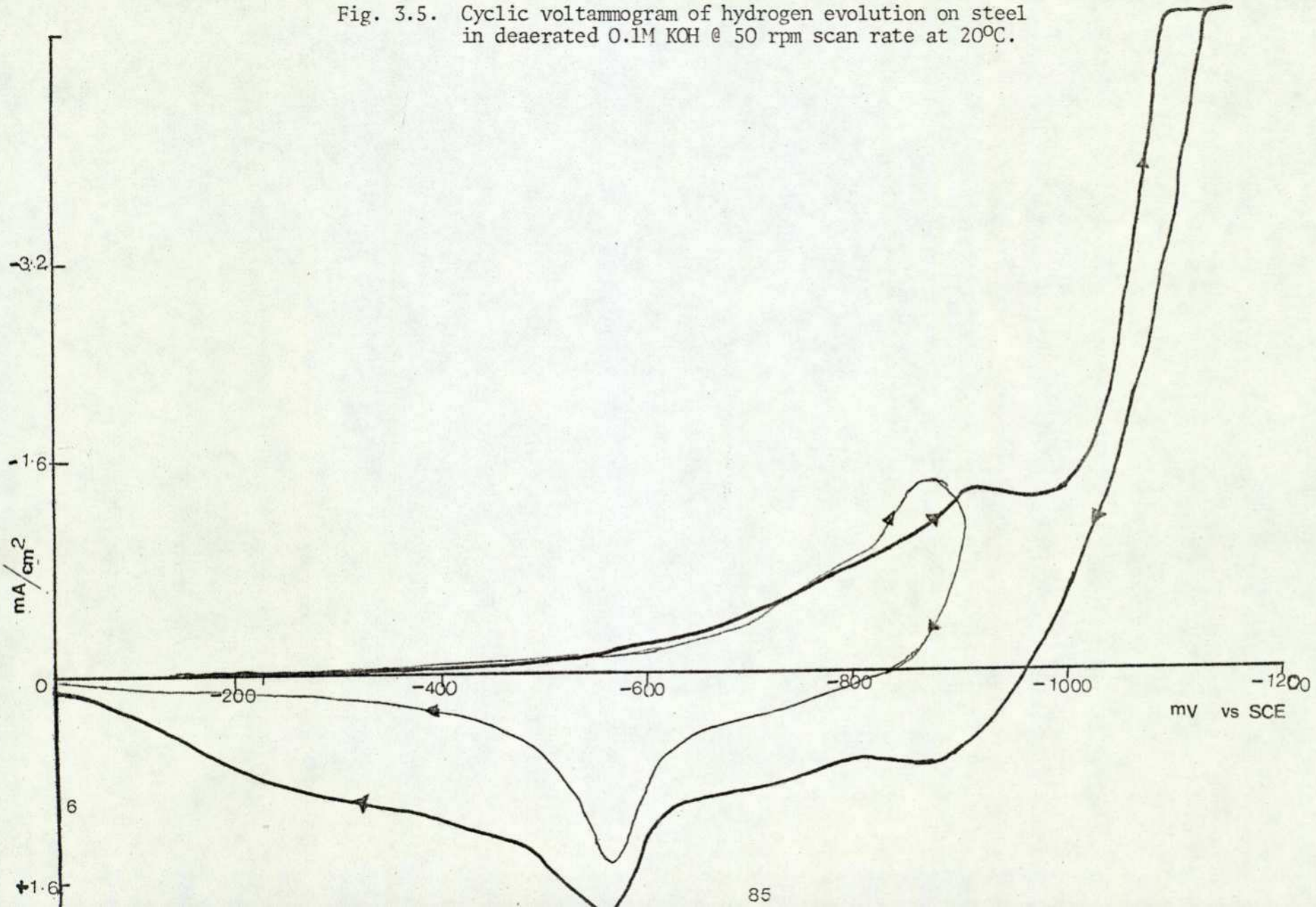
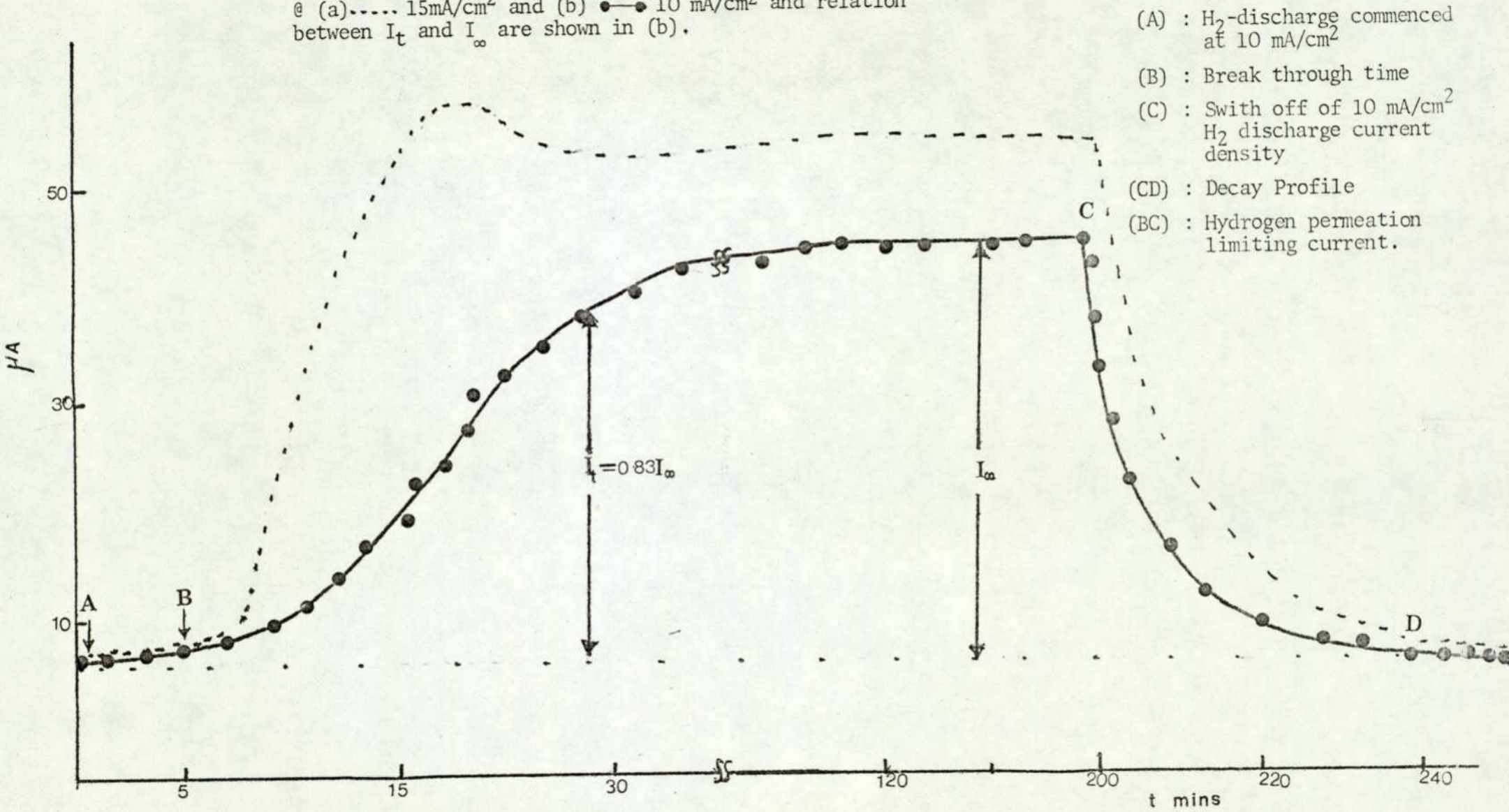


Fig. 3.6. Hydrogen permeation current/time profile @ 20°C in CN medium for hydrogen discharge current density @ (a)..... 15mA/cm^2 and (b) ●—● 10 mA/cm^2 and relation between I_t and I_∞ are shown in (b).



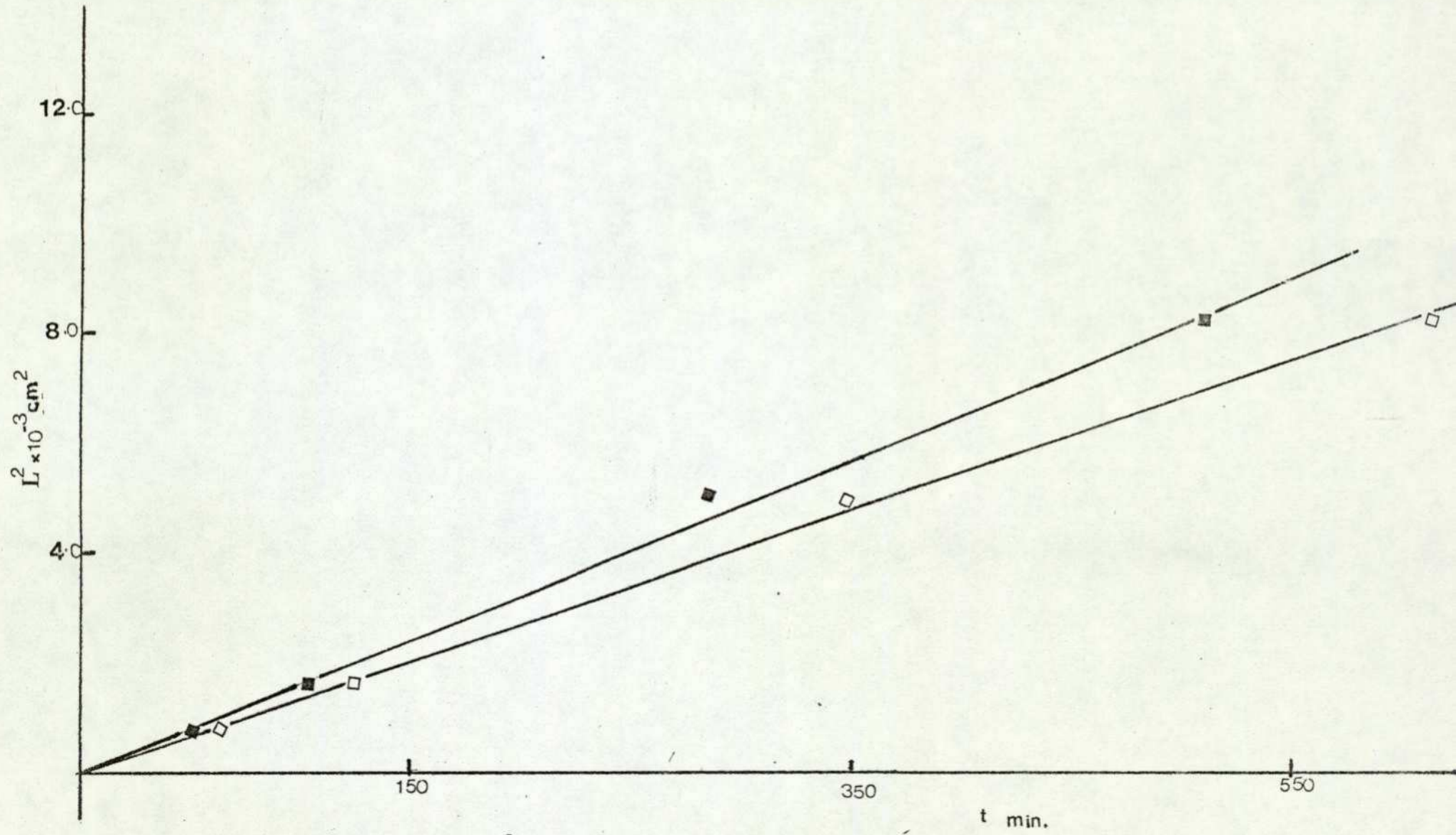


Fig. 3.7. Plot of L^2 Vs t for (a) $t = 0.83\ t_\infty$ ■—■
(b) $t = t_\infty$ □—□

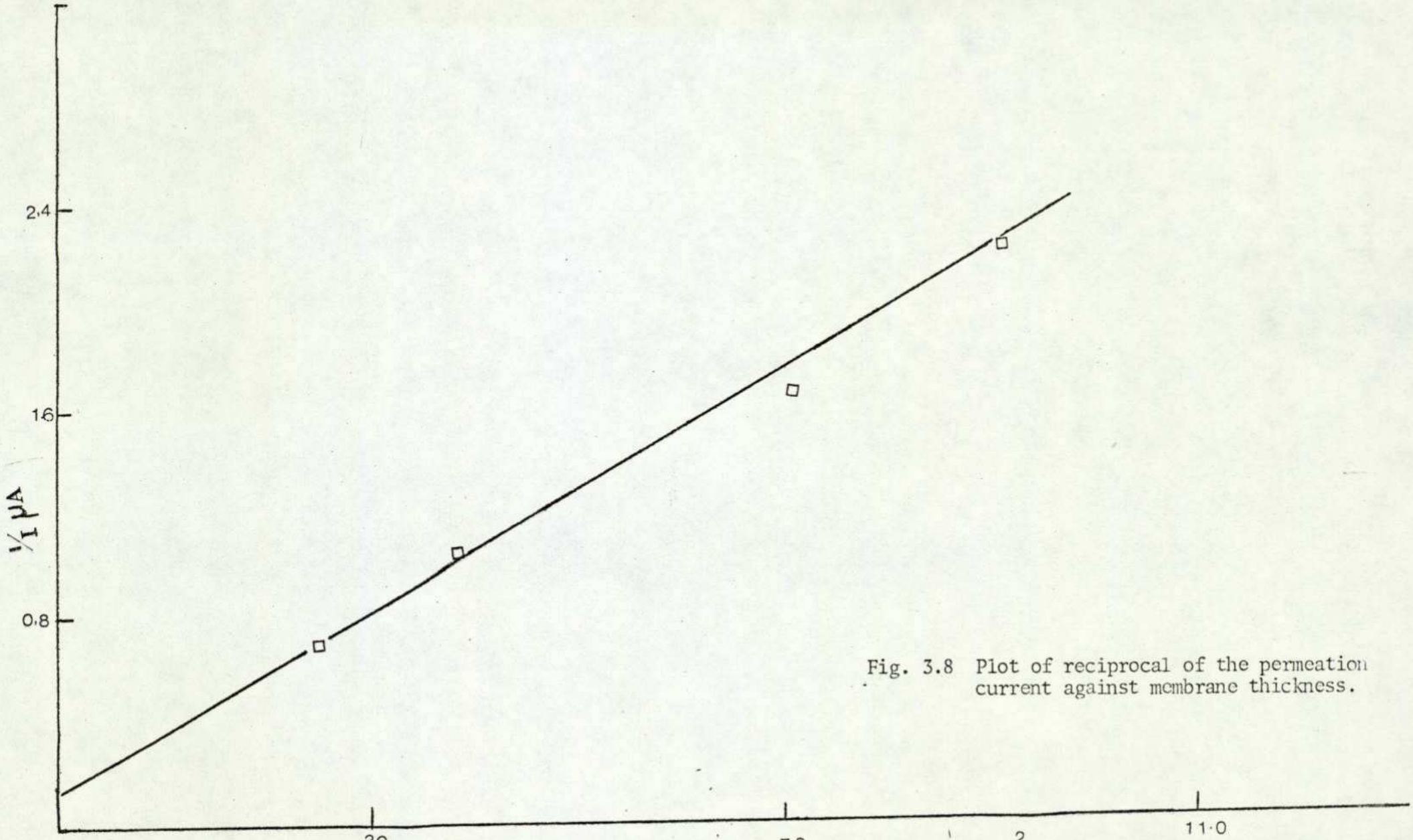


Fig. 3.8 Plot of reciprocal of the permeation current against membrane thickness.

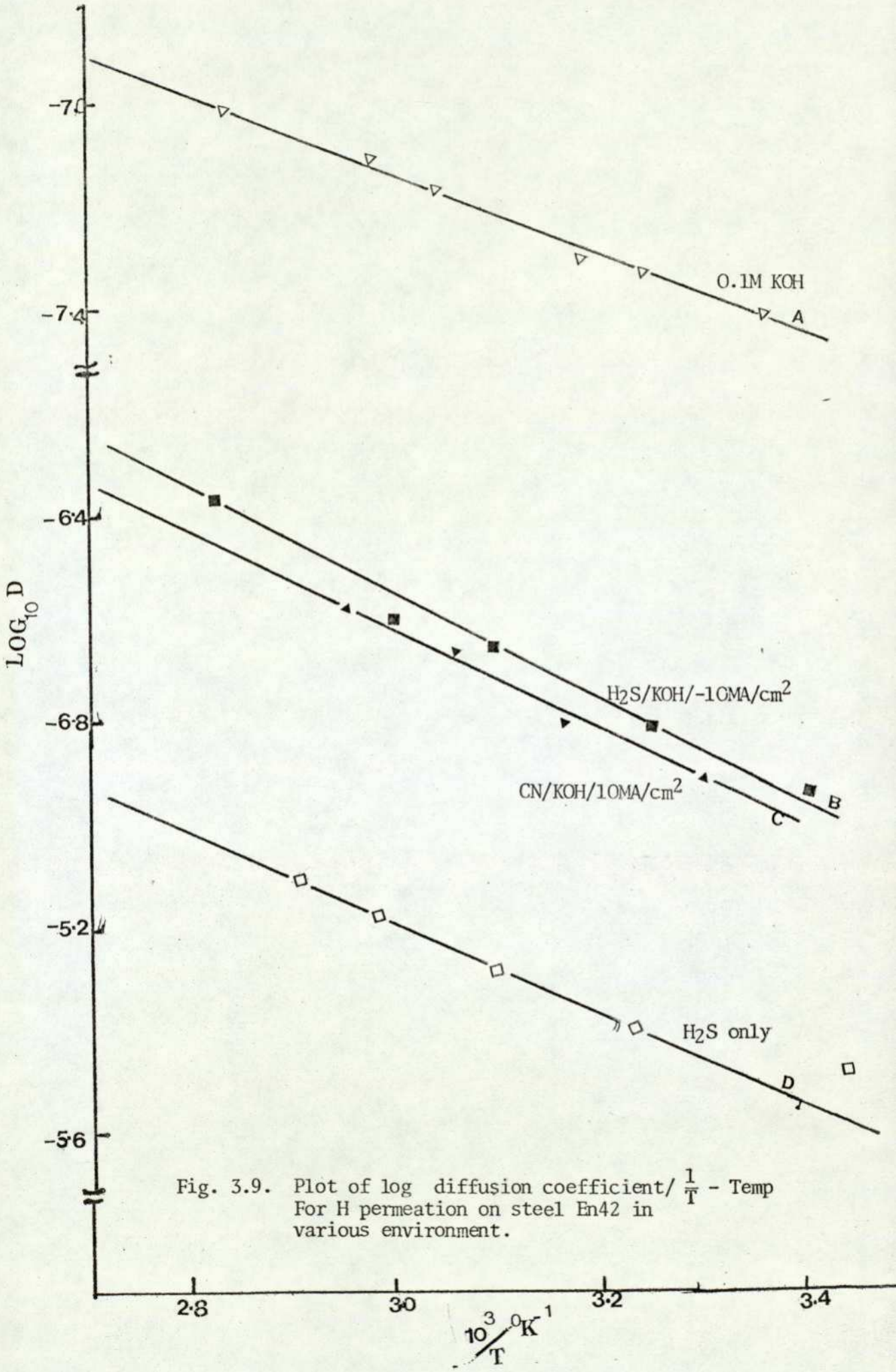


Fig. 3.9. Plot of log diffusion coefficient/ $\frac{1}{T}$ - Temp For H permeation on steel En42 in various environment.

CHAPTER FOUR

HYDROGEN PERMEATION INTO STEEL

UNDER APPLIED TENSILE STRESS

CHAPTER IV

HYDROGEN PERMEATION INTO STEEL UNDER APPLIED TENSILE STRESS

4.1. Introduction

The rate of hydrogen dissolution in steel is known to be influenced by the composition, the structural defects such as interstitial sites, grain boundaries, dislocation etc., which provide hydrogen diffusion paths in the steel.[58,92] These structural defect paths for H permeation are enlarged in size or number by the presence of residual or applied tensile stress.[92] Phalen et al[92,93] have shown that the H entry into the steel grain boundaries is further enhanced by applied tensile stress.

As the effect of stress on H absorption by steel has not adequately been established, this work proposes to investigate cn the relationship between applied stress and H permeation in steel. Also, the mechanical properties of the steel specimen would be determined.

4.2. EXPERIMENTAL TECHNIQUE

4.2.1. Mechanical Properties of Steel Specimen

En42 steel membrane was mechanically press-cut into a standard tensile test piece according to the specification of material testing organisations.[39,40] This short length strip tensile piece is shown in Fig. 4.1. below.

The tensile specimen described above was polished at the centre with a very fine emery paper and degreased with acetone before an electrical resistance strain gauge was introduced.

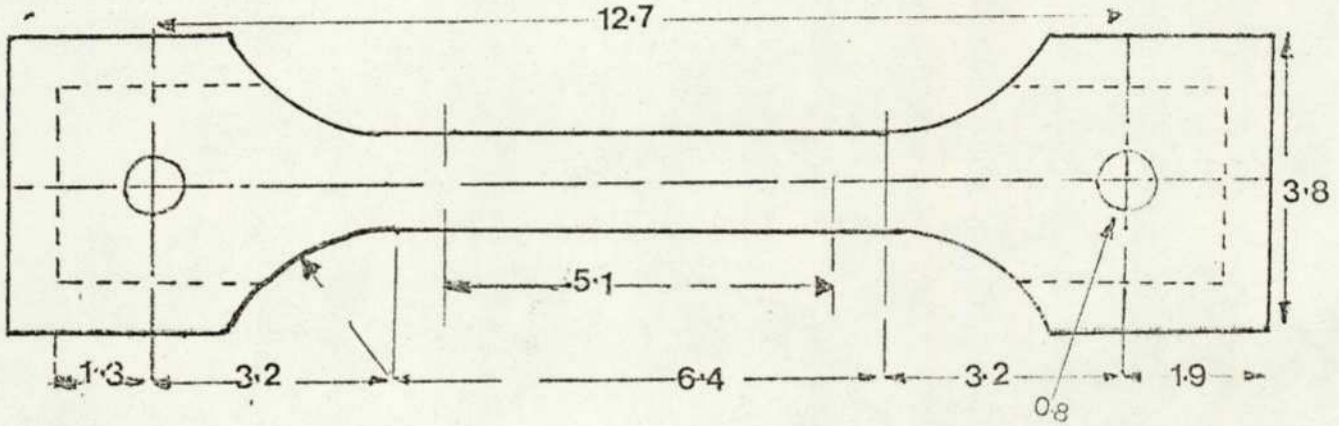


Fig. 4.1. Short length tensile strip test piece of En42 steel, thickness 0.274 cm (Dimensions in cm)

Each strain gauge used consisted of a wire or foil grid mounted on a plastic base, which in turn was bonded onto the centre of the surface of the steel specimen on which the strain was to be measured. The electrical resistance strain gauges usedin this work have gauge factor of 1.98 which was predetermined by the manufacturer. The gauge factor is defined by:

$$\text{Gauge Factor} = \Delta R \left(\frac{1}{ER}\right) \qquad 4.1.$$

where R = gauge resistance

ΔR = resistance change due to strain E

The installation of the gauges onto the tensile specimen were carried out as illustrated procedure by Coutts et al[94]. A digital strain indicator made by Vishay/Ellis, model 20 was used to record the strain while the applied stress was recorded and progressively increased on the Monsanto Type Tensometer. The applied stress (N/mm^2) and resultant strain (μ-strain) were used to compute the elastic modules for the material in the usual manner.[95,96]

4.2.2. Mechano - Electrochemical Tests; Hydrogen Permeation in Steel Under Applied Stress

The two-compartment-cell used for this investigation was basically the same as described in Chapter III section 3.2.4 and Fig. 3.1. However, the tensile specimen Fig4.1 above, was made to fit the glass ware flanges at the joint and at the same time projected above and below the joint of the two-compartment-cell. These two projections of the tensile specimen were clamped firmly to the provisions made for them on the Mosanto type Tensometer

which was held vertical for convenient application of specific stresses. Pictures of the test assembly are shown in Figs. 4.2 and 4.3.

The hydrogen permeation studies were conducted based on the previous technique in Chapter III, section 3.2.4. Thus, the anolyte and catholyte were maintained as described in section 3.2.4. The tensile diffusion membrane was initially at zero stress level while the cathode side was maintained at 10 mA/cm^2 hydrogen discharge current density in cyanide catholyte. The H permeation current was recorded by the X-t pen recorder in the usual manner. But, at the maximum H permeation current (ie. limiting current), the stress level was increased from its zero stress level at 186 N/mm^2 and simultaneously, the H permeation current was observed to increase with the applied stress and attained a higher value of limiting current corresponding to this stress level. The stress level was once more increased from 186N/mm^2 to 248 N/mm^2, 372 N/mm^2, 433 N/mm^2 and 557 N/mm^2 and the limiting current was determined respectively for these levels of applied stress. The H permeation limiting currents were similarly determined for 650 N/mm^2 and 681 N/mm^2 applied stress levels which were beyond the elastic region.

The effect of reducing the stress level rapidly to zero stress level for selected applied stress levels, while the 10 mA/cm^2 H_2 discharge current density was continuously kept, was investigated. Also, the H permeation diffusion coefficients in steel under specific applied stress levels were determined.

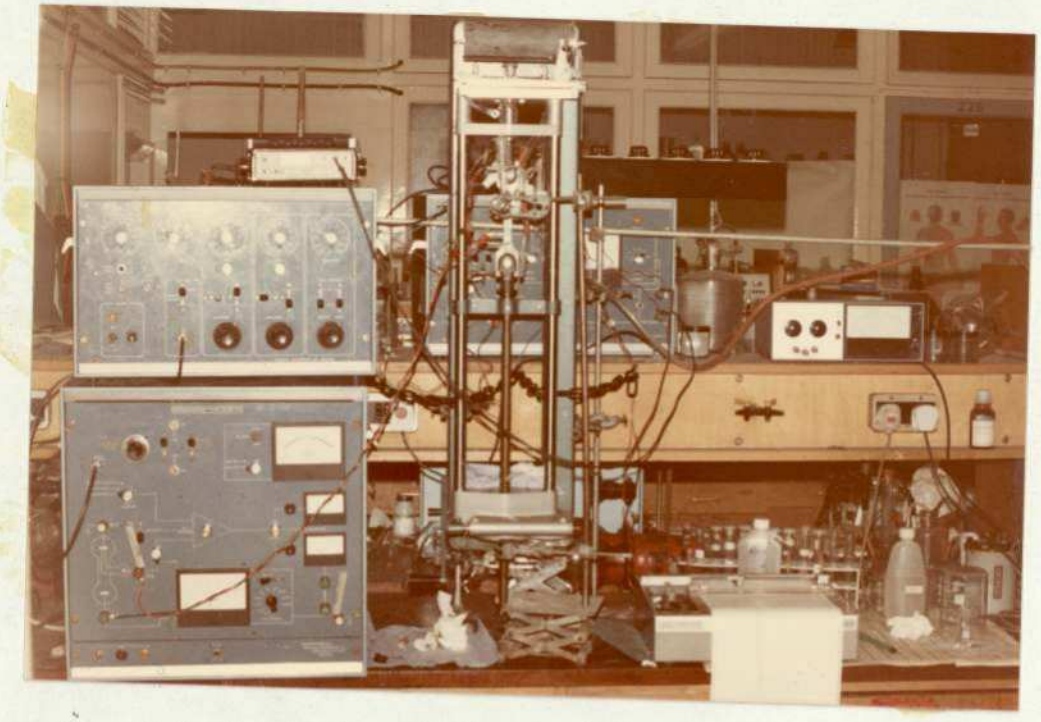


Fig. 4.2. Front view of the mounted monsanto type tensometer with the steel membrane under an applied tensile stress.

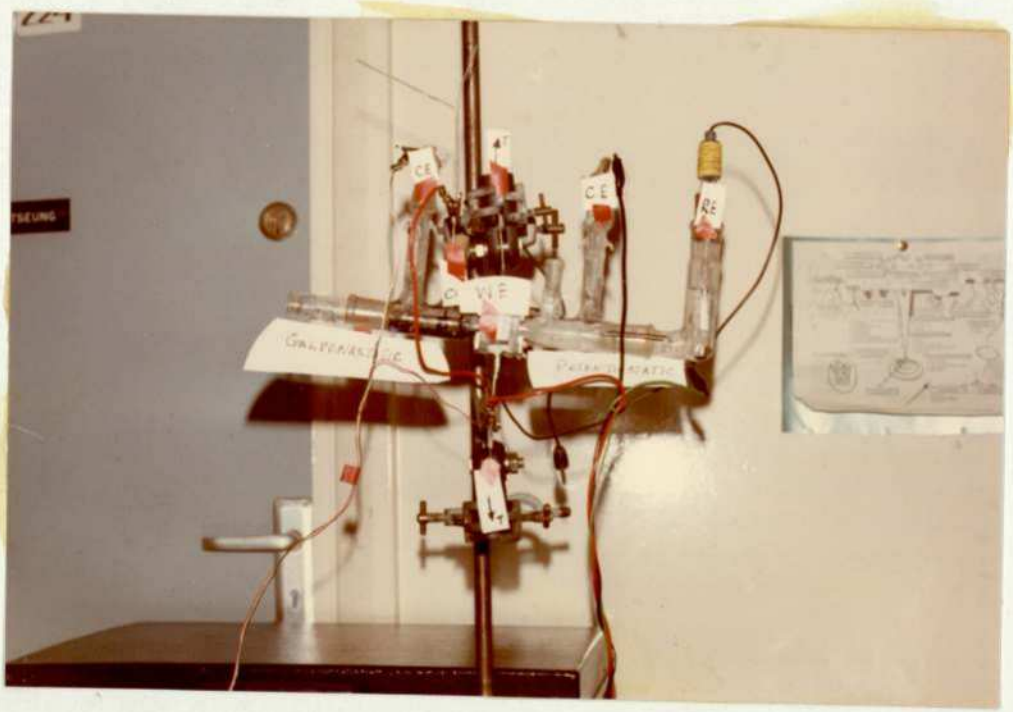


Fig. 4.3. The side view of the two compartement cell as mounted on the tensometer above. Two compartments:- Galvanostatic and Potentiostatic sides.

4.3. RESULTS

The stress-strain diagram obtained by the mechanical test on the tensile specimen of thickness of 0.274 mm is shown in Fig. 4.4. This stress-strain relation does not pass through the origin as theoretically expected. However, the curve exhibits a proportionality limit which could be defined as the greatest stress level that a material can endure without losing a straight line of proportionality between stress and strain as defined by Hook's law. The slope of the linear portion of the stress-strain curve provides the elastic modulus β, defined by:

$$\beta = \frac{P}{E} \quad \ldots\ldots\ldots\ldots\ldots\ldots \quad 4.2$$

where P : applied stress (N/mm^2) and E, the strain (μ-strain). The elastic modulus for the steel membrane used is 234×10^3 N/mm^2, which is in good agreement with the specification value given for the same material in material selector and design guide[97]. A complete plastic region of the curve, Fig.4.4, could not be obtained because the electrical resistance strain gauge peels off above an applied stress level of about 920 N/mm^2.

The H permeation is determined for stress level within the elastic region and about the plastic region. In each case, the H permeation current is allowed to attain a limiting value after a long period, first at the zero stress level before increasing the applied stress to higher values. The subsequent H permeation current monitored by the X-t pen recorder is observed to increase simultaneously with increase in applied stress levels. In effect, as the stress level is raised, the H permeation is

observed to increase to a higher value which after short period attained a limiting current value corresponding to the level of applied stress. Thus, the H permeation currents are observed to increase as the stress level increased from 186 N/mm^2, 248 N/mm^2, 372 N/mm^2, 433 N/mm^2 to 557 N/mm^2 and their corresponding limiting current are shown in Table 4.1and Fig. 4.5. These stress levels are within the elastic region of the stress/strain relation Fig.4.4. However, the permeation process at 650 N/mm^2 and 700 N/mm^2 which are beyond the elastic region are observed to produce more pronounced high current value and the limiting current is an average of the zig-zag current values recorded by the X-t pen recorder.

Diffusion coefficient of H permeation in steel membrane at 248N/mm^2 and 372 N/mm^2 applied stresses are 4.48 x $10^{-7}cm^2/sec$ and 6.25 x $10^{-7}cm^2/sec$ respectively.

However, at limiting current for 557 N/mm^2 (ie. within the elastic region), this stress level was rapidly reduced to zero stress, within seconds the permeation current is observed to increase before an expected decrease. Fig. 4.5. Suprisingly, this sudden increase at rapid reduction of the stress is about 35 µA more than the limiting current at 557 N/mm^2. At 700 N/mm^2 stress level which is within the plastic region, the increase in H permeation current when the 700 N/mm^2 stress level was rapidly reduced to zero, is only 13 µA which depicts the attainment of a permanent set in the membrane Fig. 4.5A. A plot of H permeation limiting (µA) against the corresponding applied (N/mm^2) shows that the current increases with applied stress, and this simultaneous

increase in current with load is more pronounced at the plastic region ie. above 550 N/mm^2 as shown in Fig. 4.6. However, the plot of H permeation current against the strain Fig. 4.7. shows a corresponding increase which could be approximated to a linear relationship even within the plastic region. These results could be significant in the explanation of H dissolution in steel.

TABLE 4.1.

Shows the effects of (i) applied stress (N/mm^2) and (ii) strain (μE) on the H permeation current for En42 steel of thickness 0.274 mm and cross-sectional area 3.10 mm^2 @ 10 mA/cm^2 H_2 discharge current density in cyanide catholyte @ 25°C.

Applied Load kN	Applied Stress N/mm^2	Strain μE	H Permeation Current μA
0.00	0.00	0.00	59
0.6	193	262	76
0.8	248	370	88
1.2	372	602	100
1.4	433	713	113
1.8	557	980	126
2.1	650	1120	150
2.2	681	1238	208

4.4. DISCUSSION

The stress-strain relation determined for the steel specimen used in this investigation has shown two distinct regions ie. the elastic region and above 560 N/mm^2 is the region of plasticity, Fig. 4.4. H permeation current has been investigated within these two regions as illustrated in Figs. 4.5, 4.6 and 4.7 and the data displayed in Table 4.1. Within the elastic region ie below 560 N/mm^2 Figs. 4.5 and 4.6, the H permeation current is observed to increase with increase in applied stress, but the use of a mathetical relation to quantify this mode of increase is difficult. However, the H permeation current is observed to increase with strain in the member. Figs. 4.5 . and 4.7. Thus, an approximate linear relation for the H permeation current densities with strain suggests that more active sites seems to be created by the presence of strain due to applied stress. The strain in the member is possibly influencing the lattice distortion more than stress, presumably due to the lattice elongation. Such affect could increase the defect points on the steel, consequently more H path could develop which is responsible for the increase in H permeation current particularly above the elastic region where the strain is fairly independent of applied stress.

However, Phalen et al[93] in their assessment of H permeation in steel pointed out that the number of reaction sites is controlled by the magnitude of the tensile stress. In this respect, H embrittlement has been enhanced in steel tanks by the presence of tensile stress[98]. Thus, the collection of hydrogen in the high

tensile stress region, whether the stress is applied before or after cathodic charging, suggests that preferential diffusion and acceleration of M-H reaction occurs only in steel stressed specimen.[99] The inability of detecting a hydride phase in steel[48], supports the earlier view that atomic hydrogen does enter the surface of the stress metal, diffuses to and concentrates in the region of highest tensile stress. This fact could explain the rapid increase in permeation current observed when the steel membrane was contracting as the stress is suddenly removed, or reduced to zero. This rapid increase in permeation current could be due to "squeezing out" of the dissolved H at high stress that could not be accommodated at the limited sites available at zero stress.

But, at plastic region where the strain has more dominant effect than stress, much higher H permeation current was obtained, However, when the strain is reduced, the amount of H squeezed out was observed to be much lower than in the elastic region Fig.4.5. This phenomenon suggests that the strain in the material has induced a permanent set in the steel, consequently the dissolved H has enough sites at lower stress or strain level due to the formation of plasticity in the membrane.

The diffusion coefficient D, is observed in this investigation to be independent of applied tensile stress in the steel membrane within the elastic region. A similar result[59] is obtained for AISI4340 steel. However, it is not clear the effect of strain on the diffusion coefficient in the plastic region

because the electrical resistance gauge peeled off during the long period of test. However, the permeation current change observed from the lateral contraction of the membrane with stress or strain shows that the increase in the H permeation rate with stress could possibly be due to increase in the hydrogen solubility with applied stress or strain.

Recent work[93] has indicated that as hydrogen enters the steel their tensile strength decreases markedly and corrosion in this area continues to generate more hydrogen which reacts with the steel and probably diffuse into the grain boundaries. Thus, along these grain boundaries, H diffusion may be more rapid as much of the embrittlement occurs here. In this regard, more investigation is envisaged in the next chapter to introduce electrochemical hydrogen evolution catalyst which could possibly isolate hydrogen evolution and dissolution from the corroding steel.

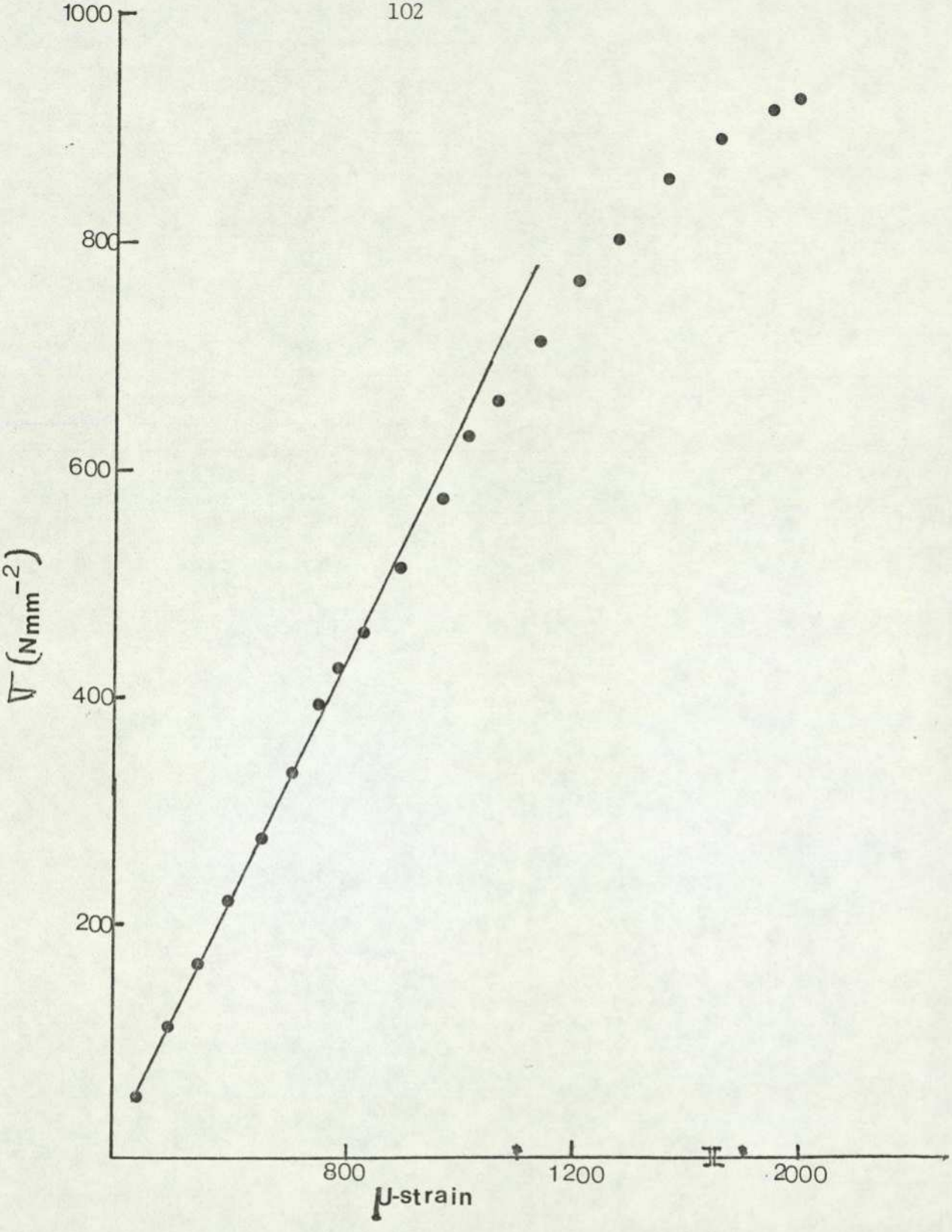


Fig. 4.4. Stress/strain relation for En42
(membrane thickness 0.274 mm)

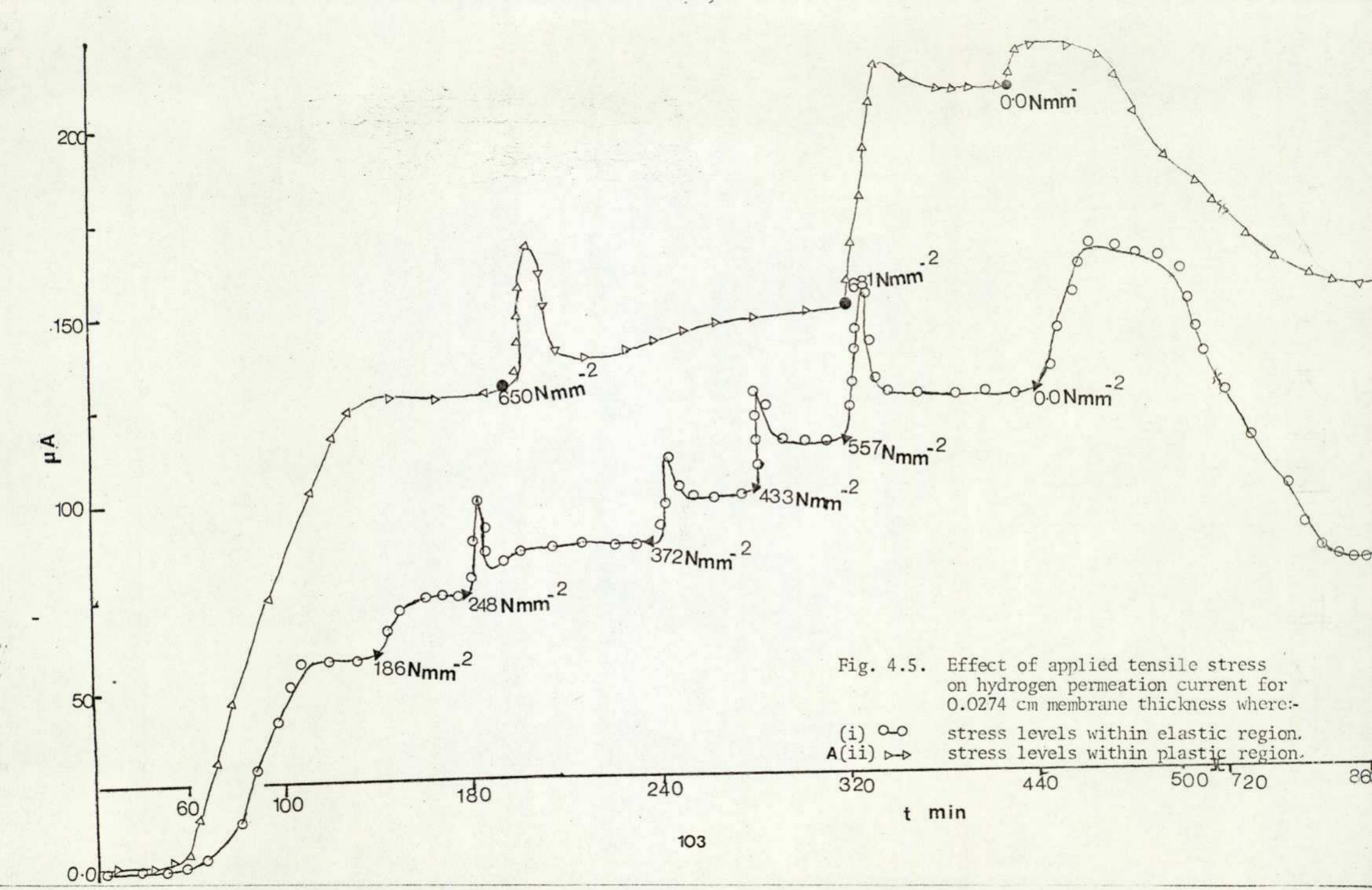


Fig. 4.5. Effect of applied tensile stress on hydrogen permeation current for 0.0274 cm membrane thickness where:-

(i) stress levels within elastic region.

A(ii) stress levels within plastic region.

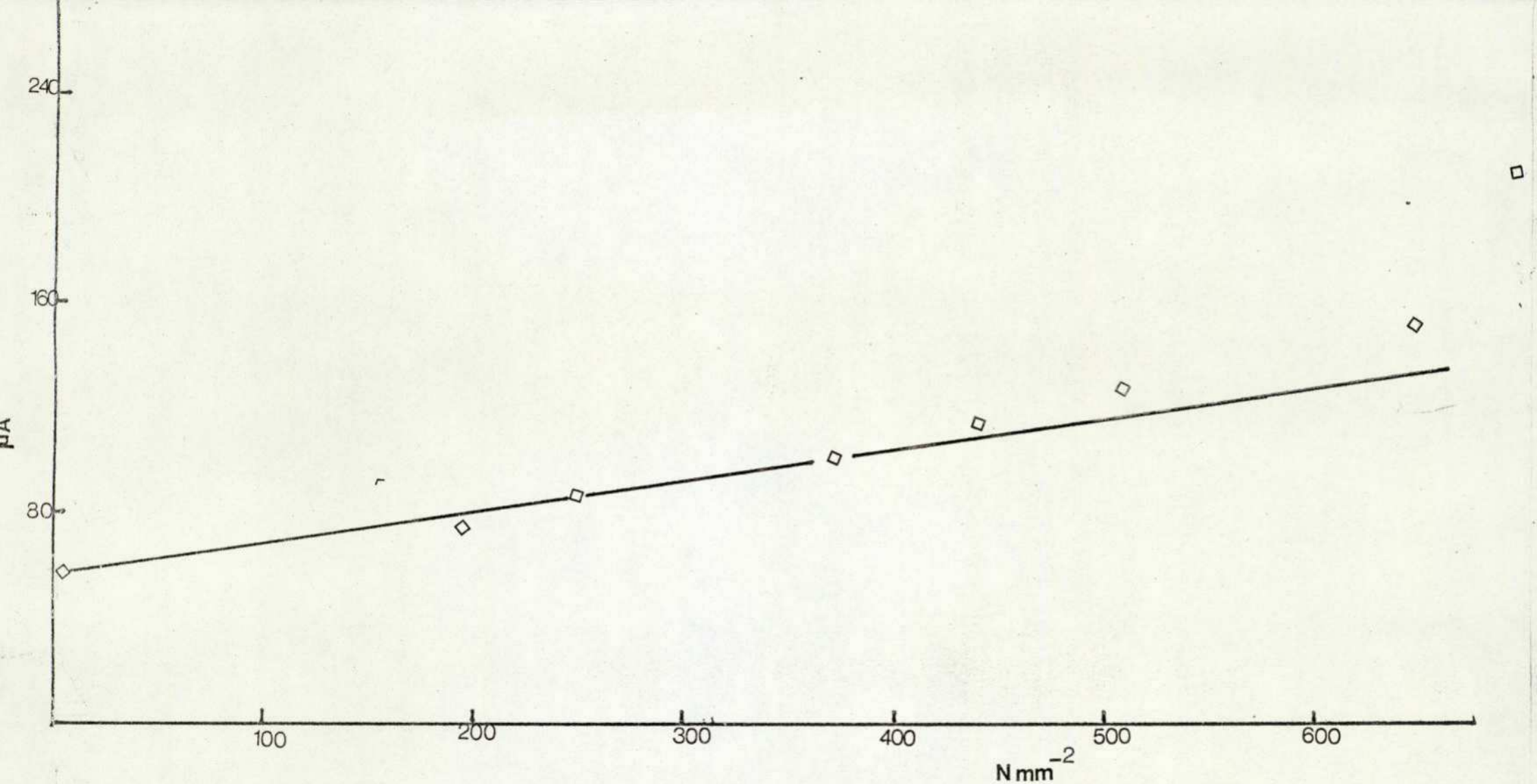


Fig. 4.6. Hydrogen permeation current (μA) against applied tensile stress (N/mm^2)

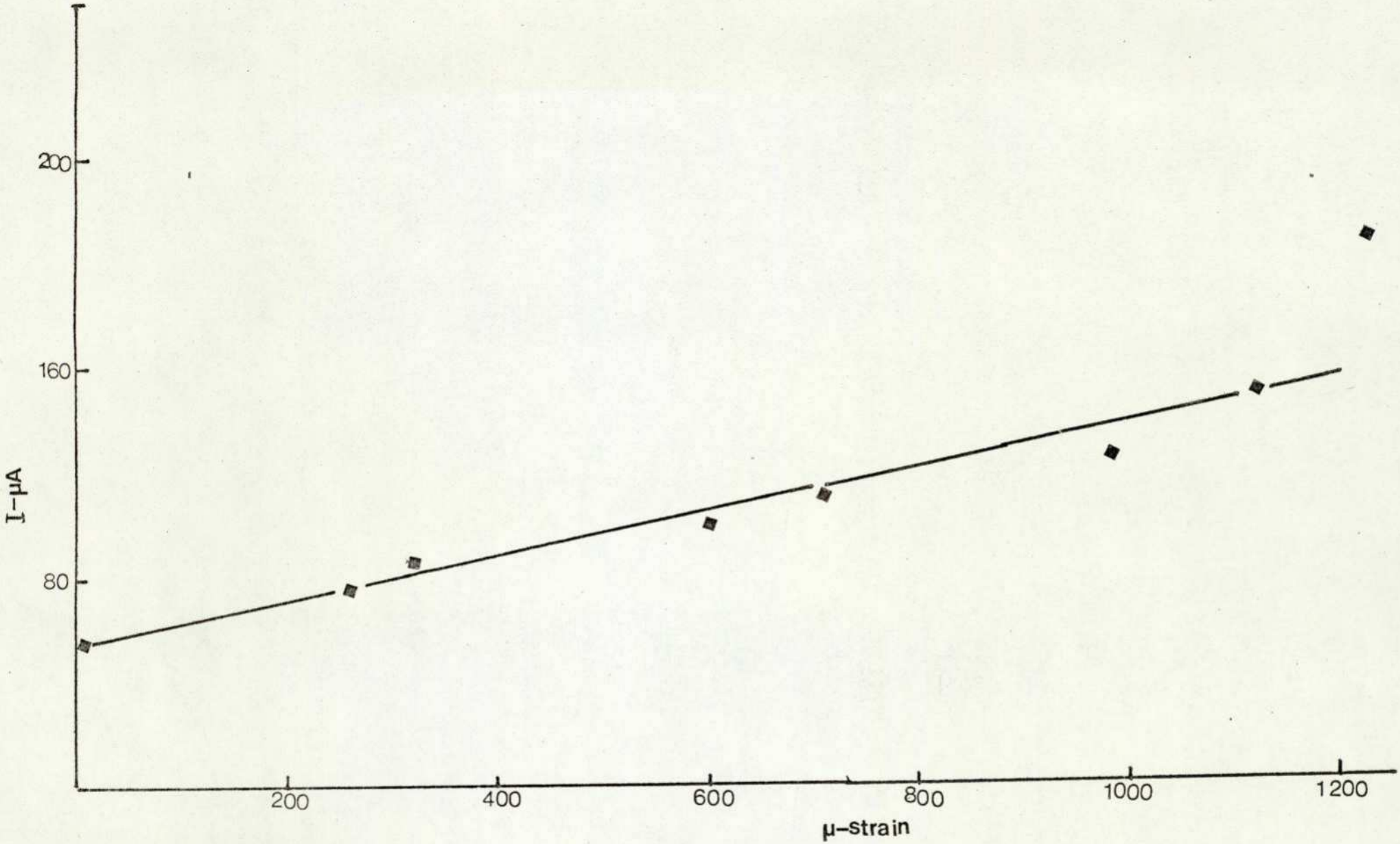


Fig. 4.7. Hydrogen permeation limiting current (μA) against strain in the membrane.

CHAPTER FIVE

THE ELECTROCATALYST FOR HYDROGEN EVOLUTION REACTION (h.e.r)

CHAPTER V

THE ELECTROCATALYSTS FOR HYDROGEN EVOLUTION REACTION (h.e.r.)

5.1. Introduction

5.1.1 A Survey of h.e.r. electrocatalyst

Hydrogen evolution reaction often accompanies many electrochemical industrial processes and it is of considerable importance in water electrolysis and diaphragm chlor-alkali cells.[100,101] The h.e.r. over-voltage influences the energy requirements of most electrochemical processes, hence extensive studies are being carried out in search of the electrocatalyst requirements for h.e.r. in most electrochemical systems. The h.e.r. over-voltage has been shown to vary periodically with atomic number of various metallic elements by earlier workers[102]. Parson and Brecter[103] pointed out that there is a close relationship between the rate of h.e.r. and the heat of adsorption M-Hads,on the metal. A volcano-type relationship was found between hydrogen over-voltage and the M-Hads bond strength.[104] The hydrogen over-voltage have a minimum value for Ni, Pd and Pt elements as compared with high over-voltage values observed for Zn, Cd and Hg elements by Bockris et al.[75] The electronic configurations of these elements are given by Ni(d^8s^2), Pd($d^{10}s^o$) and Pt(d^9s^1) compared to M ($d^{10}s^2$) characteristic of Zn, Cd and Hg elements. Based on the h.e.r. performance of the above elements and results of earlier workers,[75,104] electronic factors could play a significant role in h.e.r. performance of electrolysts.

Recently, many workers in this field have combined elements by doping etc. to achieve a compound with proper electronic properties that has high h.e.r. performance.[103, 105] In this regard, Tungsten oxide doped with platinum by implantation[105] and sodium Tungsten bronze are two of the compounds which have shown enchanced h.e.r. performance.[106] The h.e.r. performance of these electrocatalysts obtained by combination of elements has recently discouraged the common use of steel as h.e.r. electrocatalyst. Platinum is often an alternative choice to steel, but this element is expensive and often very susceptible to poisoning by trace of impurities from the cell component and electrolyte.

Therefore, from the above facts on the properties of h.e.r. electrocatalyst, it is most probable that an efficient electrocatalyst for h.e.r. can be achieved by developing a compound which has a fairly moderate M-Hads bond energy, a good electrical conductivity, corrosion resistant and most significantly a low hydrogen over-voltage. In considering these facts, recent work at The City University on an E.E.C. funded project entitled 'OPTIMISATION OF TEFLON BONDED GAS POROUS ELECTRODE', Tseung and Man[107,108] developed what could be described as a novel nickel-cobalt-sulphide, $NiCo_2S_4$ cathode catalyst which gave over 1000 MA/cm^2 at -170 mV Vs RHE in 5 MKOH at 70°C after ohmic drop correction. Recent life tests in 5 M KOH at 85°C, have confirmed that teflon bonded $NiCo_2S_4$ cathode catalyst can operate at 1.0 A/cm^2, - 130 mV Vs RHE, (Ir corrected), 85°C, for over a

test period of 3300 hours without any deterioration in performance. Moreover, this cathode catalyst $NiCo_2S_4$, is not affected by subsequent exposure to air even at 85°C.

In order to study the electrocatalyst activity, the present work aims at comparing the h.e.r. performance of iron sulphides with the $NiCo_2S_4$ cathode catalyst developed by Tseung and Man. To achieve this comparative study, this investigation proposes to determine (i) the current density - voltage performance curves and (ii) the basic electro-kinetic parameters for iron sulphides and nickel-cobalt-sulphide $NiCo_2S_4$, in different electrolyte systems.

The h.e.r. requires the presence of proton in solution, thus in acidic medium there is preponderant amount of proton while in alkaline solution water molecule is the only source. Heyrovsky, Horiute and Okamoto[109] postulated a mechanism for h.e.r. for both acidic and alkaline media. But, their mechanism does not differ markedly from the often considered mechanism put forward by Volmer and Tafel[75] which involves a charge transfer and recombination steps in alkaline medium :-

(i) $H_2O\ (\ell) + e \longrightarrow Hads + OH^-(aq)$ Volmer 5·1

(ii) $Hads + Hads \longrightarrow H_2\ (g)$ Tafel 5·2

The reaction mechanism and rate determining step changes depending on the nature of the electrocatalyst material, the condition of the surface and various other factors. However, by considering a simple electrochemical redox reaction system, the electro-kinetic parameters are defined at low hydrogen over-potential by

Bulter-volmer equation from which the Tafel equation :

$$\eta = a + b \log i \qquad 5.3$$

is derived.[75] where η : hydrogen over-voltage

i : the reaction current density

a; b : the tafel parameters for the intercept and slope respectively.

Therefore, a knowledge of the Tafel parameters, exchange current density i_o , stoichiometric number and the Arrhenius activation energy could be very useful for the elucidation of the electro-catalyst activity for h.e.r.

5.2. EXPERIMENTAL TECHNIQUE

5.2.1. Preparation and Characterisation of the Electrocatalyst for h.e.r.

(a) Nickel - cobalt - sulphide, $NiCo_2S_4$.

A high surface area nickel-cobalt-oxide was prepared from the nitrates of the respective elements by freeze-drying as improved by Tseung et al[110] and used by Man.[108] The second batch of oxide was prepared by decomposing a known mixture[110] of the nickel-cobalt-nitrates solution placed on En42 steel membrane as a support. The BET[111] surface area of the oxide powder was 74 M^2/g. These oxides were sulphided in a flowing stream of H_2S gas in the furnace at 300°C for 8 hours as described by Man. The sulphides produced from the freeze dried and air decomposed oxides were labelled A and A1 respectively and their respective sulphur content was determined.

(b) Iron Sulphide

The type B iron oxide was prepared by decomposing in air, a BDH analar grade ferrinitrate solution $\{Fe(NO_3)_3\}$ to produce a black "Cake". This resultant black ferri-oxide was ground into powder and sulphided in the stream of H_2S as above.

The type C iron sulphide was prepared by dissolving in 100 ml distilled water analar grade crystals of 9.69 g ferrous chloride and 27.58 g ferric chloride. A solution of these salts was treated with 6M NaOH solution to obtain a black precipitate which was filtered and washed several times with distilled water and dried in an oven at 75°C for 5 hours. The "Cake" produced was ground into brown powder which has a BET surface area of 102 m^2/g. This oxide was suphided in a stream of H_2S in the usual manner.

Type D was prepared by exposing the En42 steel for about six months in air. Rust was observed to cover the steel. This rusted steel was fed into a stream of H_2S in the furnace and sulphided in two batches: (i) 75°C for 18 hours and (ii) at 300°C for 8 hours to produce D_1 and D iron sulphides respectively.

The fourth type of iron sulphide involved anodizing the En42 steel in the electrolytic cell, then H_2S was introduced into the cell to reduce in situ the oxides formed to their respective sulphide. The electrochemical h.e.r was tested immediately after sulphiding.

C. X-RAY ANALYSIS

X-ray and chemical analysis confirmed that the resultant $NiCo_2S_4$ cathode catalyst possessed the thio-spinel structure[108]. The x-ray diffraction patterns determined for various types of iron oxides and iron sulphides show the following properties:- The iron oxide from the air decomposed ferric nitrate shows only the presence of α -Fe_2O_3, but the oxide from FeII/FeIII chlorides shows the presence of α -Fe_2O_3 and traces of α-FeO(OH). The x-ray pattern for iron oxide from rust in analysed to contain magnetite and haemetite ie. Fe_3O_4, and α-Fe_2O_3 respectively. Also, traces of α -FeO(OH) is evident but the x-ray patterns made it very unreliable to distinguish succinctly other forms of ferrite allotropes designated by δ and γ.

The x-ray patterns for the various grades of iron sulphides were observed to be highly indistinguishable. However, the type (B) (Table 5.1) iron sulphide shows the cubic ferrous sulphide of general formula FeS_{1-x} where $(1 < X > 0)$. The type (C) from mixed oxides is analysed to contain Troilite and pyrrholite type sulphides with general formula FeS_{1-x} and Fe_{1-x} S, where $(0.95 < X > 0.875)$ respectively. The type (D) iron sulphides obtained from rust contained iron disulphide (FeS_2), the pyrrholite ($Fe_{1-x}S$) and Troilite, FeS_{1-x}. The presence of the pyrite FeS_2 is as expected, but the absence of other homologue ie. FeS_4 etc. could be due to the temperature of preparation as reported by Reiff[112] et al and Shoesmith et al[113].

The d- spacings from this work and the JCPDS powder diffraction index are shown in the appendix. The Debye-Scherrer powder diffraction photographs were used to obtain the d- spacing of the oxides and sulphides in these analyses. And, the x-ray diffraction unit, model PW 1010, made by Phillips was of much help for these structural analysis.

(D) Sulphur Content Determination

The sulphur content of all the the sulphides were determined by Schöniger combustion unit. This technique involved the use of weighed amount of the iron and nickel-cobalt sulphides specimens which were oxidized by combustion in a stream of oxygen. The effluent gases were then absorbed and dissolved in a solution of hydrogen peroxide of known concentration to form sulphate ions which were titrated against Barium chloride solution, using Thorin solution as indicator. The result of this analysis is displayed in Table 5.1.

5.2.2. Half-Cell Electrochemical Testing

(a) Electrode Fabrication:

The freeze dried $NiCo_2S_4$ and type D iron sulphide were each mixed with I.C.I. Fluon dispersion and pested onto 100 mesh nickel screen. The catalyst/teflon ratio in each case was 10/3. The catalyst loading was between 2 and 5 mg/cm^2. The electrodes were dried at 100°C for one hour, followed by final curing at 300°C for one hour. The electrodes were 1.0 cm^2 in geometric area in all cases and 1.0 mm thick nickel wire was spot welded onto the electrode to facilitate current collection.

The second batch of $NiCo_2S_4$ produced on En42 steel membrane support was cut with mechanical shears into 1.0 cm^2 area electrode with spot welded nickel wire for current collection and other iron sulphides were prepared in the same manner.

(b) Electrochemical Test:

An electrolytic cell Fig. 5.1, consisting of platinum screen counter electrode, the saturated calomel electrode and the working electrode. The working electrode prepared as described above varied from $NiCo_2S_4$ to all the different types of iron sulphide. The electrolytes used were (i) 0.1 M KOH and (ii) 3.5 per cent Nacl at chosen temperature range. This involved, introducing each electrode into the electrolyte and cathodized at -300 mV Vs SCE hydrogen over voltage for about 120 minutes. The potentiostatic polarisation measurements were taken from the direction of high current to low current and measurements were made at steady state current density. The electrolyte was purged with nitrogen gas.

The i-v potentiostatic polarisation curves were obtained for $NiCo_2S_4$ and En42 steel in 0.1 M KOH at 25°C. Then i-v potentiostatic curves were obtained for $NiCo_2S_4$, all grades of iron sulphides including the iron sulphide prepared in situ in 3.5 per cent Nacl at 25°C. An i-v comparative study was made in each case. Finally, Tafel plots were determined for $NiCo_2S_4$ and sample D iron sulphide prepared from rust in which comparable performance was observed in 3.5 per cent Nacl. Arrehnius activation energy was investigated for these two comparable h.e.r electrocatalysts in 3.5% Nacl solution. The Ir correction was obtained for each system studied by using the interrupter technique.

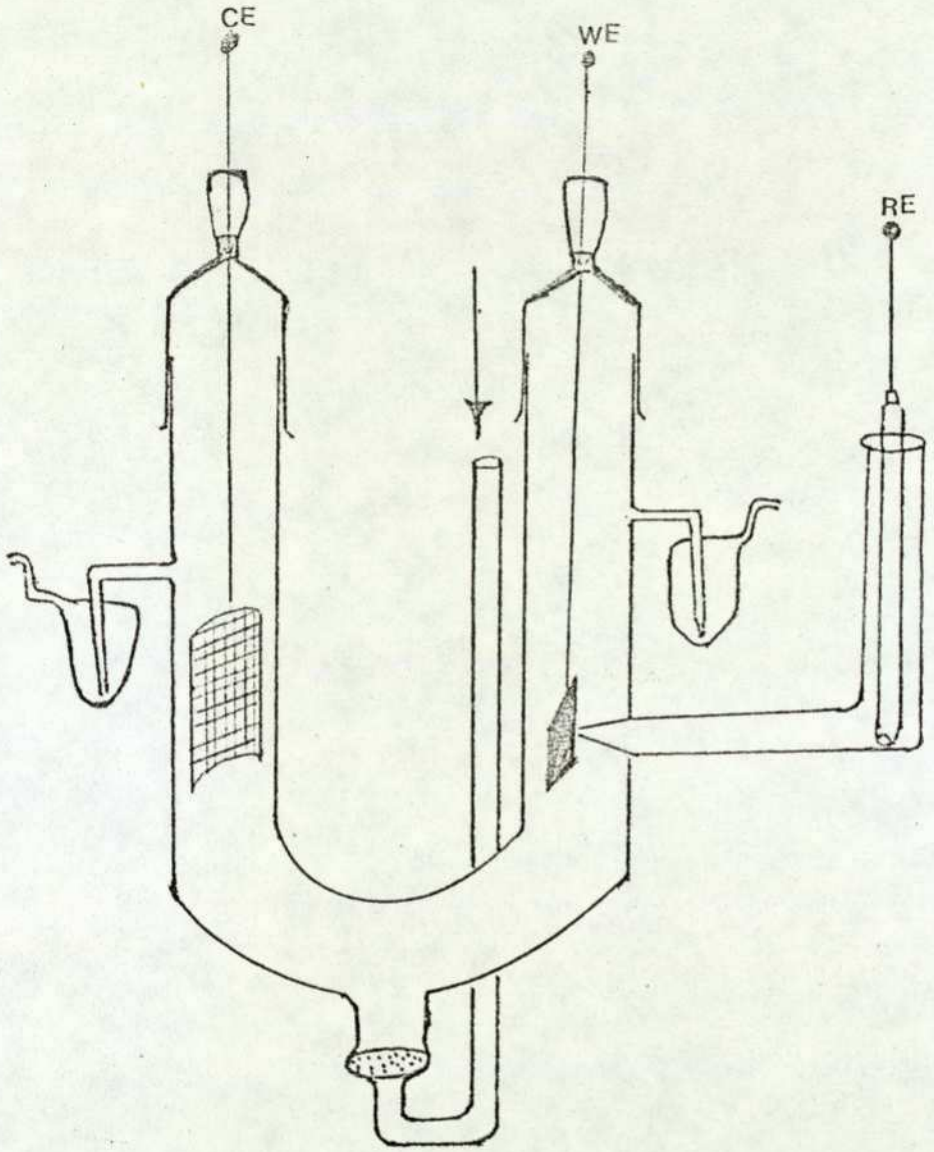


Fig. 5.1. Three compartment cell assembly for i-v performance studies of the sulphide electrodes on h.e.r.

5.3. RESULTS

Figure 5.2. shows the performance of $NiCo_2S_4$ and En42 steel for hydrogen evolution in O.1M KOH @ 25°C and Fig. 5.3 depicts the same performance of these catalysts in the absence and presence of H_2S in 3.5% sodium chloride solution. Their performances are observed to be more enhanced in presence of H_2S than without. Similar i-v curve is obtain for $NiCo_2S_4$ and steel in sea water, Fig. 5.4.

The electrochemical h.e.r performance conducted using various grades of iron sulphide is shown in Fig. 5.5. while the iron sulphide electrodes prepared direct from iron and electrode from sulphided-anodized-iron show similar performance which are much lower than the high performance of other grades. Also, there seems to be no distinguishable performance between the iron sulphide electrode prepared from iron rust and the one from mixed FeII/FeIII salts. Thus, these two electrodes gave the same electrochemical h.e.r performance @ 25°C in 3.5% Nacl solution. Fig. 5.5, but both of them show a low marginal difference of performance to a better $NiCo_2S_4$ electrocatalyst Fig. 5.6, @ 35°C .

Figures 5.7 & 5.8 show plots of log i vs. over-potential in 3.5% Nacl for 2.4 mg/cm^2 and 4.5 mg/cm^2 of $NiCo_2S_4$ and iron-sulphide (from rust) catalyst loadings respectively at temperatures 25°C, 45°C and 60°C. Reproducibility was good for both catalysts but much better on $NiCo_2S_4$. Two Tafel slopes are observed in each case at lower overpotential and the heat of activation at high

overpotential are obtained from a plot of log i vs reciprocal of the absolute temperature Fig. 5.9. The numerical value of the heat of activation E_A, may yield information on reaction mechanism (ie. E_A is expected to be high for the slow discharge mechanism, which involves breaking of a strong $O\text{-}H^+$ bond and formation of relatively weak M-H bond, while low E_A is for slow recombination mechanism, which involves breaking of two relatively weak bonds to form a strong H-H bond).

Note, the determination of Tafel parameters were made by taking measurements in the low over-voltage region (η <RT/F) in order to avoid or minimise contribution due to activation, ohmic and concentration polarisation at higher overpotentials.

TABLE 5.1

Sulphur content (w/w per cent) in iron sulphide grades and $NiCo_2S_4$ prepared in a stream of H_2S for 8 hours.

Source of Sulphides	Grade	Temperature of sulphidisation	w/w % sulphur
$NiCo_2S_4$ from freeze dried $NiCo_2O_4$ oxide	A	300°C	22.10
$NiCo_2S_4$ from Air decomposed $NiCo_2O_4$	A_1	300	18.40
FeSx from decomposition of $Fe(NO_3)_3$	B	300°C	19.4
FeSx from NaOH and mixed FeII/FeIII chlorides	C	300°C	26.8
FeSx from Rust	D	300°C	12.4
FeSx from Rust (sulphided for 18 hours)	D_1	80°C	10.2

TABLE 5.2

Kinetic parameters for h.e.r. on $NiCo_2S_4$ and FeSx prepared from iron rust. The electrolyte used is 3.5 per cent Nacl @ 25°C, 45°C and 60°C. { $NiCo_2S_4$ is prepared on the steel membrane while the FeSx is obtained by reducing the rust on the membrane with H_2S }

Electrocatalysts	Temp °C	Tafel Slope @ low	Activation Energy $\rightarrow \Delta F/R$
$NiCo_2S_4$ (catalyst loading is 2.5 mg/cm^2)	25 45 60	0.0701 0.1125 0.1620	1860.5 (η =80mV SCE)
FeSx from Rust (loading 4.5 mg/cm^2)	25 45 60	0.0875 0.1634 0.2333	2142.8 (η =75mV SCE)

DISCUSSION

The hydrogen evolution performances on various grades of iron sulphide obtained in this work Fig. 5.2, 5.7. show marked performances of two grades of iron sulphide namely grades C and D sulphides from mixed FeII/FeIII oxide and iron rust respectively. The iron sulphide from iron rust shows a better performance at lower over-potential but at higher over-potential its performance and that of grade C are found to be same. The grade B ie. from the decomposed ferric nitrate which shows a comparable performance with the first two grades C and D, but performance of only steel and steel exposed to H_2S have been found to be very poor. Fig.5.2, 5.5. Thus, the iron sulphide prepared from combined oxides of iron has shown to give a better performance than steel and iron sulphide prepared direct from steel. Fig. 5.5. Again, the performance of iron sulphide in h.e.r seems to depend on the composition of the oxides from which such sulphides are prepared. This fact is manifested in this work ie. the iron sulphide obtained direct from only Fe_2O_3 gives a better performance than iron sulphide obtained direct from steel. The iron sulphide prepared from the combination of $Fe_{1-x}O$, Fe_2O_3 and Fe_3O_4 (ie. rust) gave a much better performance than the sulphide from only the mixture $Fe_{1-x}O$ and Fe_2O_3 as shown in Fig. 5.6. There is no evidence in literature to explain this phenomenon. The difference in sulphur content, Table 5I was considered responsible

but the minimum sulphur content (12.4 w/w per cent) of rust as compared with the 19.4 and 26.8 w/w per cent for grades B and C iron sulphides respectively Table 5.1. shows the contrary. In effect, the grade D sulphide from rust with its low sulphur content gave higher performance which suggests that other factors could be responsible. As, it was not possible to measure the surface area of the various grades of sulphide because of the loss of sulphur during the degassing stage in the BET measurement,[111] we could not effectively explain these observations based on surface area of the catalysts. However, from the X-ray analysis, we observed differences in the structure of each grade of sulphide. Thus, the presence of different structure in the overall composition of the sulphide could be responsible for this observed performance. This fact supports the earlier view[114] that electronic properties of the catalyst does influence the hydrogen evolution reaction and this has been manifested in the result of this work in which the sulphide prepared from mixture of $Fe_{1-x}O$, Fe_2O_3 and Fe_3O_4 (ie. rust) gave a commanding performance compared with sulphides with fewer oxide combination.

Two grades D and D_1 (Table 5.1) of iron sulphide prepared from rust at 300°C and 80°C for 8 hours and 18 hours respectively were found to contain the same amount of sulphur and gave the same h.e.r performance. The performance compared with that of $NiCo_2S_4$ shows that at 105 mV SCE over-potential, 10mA/cm^2 and 18 mA/cm^2 for D grade of FeSx and $NiCo_2S_4$

respectively in 3.5 per cent Nacl at 25°C (Ir corrected). But, at 250 mV (SCE) overpotential, 85 mA/cm^2 and 90 mA/cm^2 for grade D iron sulphide and $NiCo_2S_4$ respectively under the same condition. These results show comparable performance Fig. 5.6. The Tafel slopes for the two h.e.r electrocatalysts determined at 25°C, 45°C and 60°C as well as the Arrhenius activation energy show identical values, Table 5.2. Since the Tafel slopes at lower overpotential are relatively identical under the same experimental conditions, this strongly suggests that the reaction mechanism remains the same for the two electrocatalysts.

It follows, however, that this comparable kinetics studies of iron sulphide and $NiCo_2S_4$ have shown that both electrocatalysts have comparable hydrogen evolution performance. Thus, the application of anyone of them could be as effective as the other for the prevention of hydrogen embrittlement in a corroding steel envisaged in the next chapter.

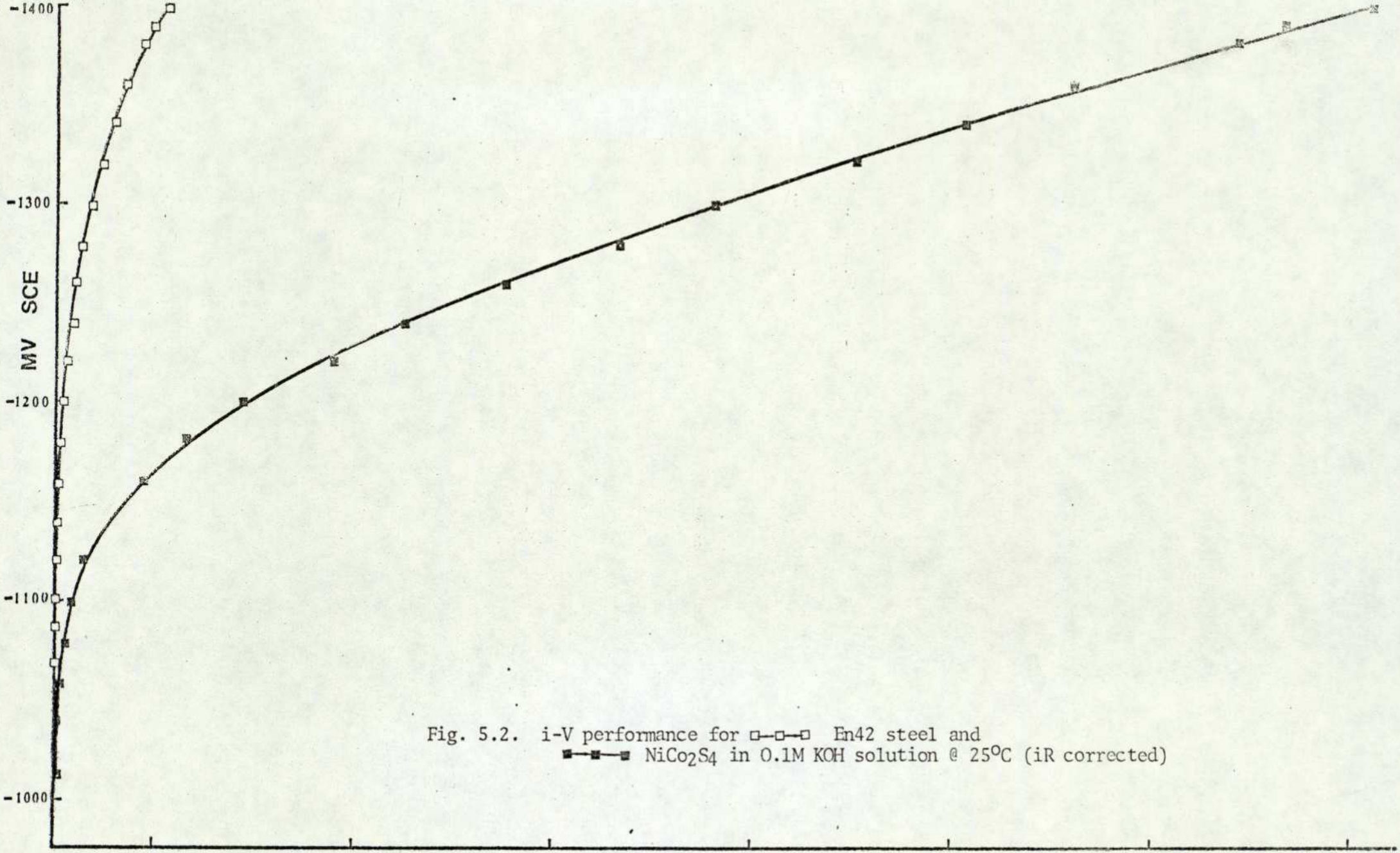


Fig. 5.2. i-V performance for □—□—□ En42 steel and
■—■—■ $NiCo_2S_4$ in 0.1M KOH solution @ 25°C (iR corrected)

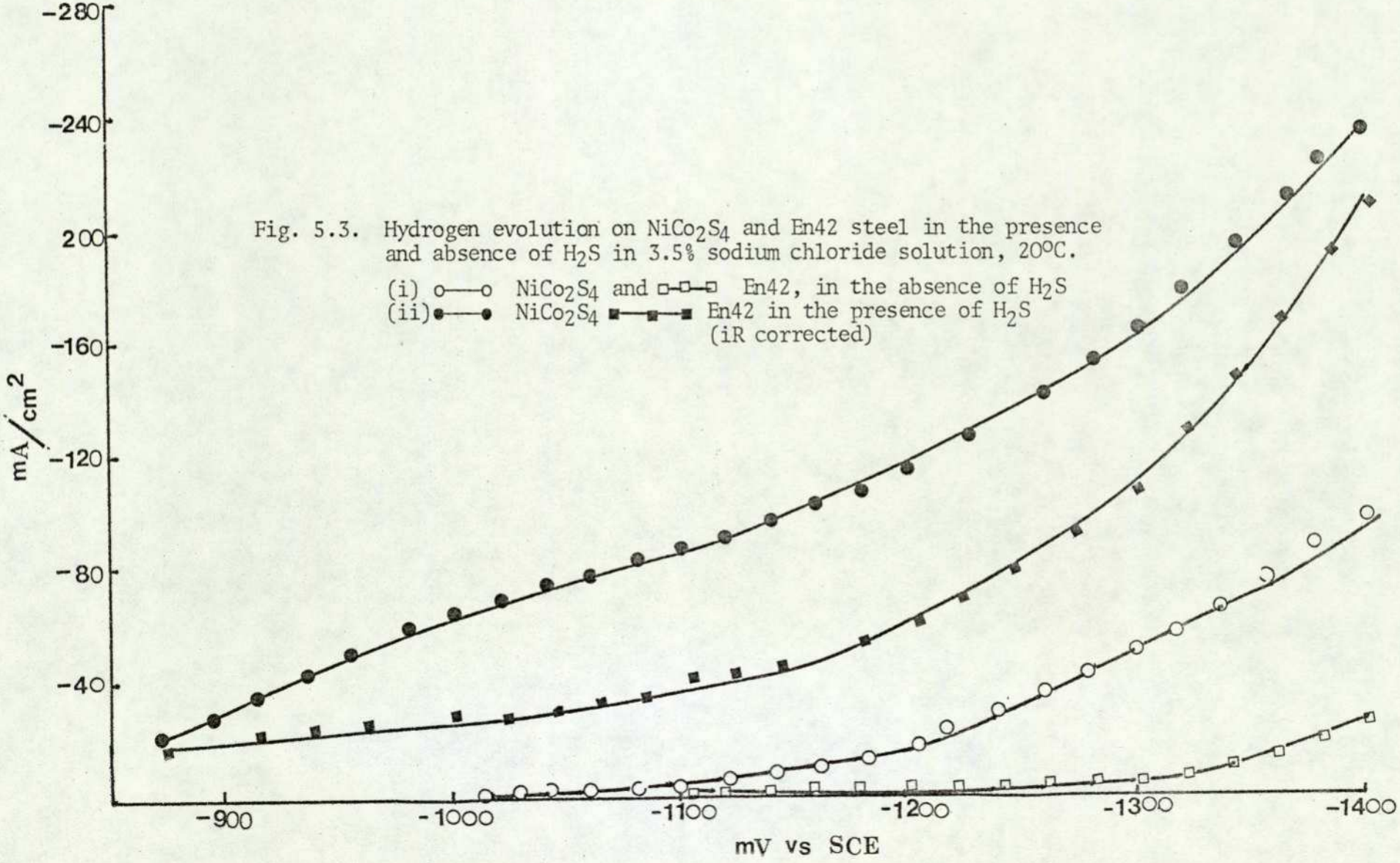


Fig. 5.3. Hydrogen evolution on $NiCo_2S_4$ and En42 steel in the presence and absence of H_2S in 3.5% sodium chloride solution, 20°C.

(i) o—o $NiCo_2S_4$ and □-□-□ En42, in the absence of H_2S
(ii) ●—● $NiCo_2S_4$ ■—■—■ En42 in the presence of H_2S (iR corrected)

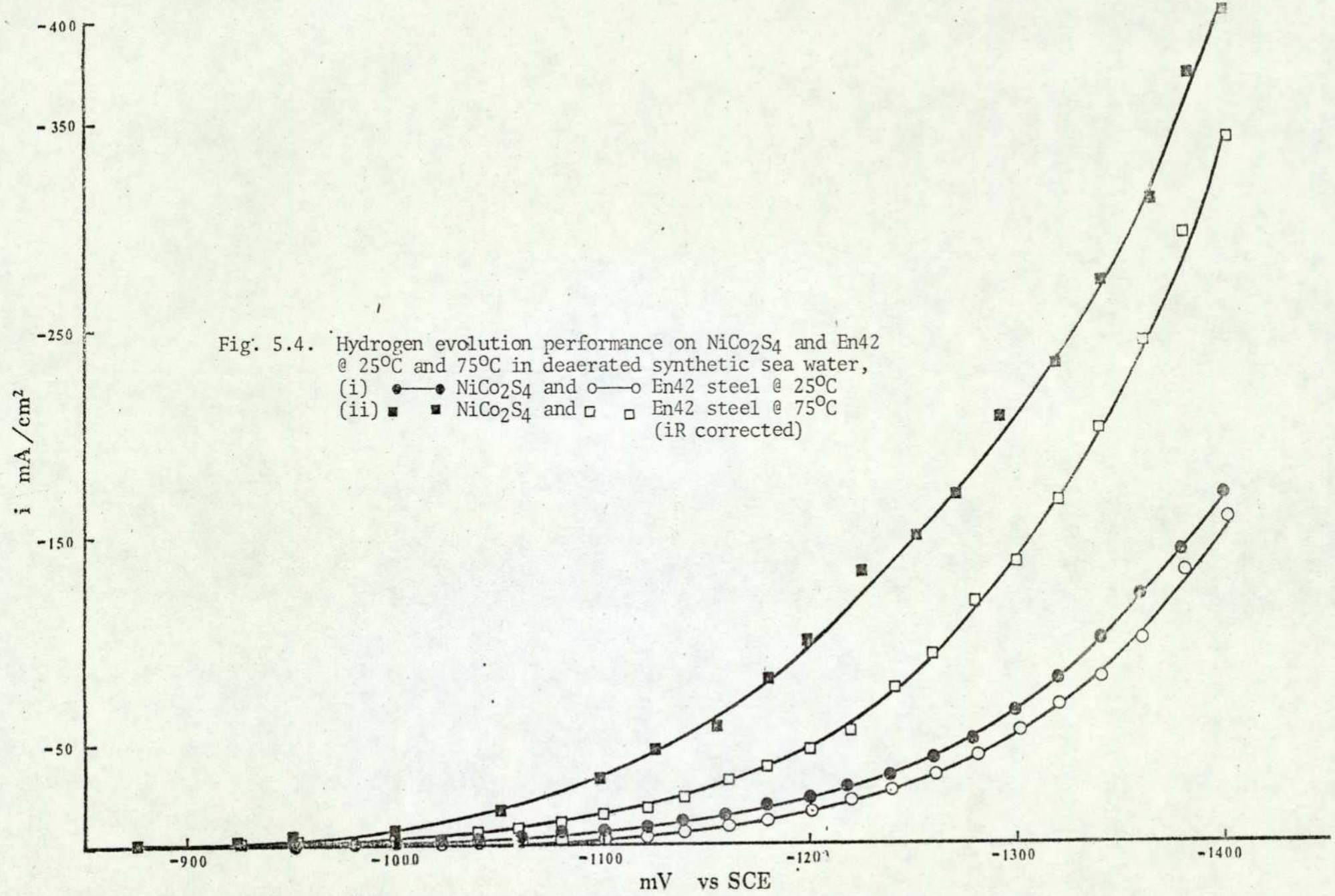


Fig. 5.4. Hydrogen evolution performance on $NiCo_2S_4$ and En42 @ 25°C and 75°C in deaerated synthetic sea water,
(i) ●—● $NiCo_2S_4$ and o—o En42 steel @ 25°C
(ii) ■ ■ $NiCo_2S_4$ and □ □ En42 steel @ 75°C
(iR corrected)

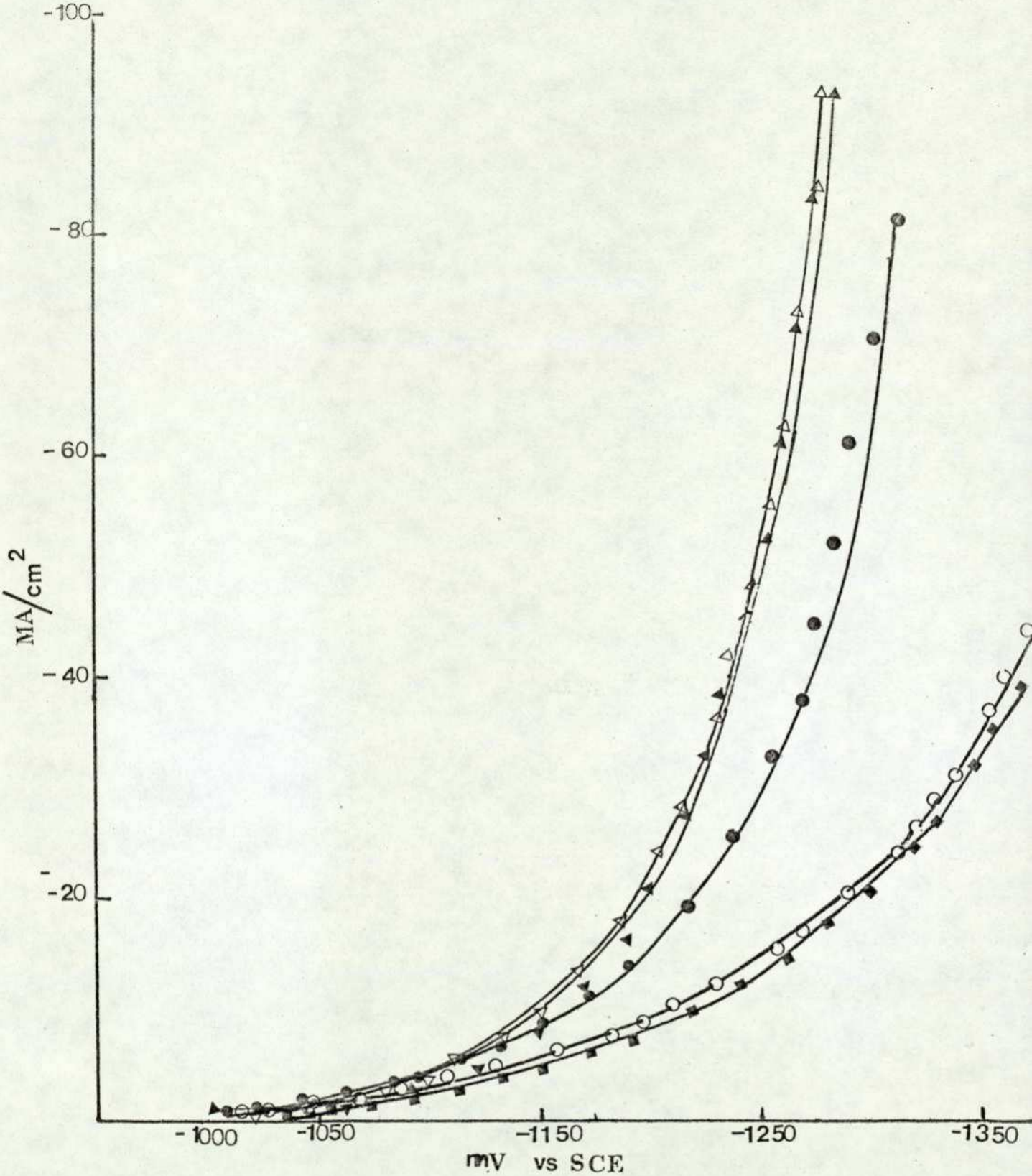


Fig.5.5. Hydrogen evolution performance on various grades of iron sulphides. (a) ■—■ En42 steel (b) o—o En42 steel exposed to H_2S for 10 hours @ 300°C. (c) ●—● FeSx from $Fe(NO_3)_3$ (d) ▲—▲ FeSx from rust and (e) Δ—Δ FeSx from mixed chlorides of iron. (iR corrected, 3.5% Nacl @ 20°C).

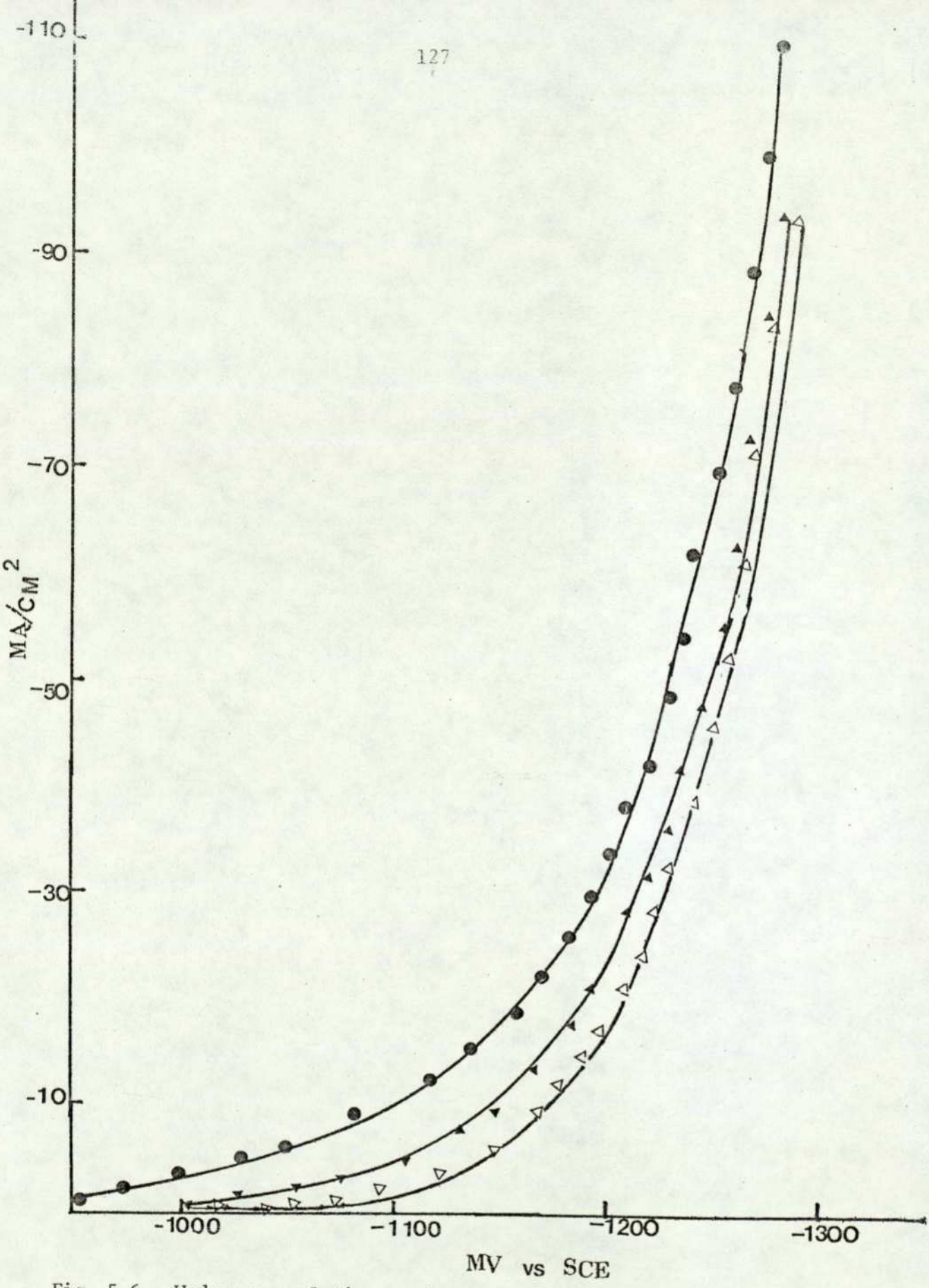


Fig. 5.6. Hydrogen evolution performance on
(a) o—o $NiCo_2S_4$; (b) ▲—▲ FeSx from rust and
(c) △—△ FeSx from mixed chlorides of iron.
iR corrected in 3.5% Nacl @ 35°C.

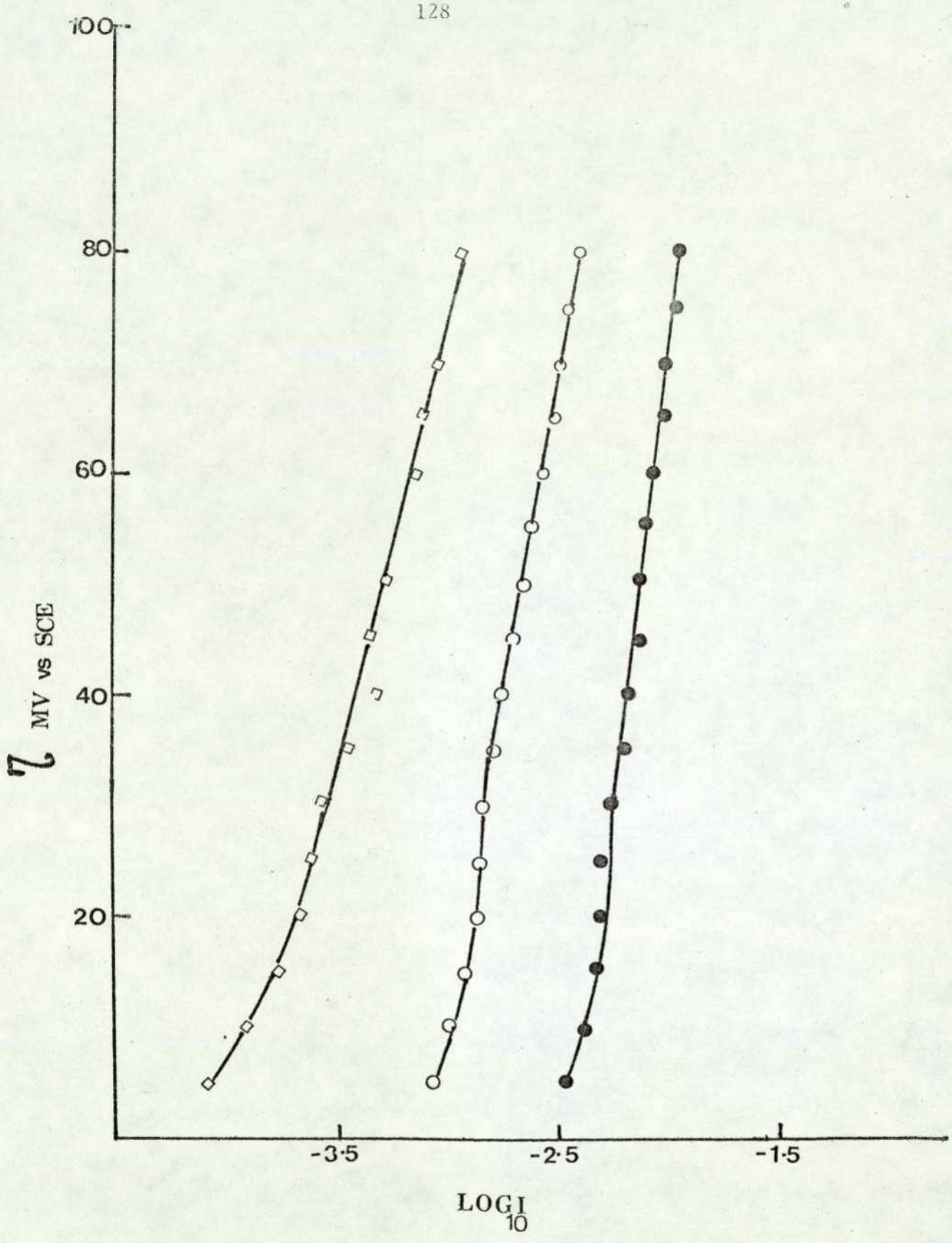
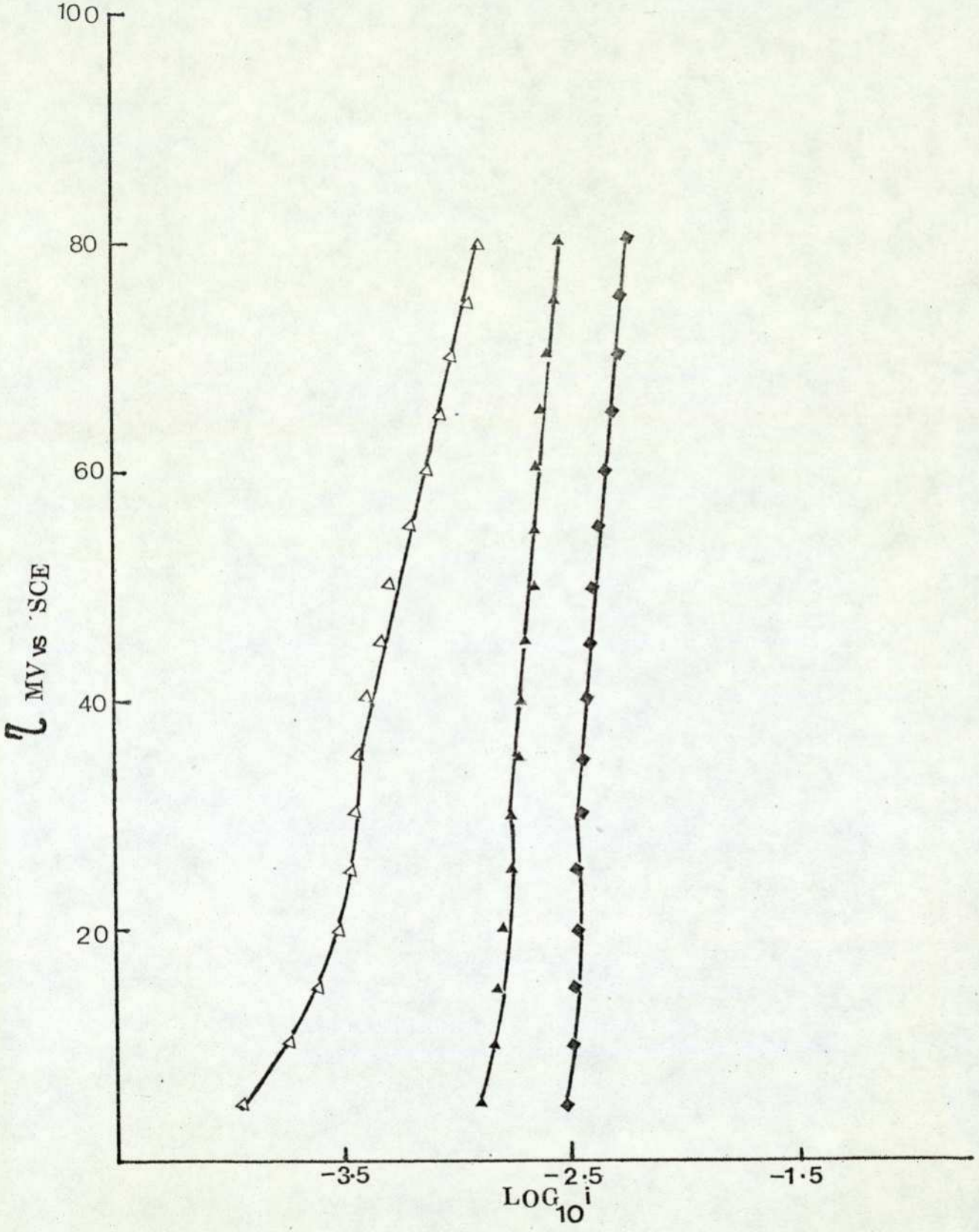


Fig. 5.7. Tafel plot of precathodized $NiCo_2S_4$ electrode in 3.5% Nacl @□25°C,○44°C and●64.5°C.



5.8. Tafel plot of precathodized FeSx from iron rust in 3.5% Nacl @△25°C,▼45°C and■60°C.

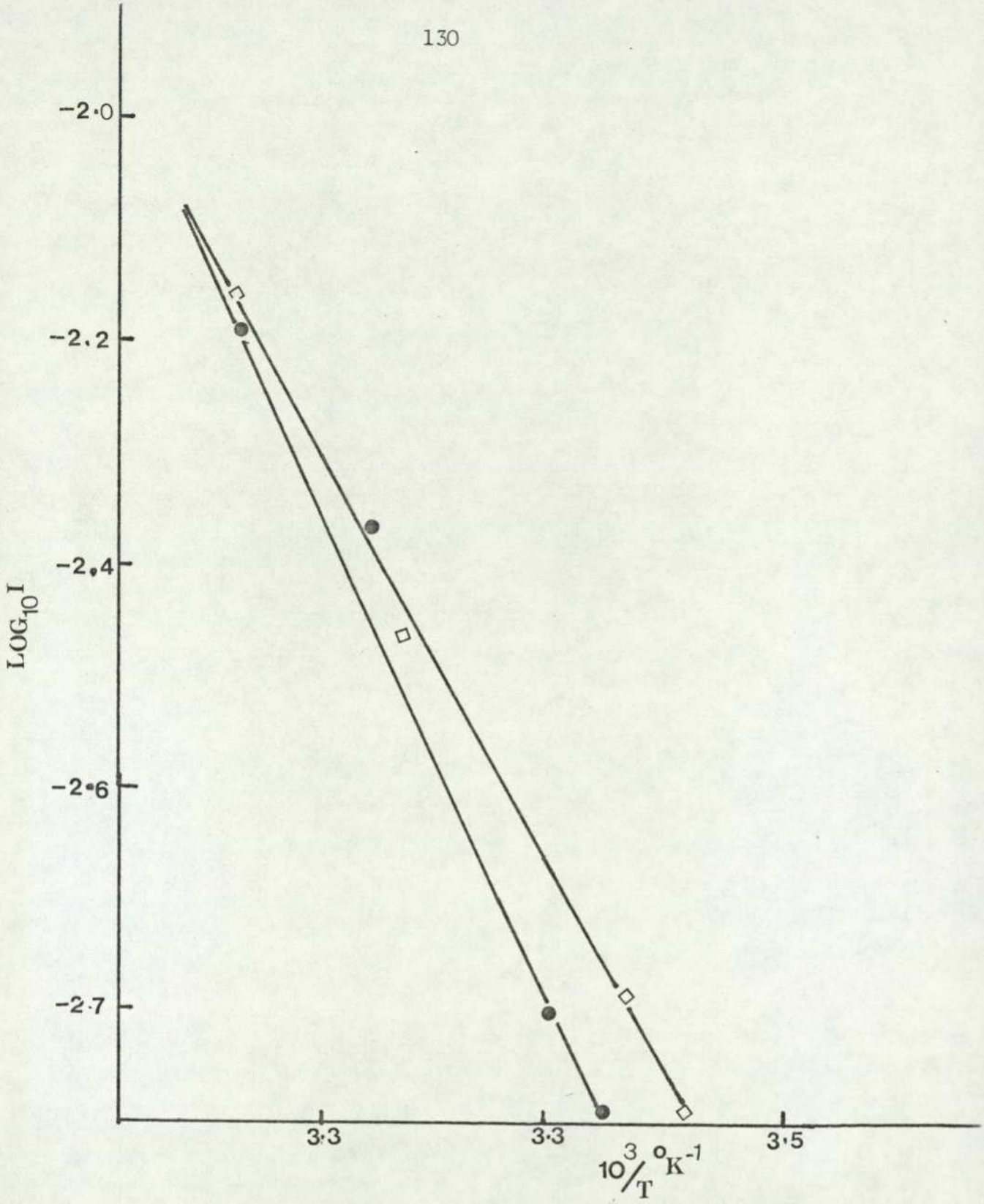


Fig. 5.9. Plot: $Log_{10}i$ Vs $\frac{1}{T}$ for FeSx from $\frac{10^3}{T}$ K

□ Iron rust and● $NiCo_2S_4$ in 3.5% Nacl at H_2 over potential (η) 80 mV SCE and 75 mV SCE respectively.

CHAPTER SIX

HYDROGEN EMBRITTLEMENT IN STEEL

CHAPTER VI

HYDROGEN EMBRITTLEMENT IN STEEL

6.1. Introduction

Hydrogen evolution is among the varying cathodic reactions which accompany the corroding steel structure in some environments, (equation 2, chapter 1). Although the majority of the H_2 produced on the cathodic areas is evolved as gas and assists the removal of corrosion products, some of it diffuses into the steel in the atomic form and can render it brittle. As pointed out in Chapters III & IV, the presence of impurities such as arsenic, H_2S, Co_2, CN^- etc reduce the formation of H_2 gas on the steel, consequently, the amount of atomic hydrogen diffusing into the steel, and the brittleness are increased. As well as causing brittleness, the absorbed H atom combines to form molecular hydrogen on the surface of inclusions and voids within the steel. Thus, a gas pressure is set up in the voids and this may be sufficient to cause blisters to appear either during pickling or particularly during processes leading to stress corrosion damage[20]. Hydrogen evolution and consequent diffusion of H atom into steel is vulnerable in localized corrosion sites where ingress of oxygen or any other reducible species is restricted. It has recently been observed that the electrochemical conditions (ie. solution pH and electrode potential) at the tip of an advancing stress corrosion crack in steel exposed to 3.5 per cent sodium chloride solution are favourable for hydrogen evolution regardless of the externally

applied potential or the pH of the bulk solution.[115] Similarly, Brown[61] found that the solution inside a fissure on the surface of a specimen becomes very acidic (from pH 6.5 to pH 3.5) and that metallic ions are present. He emphasised the point that, on plotting the combination of pH and potential observed during cracking on a Pourbaix diagram, the points always fall in that region where hydrogen evolution is possible. He states that 'there does not appear to be any valid reason to require a mechanism other than hydrogen embrittlement to account for the cracking of high strength steels in salt water'. For low alloy steels, without applied potential, Snape[61] attributes failure mainly to hydrogen embrittlement. Thus, the failure of a metallic structure could be the responsibility of stress corrosion cracking and/or the hydrogen embrittlement where the specific cause célébre in any environment is not clear.

Kennedy and Whittaker[61] emphasized the practical importance of distinguishing between the cracking due to hydrogen and that due to anodic attack at the crack tip, since such information is necessary in deciding on a protective treatment. If the mechanism of fracture can be shown to be of the second type, then coating consisting of a metal anodic to the basis of the metal should provide cathodic protection at the gaps (at least for some time), whereas, if the mechanism of failure is connected with hydrogen, the choice of an anodic material is likely to be disastrous; phosphating and painting may be more suitable. They discuss methods of distinguishing between the

two types of failures, reaching the conclusion that various techniques, such as changes in cathodic polarization and fractographic techniques are of some value in determining failure mechanism but absolute diagnosis is not yet possible.

One of the major problems in off shore gas and oil pipelines is their susceptibility to stress corrosion cracking due to hydrogen embrittlement.[62] The problem is particularly serious in riser pipes which carry the hot crude oil or gas from the ocean bed to the underwater pipes which transport the fuel to the shore. The riser pipes are subjected to considerable stress caused by oil or gas pressure as well as the pounding action of the waves. An added factor - the presence of H_2S which is strongly adsorbed and dissociates very easily on the steel structure. This reduces the possibility of H atom recombining as H_2 molecule[87] consequently most of the H produced in the dissociation process diffuses into the metal, thereby reducing the energy needed for creating new surfaces when a dislocation pile up is transformed into true crack.

6.1.2. Possible Mechanism and Prevention

The contribution of earlier workers[46,59] and the results based on the present work (ie. Chapters III and IV) have shown that the presence of H_2S increases the rate of hydrogen permeation into steel. The action of H_2S is generally assumed to be due to the poisoning of the H atom recombination sites by strongly adsorbed $S^{=}$, thereby forcing the H atoms to diffuse

into the metal lattice.[55] Hence, this phenomenon could be responsible for the internal corrosion of pipelines and equipment which are encountered in most oil and gas production units. However, the degree of internal corrosion attack will vary with the production site and this will change during the production life of the well and also as operating procedures and the production rate change. This is because the rate and type of corrosion is dependent on various parameters, such as the amount of water co-produced with the gas and/or crude oil, the presence and concentration of carbon dioxide and/or hydrogen sulphide, the pH, the salt content and ingress of oxygen. Thus, the corrosion can be classified into two basic types, namely "Sweet" corrosion due to the presence of the Co_2 and water, and "Sour" corrosion, due to the presence of H_2S.

In both cases, the rate of the cathodic hydrogen evolution is increased, leading to hydrogen embrittlement and premature failure. Moreover, in the presence of carbonic acid, the pitting corrosion of the steel is increased; the presence of pits would enhance the possibility of stress corrosion. The evolution of hydrogen can be written as :

$$H^+ + e \rightarrow Hads \qquad 6.1$$

$$Hads + Hads \rightarrow H_2 \qquad 6.2$$

In sour pipes, H_2S reacts with steel to form iron sulphides. On such surfaces, reaction (6.2) is the rate determining step and the possibility of adsorbed H atom into steel would be greatly enchanced :

$$X\ H_{ads} + Fe \rightarrow Fe(H)_X \qquad 6.3$$

This will then result in hydrogen embrittlement, which has been identified as the main cause of stress corrosion in the internal gas and crude pipelines.[62]

The present protective measures[62] include:

(i) Proper design : This eliminates abrupt changes of flow direction. This will minimize local effects.

(ii) Proper selection of material : The method is often constrained by cost and practical considerations. In certain areas chromium steels have been used but mechanical requirements and the possibility of their cracking in high chloride, and high temperature environments restrict their large scale use.

(iii) Coatings : These have the disadvantage that, over a period of time, pores and cracks develop and severe localized attack results.

(iv) Inhibitors : This is the most favoured method at the moment. Basically, these are organic molecules incorporating active polar groups containing sulphure, nitrogen or phosphorous, eg. alkylamines or amides. These compounds adsorb on the metal surface and decrease the rate of electrochemical reaction. However, the inhibitors have to be added either continuously or at specific time intervals. Moreover, it is not certain whether it would be very effective in sour pipes, since the inhibitors cannot stop the reaction between H_2S and steel.

The present work proposes a novel technique for the prevention of hydrogen embrittlement in steel. The technique ensures that when the steel is being corroded, the cathodic hydrogen evolution reaction occurs on highly efficient hydrogen evolution electrocatalyst sites instead of on the steel. In this way, the amount of Hads available for diffusion into steel will be greatly reduced. The active hydrogen evolution electrocatalysts ie. Nickel dicobalt tetra-sulphide, $NiCo_2S_4$ and iron sulphide, being considered in this investigation have been demonstrated in Chapter V to have low hydrogen over-voltage, high corrosion resistance and possess electrical conductivity.

In order to demonstrate the efficacy of this technique, anyone of these active electrocatalysts is provided before the steel to be protected from hydrogen embrittlement is exposed to the corrosive environment, and/or may be provided whilst the steel is so exposed.

Several applications of these active electrocatalysts have been demonstrated these include : An electrode (ie. Section 5.2.2, chapter V) made from anyone of these electrocatalysts may be electrically connected to the steel to be protected against hydrogen embrittlement. However, the technique will not, in general, be suitable for use in the protection of pipelines etc. and, for such applications, it is preferred to coat the active electrocatalyst directly onto the surface to be protected. This is achieved by coating the surface of the steel with a solution of the mixed nitrates which decomposes on heating

with or without a chemical inert binder and then converting the mixed oxides by treating with H_2S or another sulphur containing compound eg. carbon disulphide, CS_2.

This technique has proved very effective in preventing hydrogen permeation in steel in this work and possibly will be very useful for the prevention of hydrogen embrittlement in oil and gas pipe lines.

6.2. EXPERIMENTAL TECHNIQUE

6.2.1 METHODS OF PROTECTION OF STEEL FROM HYDROGEN EMBRITTLEMENT:

6.2.1A Electrically Connected Steel to an Electrocatalyst.

The H permeation current was the manifestation of H atom absorbed at the cathode side of the bielectrode steel membrane, diffused through the membrane and was de-electronated at the anode side of the same membrane, Chapter III. These principles and the two compartment cell techniques would be used in this chapter to investigate the possibility of preventing hydrogen permeation, by (i) electrically connecting and/or (ii) bonding the cathode side of the bielectrode steel membrane to a more efficient and active hydrogen evolution catalyst (ie. $NiCo_2S_4$ or iron sulphide).

The aim of this investigation has been realized by using the two compartment cell Fig.6.1, which has an additional column to hold the catalyst in the cathodic compartment. As described in Chapter III, the steel membrane (En42 grade) separated the two compartments at the joint. The constituents

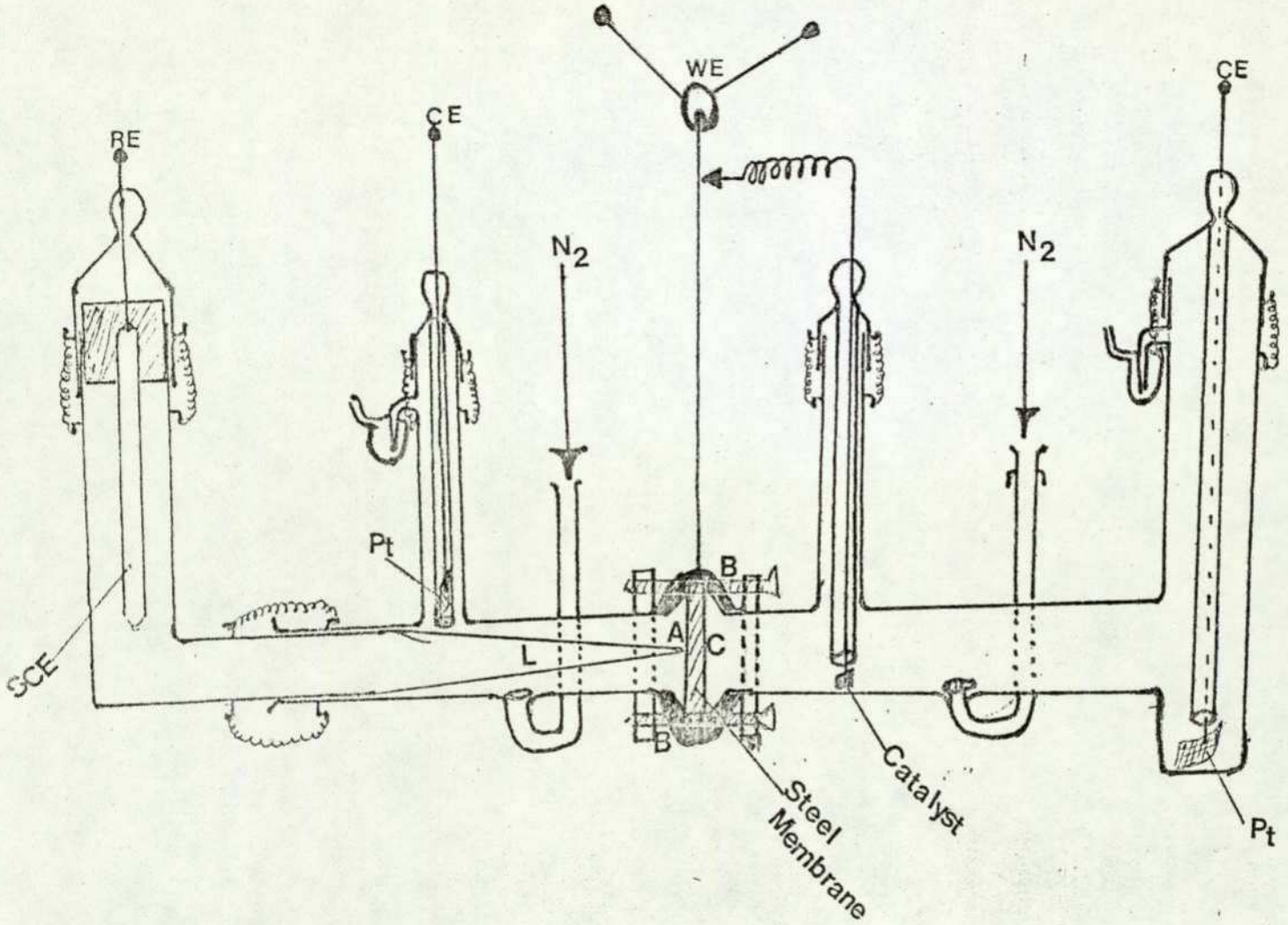


Fig 6.1 The bi-electrode diffusion cell assemby with a catalyst column in the Cathode compartement (C) and luggin capillary (L) in the Anode compartment (A); (B) shows the aluminium brackets and steel screws.

of the anolyte was maintained as in Chapter III and the electro-deposition of thin layer of palladium on the anodic side of the membrane was accomplished in the same manner. The catholyte was changed to satisfy some specific conditions in these series of investigations:-

(a) $NiCo_2S_4$ Catalyst Used To Protect Steel From Hydrogen Embrittlement In 0.1M KOH/H_2S.

In the first case, the catholyte was 0.1M KOH at 25°C. The $NiCo_2S_4$ catalyst electrode was electrically connected to the cathodic side of the bielectrode steel (En42) membrane to be protected from H embrittlement and maintained at 10 mA/cm^2 hydrogen discharge current density as shown in Fig. 6.1 and electrical circuit in Chapter III.

There was no hydrogen permeation current monitored due to the presence of $NiCo_2S_4$ which is in electrical contact with the steel substrate being protected. Thus, after a long period of time, the $NiCo_2S_4$ catalyst was disconnected from the steel which was still maintained at 10 mA/cm^2 hydrogen discharged current and within seconds, the H permeation current was monitored by the X-t pen recorder. The H permeation was allowed to increase until it attained its limiting current value, the $NiCo_2S_4$ was once more electrically connected to the steel. The H permeation was observed on the X-t pen recorder to decrease rapidly to its zero current value. Hence, by this make-and-break device between the electrical connection of $NiCo_2S_4$ to steel, the process could be used to demonstrate the effective protection of steel

from H embrittlement by the $NiCo_2S_4$ catalyst application.

H_2S gas has been noted to induce H permeation into steel (chapter III), and the effect of protecting the steel from H embrittlement by using $NiCo_2S_4$ catalyst in H_2S environment was investigated. In the manner as described above, the catholyte was 0.1M KOH in the first instant at 25°C and later increased to 75°C. The steel and the $NiCo_2S_4$ catalyst were electrically connected and maintained at 10 mA/cm^2 in the potentiostat. After about one hour, the H_2S gas was introduced to saturate the 0.1M KOH catholyte at 25°C. As soon as H_2S was introduced, a small H permeation current was monitored by X-t pen recorder. This current increased and attained its maximum value of about 5 μA. But after a long period, as soon as the $NiCo_2S_4$ catalyst was disconnected from the steel, the H permeation current increased very sharply and within 120 seconds attained a maximum value of over 160 μAmpere. After a prolonged period of time, the $NiCo_2S_4$ was re-connected to protect the steel and within seconds, the H permeation current was observed to decrease very rapidly to its initial current value.

In the same system at 75°C, introduction of H_2S gas gave a H permeation current while the $NiCo_2S_4$ catalyst was still protecting the steel but after a long period, the catalyst was disconnected. The H permeation current shot up to just under 400 μA, but on reconnection of the $NiCo_2S_4$ catalyst to protect the steel, the H permeation was observed to decrease very sharply to its initial value. Thus, the $NiCo_2S_4$ catalyst

protects the steel from H embrittlement even at above room temperature.

(b) $NiCo_2S_4$ Catalyst Used To Protect Steel In 3.5% Nacl Solution/H_2S.

The effect of electrically connecting the $NiCo_2S_4$ on the H permeation rate of steel to be protected in the presence and absence of H_2S in 3.5 per cent Nacl solution at 25°C and 75°C were investigated. This was accomplished by maintaining the requirements as described above. The catholyte in this case was 3.5 per cent Nacl. In the same manner, the $NiCo_2S_4$ catalyst was electrically connected to the steel to be protected and maintained at 10 mA/cm^2 hydrogen discharge current density. As expected, there was no H permeation current monitored for a long period. But, as soon as the $NiCo_2S_4$ catalyst was electrically disconnected, the H permeation increase fairly gradual to a maximum of just over 80 μA. To continue the protection of the steel, the $NiCo_2S_4$ was reconnected and within seconds, the H permeation current decreased fairly rapidly to its initial zero current.

But, under the same condition above, the H_2S was introduced into the 3.5% Nacl catholyte at 25°C. As soon as the H_2S was introduced into catholyte, H permeation was observed and it increased to maximum value of about 50 μA. At this H permeation current value (50 μA), the $NiCo_2S_4$ was electrically disconnected from the protected steel. Within seconds, the H permeation current shot up rapidly to about 200 μA maximum

current value which later decreased vary steeply as soon as the $NiCo_2S_4$ was electrically reconnected to protect the steel. At 75°C in the system, H permeation current (100 μA) was observed as soon as the H_2S was introduced into the catholyte, whilst the steel was being protected by the catalyst. But, after a prolonged time period, the catalyst was electrically disconnected from the protected steel. The H permeation current was observed to shoot up tremendously to a maximum value of about 500 μA within seconds. After short period, the $NiCo_2S_4$ was reconnected to protect the steel and simultaneously, the H permeation current was observed to decrease very steeply to a value little above its initial current value.

(c) Iron Sulphide Catalyst Used To Protect Steel From Hydrogen Embrittlement.

However, although the use of $NiCo_2S_4$ electrocatalyst in the above investigation have proved very effective, iron sulphide has been shown (chapter V) to possess high activity for hydrogen evolution. In this respect, it is surprisingly found that iron sulphide (ie. grades D from oxides of mixed chlorides and D from iron rust,both in chapter V) exhibited a low overpotential for the cathodic evolution of hydrogen, accordingly,these iron sulphide is suitable as an active catalyst for use in accordance with the present investigation. Thus, the effect of electrically connected iron sulphide electrode on the protection of steel from H embrittlement was investigated. Basically,

the above principle was used for the investigation. Thus, the iron sulphide electrode and the steel being protected were electrically connected and maintained at 10 mA/cm^2 H_2 discharge current in 3.5% Nacl at 25°C. There was no H permeation current, but as soon as the iron sulphide electrode was electrically disconnected from the steel, the H permeation current was monitored which increased to a maximum H permeation current (18 μA) which decreased to its zero value as soon as the iron sulphide electrode was reconnected to protect the steel.

In the presence of H_2S in the same system at 25°C, H permeation current (30 μA) was observed as soon as the H_2S gas was introduced into the 3.5% Nacl catholyte whilst the steel was being protected by the iron sulphide. However, at a prolonged time period, the iron sulphide was electrically disconnected from the protected steel and at the same time the H permeation current increased to about 80 μA within mintues. But, the steel was once more protected by reconnecting the iron sulphide electrode, the current (80 μA) was observed to decrease to about its initial value (30 μA). At 75°C, the introduction of H_2S into the 3.5% Nacl catholyte brought about H permeation current of about 60 μA whilst the steel was protected by the iron sulphide. When the iron sulphide was electrically disconnected from the steel being protected, the H permeation increased very sharply to a maximum value (210 μA).

(Note: the $NiCo_2S_4$ and iron sulphide electrodes used for the above investigations were prepared as described in chapter V, section 5.2.2)

(d) Protection Of Steel Under Tensile Stress From Hydrogen Embrittlement.

The effect of $NiCo_2S_4$ catalyst electrically connected to the steel membrane for the prevention of H embrittlement whilst the steel was under applied tensile stress was investigated. The two compartment cell and cell assembly both in Figs. 4.2 & 4.3 of chapter IV were used for the test. Basically, the steel membrane was connected to the $NiCo_2S_4$ electrode and maintained at 10 mA/cm^2 H_2 discharge current density. Initially, the steel membrane was at zero stress level at 10 mA/cm^2 H_2 discharge current density at the cathode side. There was no H permeation. The H permeation current was not observed even when the applied stress was increased from 0.00 N/mm^2 to 433 N/mm^2, but at 681 N/mm^2 stress level there was H permeation which attained a maximum value of 6 μA. After a considerable time period at the 681 N/mm^2 applied stress level, the $NiCo_2S_4$ catalyst was electrically disconnected and within seconds, the H permeation current was observed to increase very sharply to about 160 μA. Again, the $NiCo_2S_4$ was reconnected at the same stress level (ie. 681 N/mm^2); the H permeation was observed to decrease rapidly to its initial value. The final stress level 681 N/mm^2 was within the plastic deformation of the steel, thus when the stress was reduced to zero, the H permeation current further increased before an expected decrease. This observed phenomenon of an increase in H permeation current when the stress level is suddenly reduced to zero stress level has been explained earlier

as the lendency of steel member "squeezing out" of the unaccommodated H at the zero stress level. Thus, the effectiveness of this technique could possibly be extended to the protection of structures under the influence of service stress from hydrogen embrittlement in most environment.

6.2.1B. FORMATION OF ADHERENT CATALYST ON THE STEEL AS A METHOD OF PROTECTION FROM HYDROGEN EMBRITTLEMENT

(a) Protection of steel by the formation of electrocatalyst conducting coating.

The technique of electrically connecting the active catalyst to the steel whilst protected from H embrittlement, will not, in general, be suitable for use in the protection of pipes etc. and, for such applications, it is preferred to coat the active catalyst directly onto the surface to be protected.

This was realised by using a piece of 1 cm^2, 0.0381 cm thick of En42 steel membrane which was roughened with coarse emery paper 2.05g of Analar nickel nitrate and 4.10g of cobalt nitrate was dissolved in 10 cc of distilled water. The solution was pipetted onto the roughness side of the membrane. This membrane was then heated at 100°C for 2 hours in an oven, and the temperature was then raised to 400°C for one hour. Thereafter, it was transferred to a tube furnace and heated at 300°C for 10 hours whilst a continuous stream of carbon disulphide, CS_2 was passed over the specimen. The sulphur content of the $NiCo_2S_4$ coating was 24.8 per cent. The electrical resistance of the

coating on the steel support was 0.8 ohm and the thickness was about 0.0086 cm.

The $NiCo_2S_4$ coated surface of the steel membrane was made the cathode face in the two compartment cell Fig. 6.1. The effect of $NiCo_2S_4$ coating on the protection of steel from H embrittlement was observed to be greetly enhanced by this technique. This effect was however investigated in the presence of H_2S with and without the application 10 mA/cm^2 H_2 discharge current density to the cathode side of the membrane. Other methods of metal - catalyst bonding were investigated. These include the use of P.V.C. - catalyst and teflon - catalyst adherent mixtures, but these proved very ineffective possibly due to the formation of insulating coating and the presence of micro pores.

(b) The formation of iron sulphide coating on steel in situ

In accordance with the present work, the formation of iron sulphide with steel can readily be formed as a coating in situ. For instance, a coating of rust which has naturally or deliberately been formed on the steel surface can be readily be converted to iron sulphide by treatment with a suitable sulphur containing compounds ie. H_2S or CS_2. This has been achieved in this work by passing H_2S gas into 0.1M KOH in which the anodized steel was reduced in situ to form the iron sulphide. The steel was anodized at +200 mV Vs SCE for 30 hours in 0.1M KOH solution at 25°C and the H_2S gas was introduced for 10 hours before the test commenced in 3.5% Nacl catholyte. In the same manner,

the H_2S was introduced into the 3.5% Nacl catholyte. The H permeation current was observed as soon as the H_2S was introduced. This initial H permeation current was small but increase in the temperature of the bath further increasedthe H permeation current.

6.3. RESULTS

6.3.1. Electrical connection of steel to active catalyst

The concept of using a more active hydrogen evolution catalyst for the prevention of hydrogen embrittlement of steel in hydrogen environment etc. is based on the low-overpotential for hydrogen evolution possessed by these active catalysts. In this study, the use of active hydrogen evolution electrocatalysts ie. $NiCo_2S_4$ and iron sulphide prepared as described in chapter V, for the protection of steel from hydrogen embrittlement has been shown to prove effective. The current-voltage curve of teflon bonded $NiCo_2S_4$ electrode and a piece of steel for H_2 evolution in 0.1M KOH at 25°C has shown that the hydrogen evolution overpotential on $NiCo_2S_4$ is very much lower than of steel, Fig. 5.2 in chapter V.

This is shown in Fig. 6.2 in which a 1 cm^2 piece of PTFE bonded $NiCo_2S_4$ was connected electrically to the hydrogen evolution side of the steel membrane in the cell. As can be seen from Fig. 6.2, there was no hydrogen diffusion through the steel membrane when the $NiCo_2S_4$ electrode was connected (A-B). However, when the electrode was disconnected (C), the anodic current built up, indicating hydrogen permeation which continued

until the electrode was reconnected (D) when it dropped back to its original value (E).

The same is true when the experiments were performed in a flowing stream of H_2S in 0.1M KOH at 25°C and 75°C respectively as shown in Fig. 6.3. Figure 6.4 gives the corresponding results when the tests were done in the presence and absence of H_2S gas in 3.5% Nacl at 25°C and 75°C respectively. These results in Fig. 6.4 have shown that PTFE bonded $NiCo_2S_4$ is also effective for the protection of steel in Nacl solution even at above room temperature. Thus, Fig. 6.4 shows the results of an experiment similar to that described above with reference to Figs. 6.2 and 6.3. Curve 1 in Fig. 6.4 being 25°C in the absence of H_2S, curve 2 being for 25°C in the presence of H_2S. In each case, (A) represents the connection of the steel membrane and the PTFE/$NiCo_2S_4$/nickel screen electrode, (B) represents the commencement of galvanostatic H_2 discharge at 10 mA/cm^2, (C) the introduction of H_2S gas, (D) the disconnection of the membrane and the electrode and (E) their reconnection.

The tests for the protection of steel from hydrogen embrittlement were carried out using iron sulphide prepared from rust or oxides from mixed chlorides in the presence and absence of H_2S in 3.5% Nacl solution as the electrolyte. With reference to Fig. 6.2, Fig. 6.5 shows the effect on the hydrogen diffusion rate through the steel membrane when it is connected and disconnected to an iron sulphide electrode. The test was carried out in 3.5% Nacl solution at 25°C. The

iron sulphide electrode was connected and there was no diffusion of hydrogen A-B, but the diffusion current built up B-C as soon as the iron sulphide electrode was disconnected B and again reconnected C, the diffusion current decreased to E.

The same tests were carried out in the presence of H_2S in 3.5% Nacl solution at 25°C and 60°C respectively. In Fig. 6.6. (A) represents the connection of the electrode to the steel membrane. (A_1) the introduction of H_2S, (B) disconnection and (C) reconnection of the electrode. These results show the marked effect of the iron sulphide electrode on the rate of H_2 diffusion through the steel membrane. Thus, these results confirm the suitability of iron sulphide as an active substance for use in the present work.

The diffusion of H into steel has been shown to increase with tensile stress on the steel (chapter IV). The effect of protecting H embrittlement in steel under tensile stress has been investigated. Fig. 6.7 shows (A) the electrical connection of $NiCo_2S_4$ to steel under tensile stress and there was no H-diffusion until the stress reached 681 N/mm^2 but at (C), the electrode was disconnected at the same applied tensile stress 681 N/mm^2, the diffusion current built up (CD), reconnection at (D), the diffusion current decreased to (CE). The applied stress was finally decreased to 0.00 N/mm^2 and the current increased to (EF). Thus, the active catalyst has proved its capability towards protecting steel under stress from H permeation.

6.3.2. Steel is coated with active catalyst against H embrittlement protection

In order to minimize the dissociation of H_2S on the steel whilst protected by electrically connected to the active catalyst, the catalyst was coated on to the steel before exposure to H_2S environment. The steel and an uncoated sample of steel were then tested in the two compartment cells as described above. Results in Fig. 6.8 are far more promising than the uncoated specimen ($\sim$12 $\mu A/cm^2$) as opposed to 55 $\mu A/cm^2$ for an unprotected specimen; 26 $\mu A/cm^2$ as opposed to 124 $\mu A/cm^2$ at 75°C). All the tests were conducted in 3.5% Nacl solution in stream of H_2S. In all these tests, the side of the membrane which was exposed to H_2S was not subjected to galvanostatic control of H_2 discharge. Thus, the effect of H_2S dissociation on the H_2 permeation rate was evaluated (ie. the other side of the membrane was controlled at an anodic potential to de-electronate the hydrogen ie. - 410 mV Vs SCE).

However, Fig. 6.9 shows the effect of holding the H_2S side at 10 mA/cm^2 galvanostatic current density. This again shows the $NiCo_2S_4$ coated specimen is far better than the unprotected specimen in reducing the rate of H permeation.

In the case of steel coated with iron sulphide, the steel was anodized and reduced in a stream of H_2S. The H-diffusion on this specimen was conducted in 3.5% Nacl solution at 25°C.

6.4. DISCUSSION

The significance of the results obtained from this investigation is that it provides one possible method of protecting the steel or any metal alloy from hydrogen embrittlement. Thus, this technique ensures that when the steel is being corroded, the cathodic hydrogen evolution reaction occurs on a highly efficient sites instead of on the corroding surfaces. In this way, the absorption and permeation of H into the steel is minimized and the hydrogen embrittlement is prevented. The supression of the H permeation by electrically connecting and/or bonding the active catalyst to the steel to be protected is the manifestation of the immense effective activity of these catalystsused in this respect. The active catalysts possess very low hydrogen over-potential, high corrosion resistant and most importantly they are not poisoned by H_2S because they prepared from it. Therefore, it could be used both in 'sour' and 'sweet' corrosion environments.

In 'Sour' corrosion environment ie. the introduction H_2S in the electrolyte shows the H permeation current is observed due to dissociation of H_2S on the steel whilst protected by the catalyst, Figs. 6.3, 6.4 & 6.6. In this respect, coating or bonding active catalyst on the steel before exposure to H_2S is highly recommended. However, care must be taken to ensure that the bonded catalyst and steel substrate being protected are in electrical contact. In such an application, since the catalyst is so much more active than steel, it will function

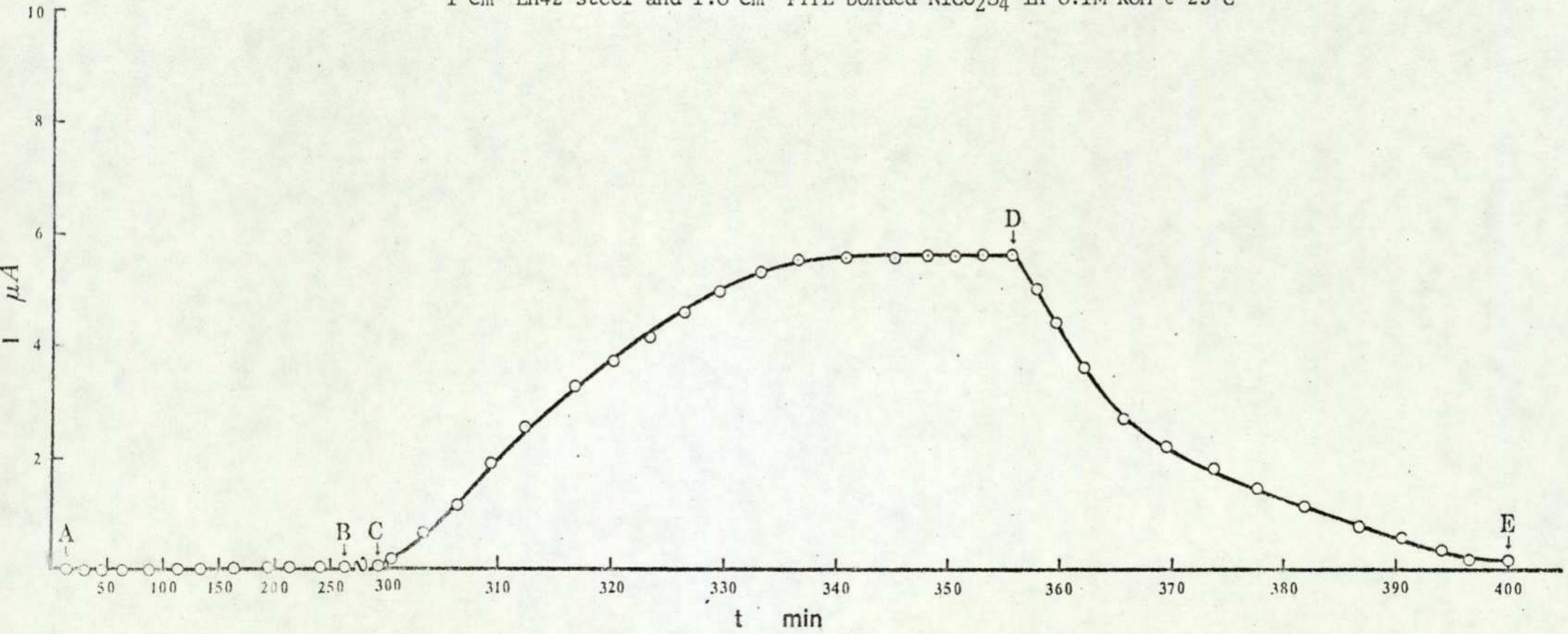
more than adequately provided the catalyst - metal bond is mechanically stable.

Thus, there is a possibility of incorporating $NiCo_2S_4$ or iron sulphide as a part of a conducting paint system. This will open the possibility of using it both in sour pipes as well as other marine structures and in other areas where hydrogen embrittlement could be a problem. Therefore, the technique proposed in this work ie. the idea of using active hydrogen evolution catalyst to prevent the possibility of hydrogen embrittlement of steel is novel and possibly will open a new prospect towards prolonging the life span of metallic alloys in most environments.

Fig. 6.2. Effect on connecting a $NiCo_2S_4$ electrode on the H_2 permeation rate of steel, H_2 evolution current density maintained at 10 mA/cm^2

AB : catalyst connected to the steel
C : catalyst disconnected from steel
CD : H permeation current
DE : catalyst connected

1 cm^2 En42 steel and 1.0 cm^2 PTFE bonded $NiCo_2S_4$ in 0.1M KOH @ 25°C



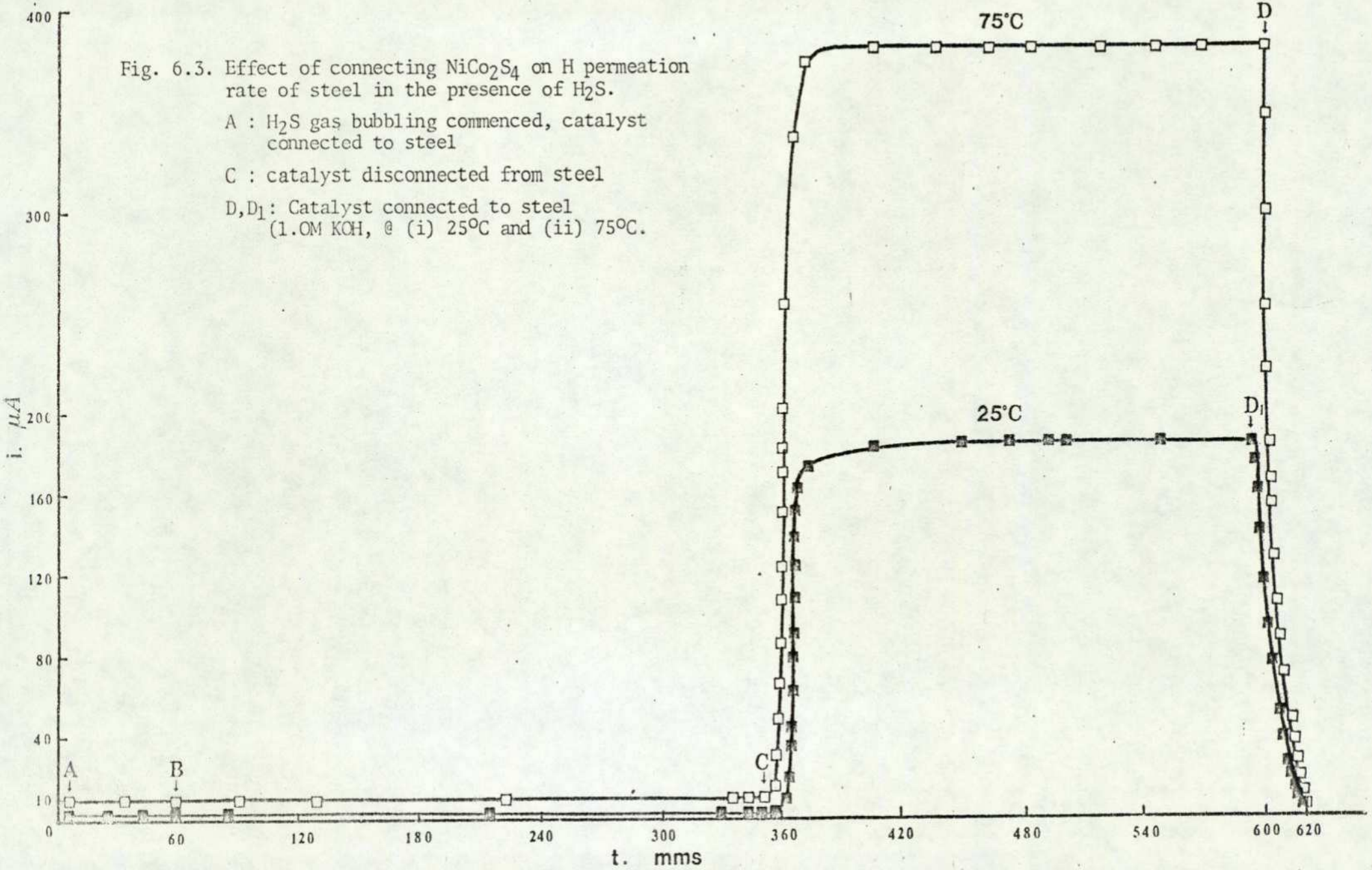


Fig. 6.3. Effect of connecting $NiCo_2S_4$ on H permeation rate of steel in the presence of H_2S.

A : H_2S gas bubbling commenced, catalyst connected to steel

C : catalyst disconnected from steel

D, D_1: Catalyst connected to steel (1.0M KOH, @ (i) 25°C and (ii) 75°C.

Fig. 6.4. Effect of connecting the catalyst on the H-permeation rate of cell in the presence and absence of H_2S in 3% Nacl solution.

A : Steel (En42) and $NiCo_2S_4$ connected

B : Galvanostatic H_2-discharge commenced at 10mA/cm2

C : H_2S gas introduced into 3% Nacl solution.

D : Catalyst is disconnected from steel

E : Catalyst is connected to steel

(3% Nacl solution maintained at

(a) 25°C in the absence of H_2S

(b) 25°C, and

(c) 75°C both in the presence of H_2S.

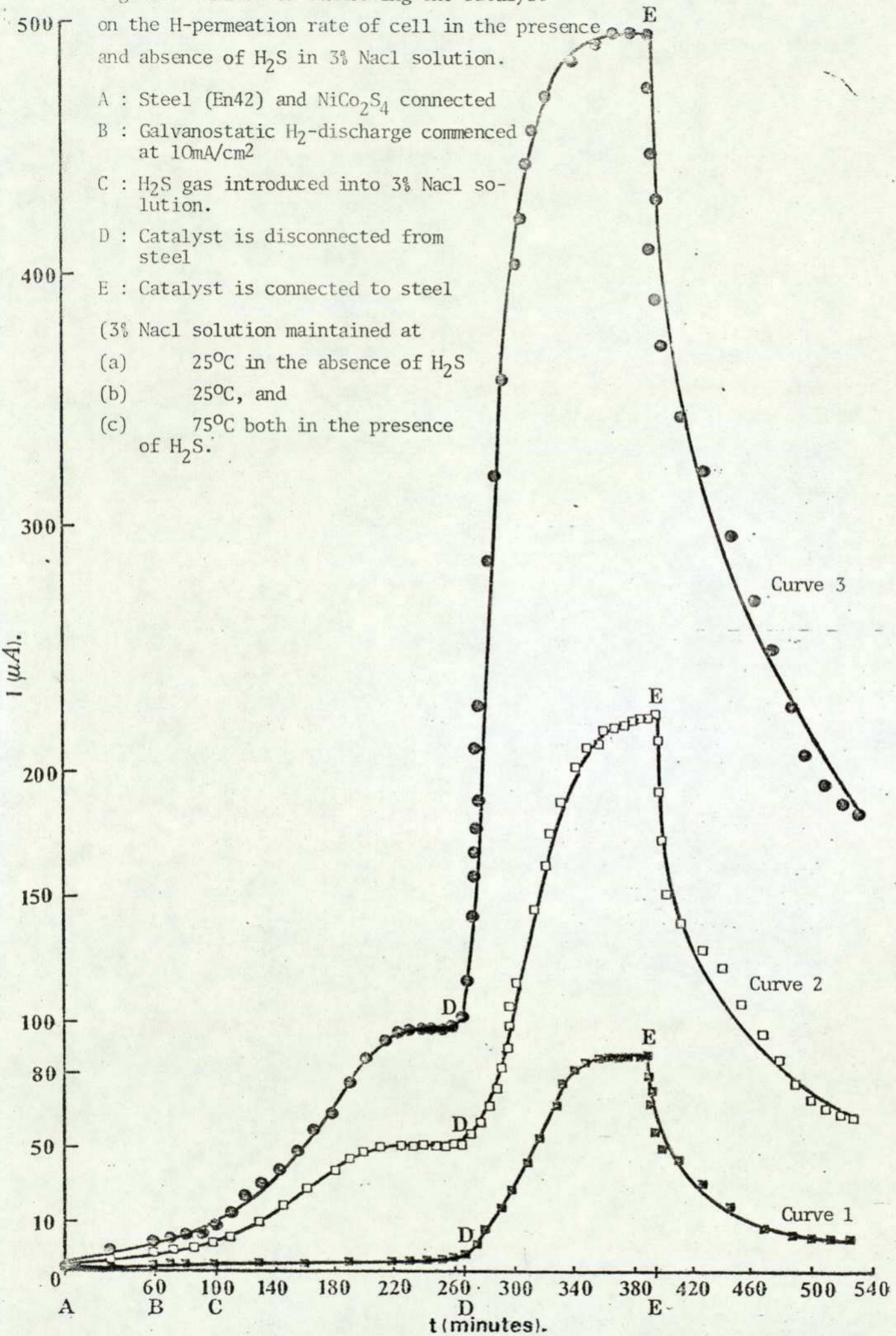


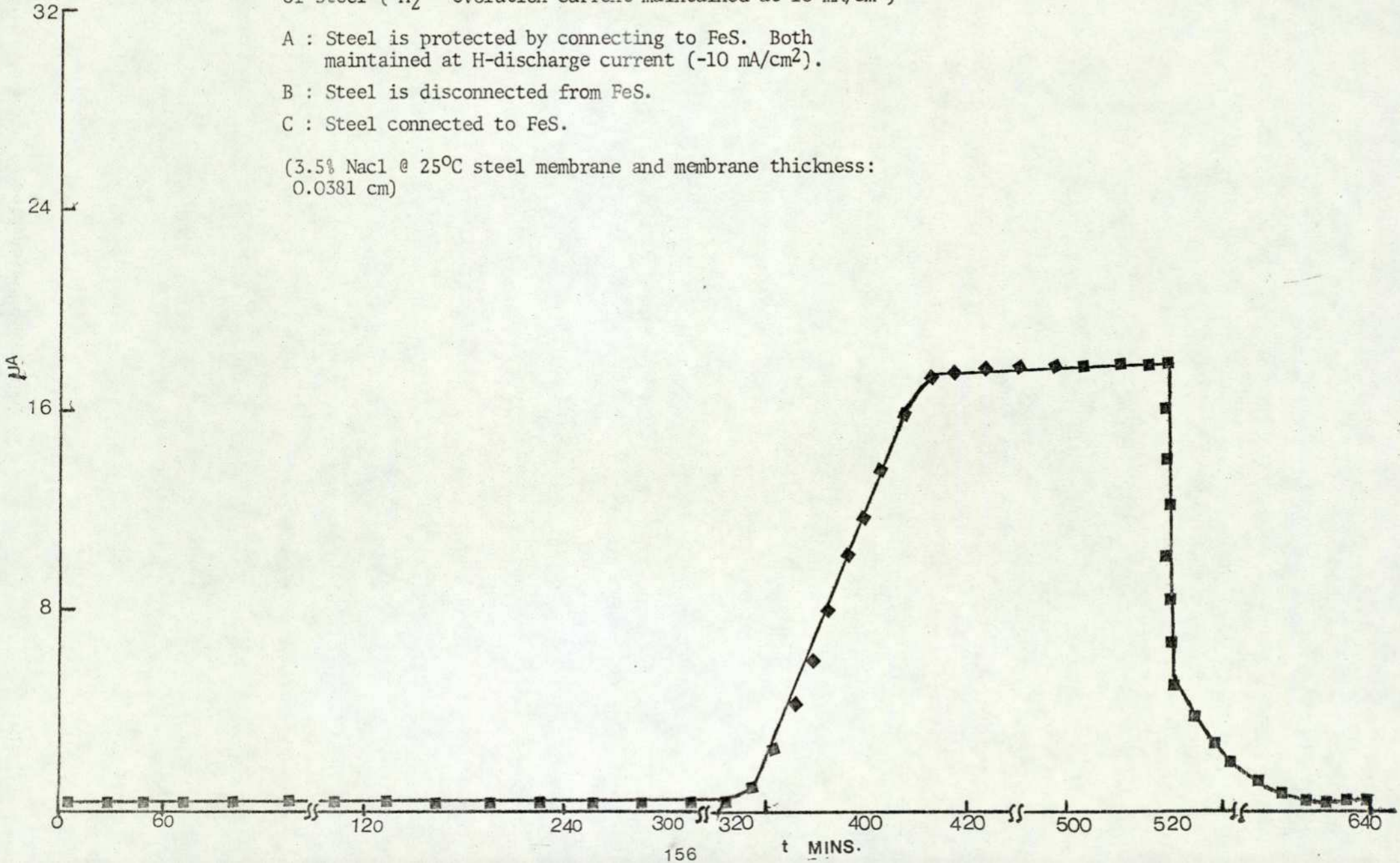
Fig. 6.5. Effect of connecting FeS electrode on the H-permeation rate of steel (H_2 - evolution current maintained at 10 mA/cm^2)

A : Steel is protected by connecting to FeS. Both maintained at H-discharge current (-10 mA/cm^2).

B : Steel is disconnected from FeS.

C : Steel connected to FeS.

(3.5% Nacl @ 25°C steel membrane and membrane thickness: 0.0381 cm)



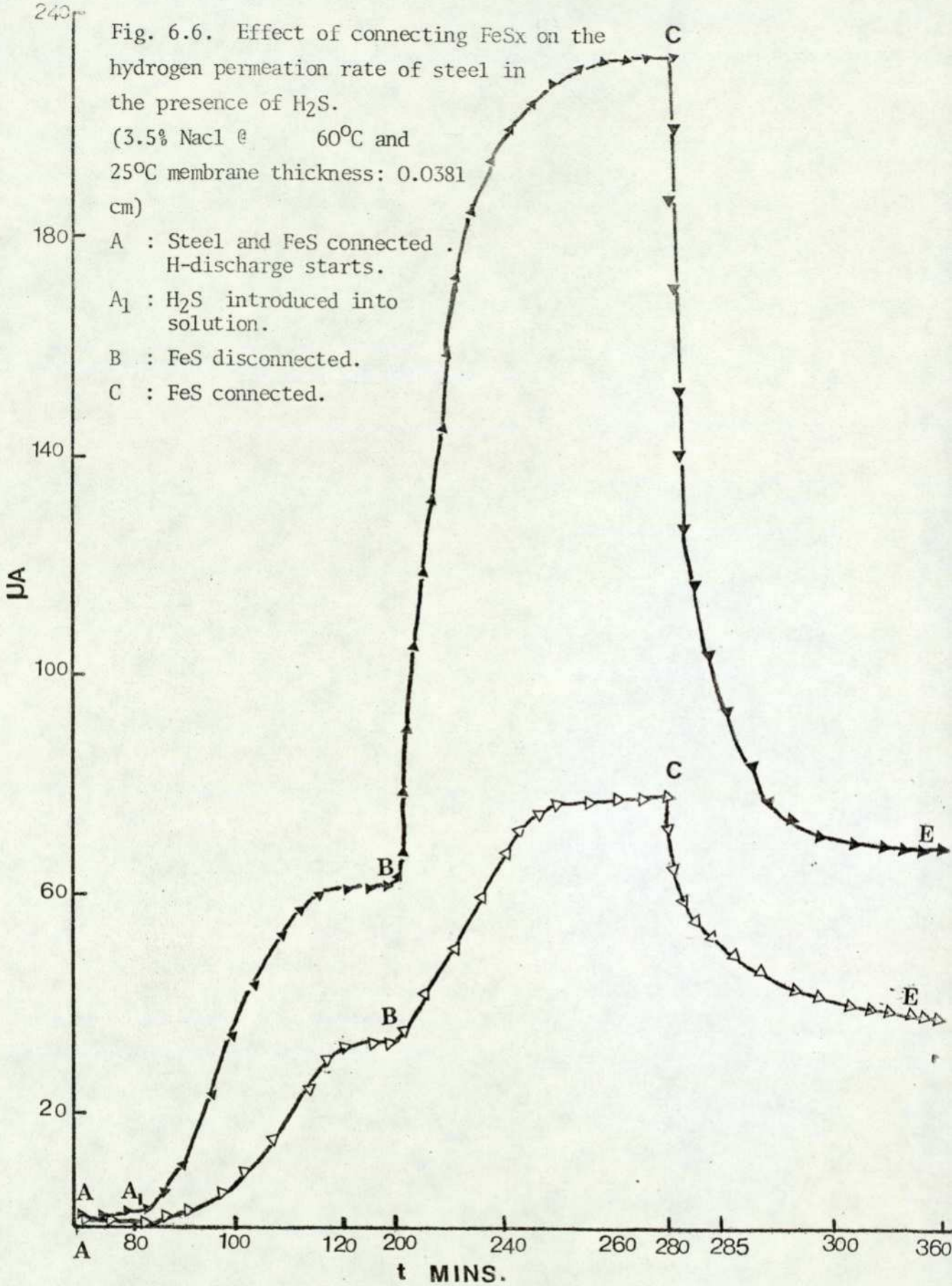


Fig. 6.6. Effect of connecting FeSx on the hydrogen permeation rate of steel in the presence of H_2S.
(3.5% Nacl @ 60°C and 25°C membrane thickness: 0.0381 cm)

A : Steel and FeS connected . H-discharge starts.

A_1 : H_2S introduced into solution.

B : FeS disconnected.

C : FeS connected.

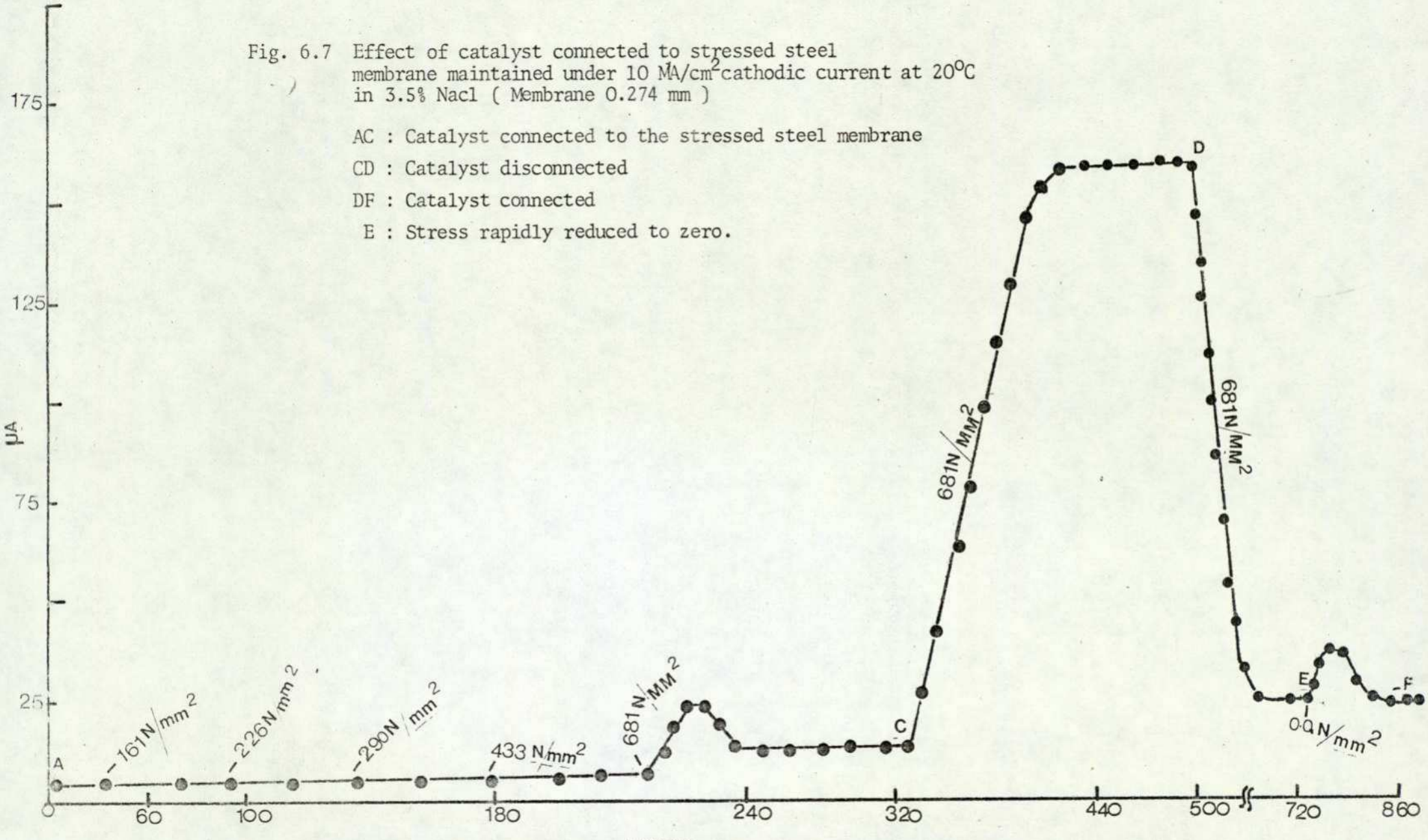
Fig. 6.7 Effect of catalyst connected to stressed steel membrane maintained under 10 MA/cm^2 cathodic current at 20^{0}C in 3.5% Nacl (Membrane 0.274 mm)

AC : Catalyst connected to the stressed steel membrane

CD : Catalyst disconnected

DF : Catalyst connected

E : Stress rapidly reduced to zero.



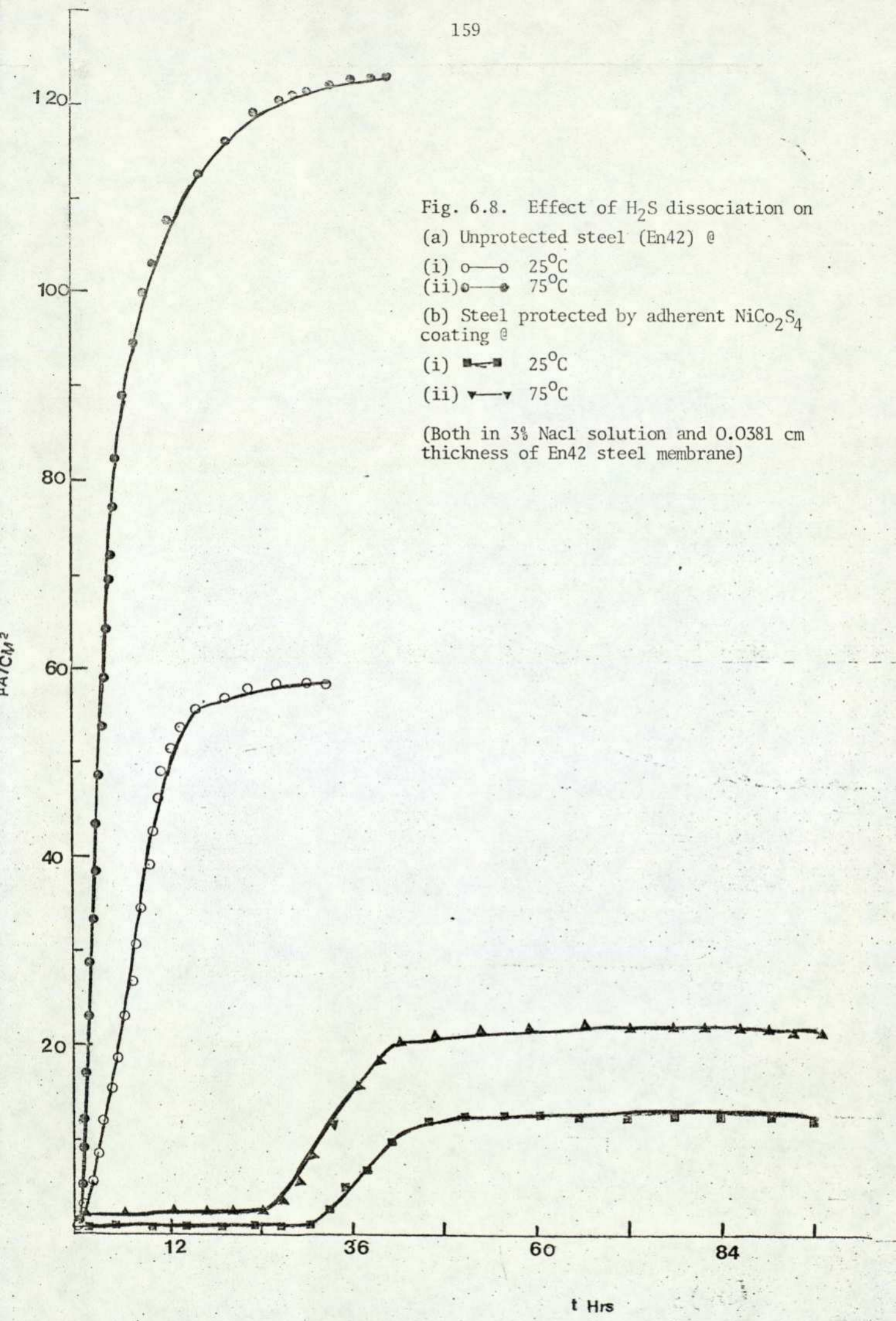


Fig. 6.8. Effect of H_2S dissociation on

(a) Unprotected steel (En42) @

(i) o—o 25°C
(ii) o—● 75°C

(b) Steel protected by adherent $NiCo_2S_4$ coating @

(i) ■—■ 25°C

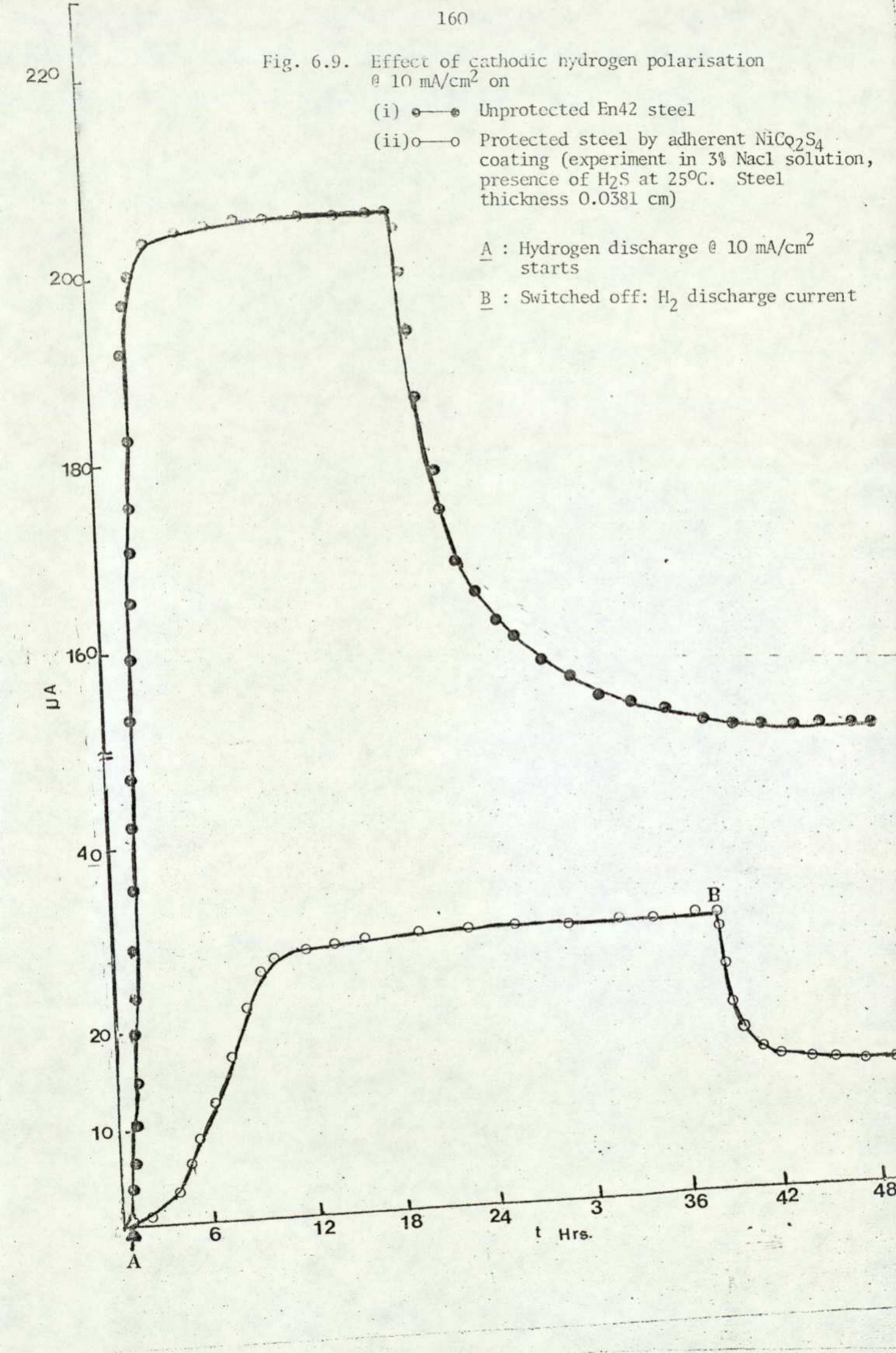
(ii) ▼—▼ 75°C

(Both in 3% Nacl solution and 0.0381 cm thickness of En42 steel membrane)

Fig. 6.9. Effect of cathodic hydrogen polarisation @ 10 mA/cm^2 on

(i) ⊙——⊙ Unprotected En42 steel

(ii) o——o Protected steel by adherent $NiCo_2S_4$ coating (experiment in 3% Nacl solution, presence of H_2S at 25°C. Steel thickness 0.0381 cm)



CHAPTER SEVEN

CONCLUSIONS AND SUGGESTION FOR FURTHER WORK

CHAPTER VII

7.1. CONCLUSIONS AND SUGGESTION FOR FURTHER WORK

7.1.1. Conclusions

A prior assessment of the susceptibility of metallic material to stress corrosion cracking could possibly be one of the ways of preventing SCC. Traditional methods often used for the assessment of metallic material susceptibility to SCC have proved time consuming, and in one particular case, the determination of K_{ISCC} is quick only in H_2S environment. But, H_2S being very toxic, elaborate safety conditions are required before this method could be used. Thus, this makes its adoption for K_{ISCC} determination very cumbersome and unattractive for potential users.

The significance of the present finding is that K_{ISCC} determination for metallic material is made simple, rapid and reliable. Thus, the adoption of the electrochemical technique introduced in this work could possibly provide a better technique for the assessment of the susceptibility of material to SCC by a more accurate determination of K_{ISCC}.

Stress corrosion cracking and hydrogen embrittlement are the combined insidious form of failure of metallic structure in most environment. This combined effect makes the mechanism of failure of a corroding structure under the influence of service load very unreliable to elucidate, consequently the application of preventive measures are often confusing. Thus, the isolation of hydrogen evolution from the corroding metallic structure

could be a better technique of protecting a metallic structure from hydrogen embrittlement.

In this respect, the present work has introduced the use of some active hydrogen evolution electrocatalysts to isolate the hydrogen evolution from a corroding structure. The significance of the use of the active electrocatalysts (ie. $NiCo_2S_4$ and for iron sulphide) are:-

(i) It has been proved in this work that the idea of using an active hydrogen evolution catalyst to reduce the possibility of hydrogen embrittlement of steel is effective,

(ii) Since the H_2 evolution over-potential on the active electrocatalysts is much lower than for steel during the corrosion of the steel the H_2 evolution would prefer the active sites on the electrocatalyst instead of on steel.

(iii) The active catalyst ie. $NiCo_2S_4$ and iron sulphide could function even in H_2S environment, and

(iv) The active electrocatalyst could possibly be incorporated as a part of paint system for use in 'sour' pipes and other marine structures and other areas where hydrogen embrittlement is a problem.

Thus, these techniques introduced in this work for the determination of K_{ISCC} value and the isolation of hydrogen evolution from a corroding metallic structure should throw light on the choice of material in the design of components and possibly eliminates the failure of such components by hydrogen embrittlement.

7.1.2. Suggestions For Further Work

The method of the determination of K_{ISCC} proposed in this work can detect any crack growth, as long as electrolyte can penetrate into the crack. This principle has been confirmed by the different electrochemical steady state and pulse techniques used in this work for various environments. Two parameters were determined in these measurements ie. the applied mechanical tensile load which was operated manually while the current was recorded by the electronic potentiostat. The determination of K_{ISCC} could further be improved, by providing an automatic device for the application of the load levels and an integration of an X-t pen recorder to monitor the current and the corresponding load levels.Such an automatic test assembly could improve the rate of testing, provided the test specimens are adequately insulated.

The significance of the prevention of H_2 embrittlement in steel proposed in this work is to ensure that when the steel is being corroded, the cathodic hydrogen reaction occurs on highly efficient $NiCo_2S_4$ sites instead of on the steel. In this way, the amount of Hads available to cause H embrittlement in the steel will be greetly reduced. The method of application of the active catalyst proposed in this work by connecting the active catalyst electrode to the steel is useful in mechanistic studies and protection against hydrogen embrittlement of a metal which is being electroplated. It could

prove impossible to use such configuration in a real industrial situation, therefore, it is necessary to devise methods of improving on the formation of adherent $NiCo_2S_4$ and iron sulphide coating on steel as proposed in this work.

In this respect, it will be very desirable to determine the actual composition, operating conditions, typical concentrations of water, Cl^-, H_2S, $H\,Co_3^-$ level in oil and gas pipe lines as well as protective procedures in current use. This information will then enable the application of the active catalyst under more realistic conditions. Also, it will assist to examine the effectiveness of various coating methods ie.

(i) The decomposition of nickel-cobalt nitrates onto the steel substrate followed by reaction with CS_2 to form the $NiCo_2S_4$. The use of CS_2 instead of H_2S will reduce the possibility of hydrogen permeation into the steel during the coating process.

(ii) Electrophoretic deposition of $PtFe/NiCo_2S_4$ dispersion onto steel substrates, followed by curing at 300^o - 350^oC. The use of electrophoretic deposition should enable the interior of pipes to be coated effectively on an industrial scale.

(iii) It will be necessary to evaluate the use of $NiCo_2S_4$ or iron sulphide as an admixture to existing protective paint systems. In order for this process to work, it is necessary

to ensure that the $NiCo_2S_4$ or iron sulphide phase is continuous. If the active catalyst particles are electrically insulated by the paint components, the particles cannot function at all. Thus, it will be desirable to examine the coatings by scanning electron microscopy and electrical resistivity measurements.

Possibly, a life long electrochemical evaluation tests could be recommended for each coating system under varying conditions, such as temperature, pH in 'sweet' and 'sour' oil and/or gas environment. At the same time, the coated steel substrate could be tested under the applied tensile stresses for hydrogen embrittlement susceptibility. Finally, a further in situ formation of adherent iron sulphide on the steel substrate could be very effective, hence this technique is highly recommended for further improvement.

REFERENCES

1. Uhlig, H.H. 'The cost of corrosion to United States' Chem. Engineering News, 27, 2764, 1949 and (ii) Corr. Sci. 6, 29, 1950.

2. Controlling Corrosion Vols. 1-6. Department of Industry, Committee on Corrosion Pub. by Dept. of Industry and the Central Office of Information (CFIT), London 1976.

3. Henthorne, M. Corrosion and the Process Plant: Collection of Chemical Eng. Reviews 1971 - 1972; (ii) Carpenter Technology Corp., Chem. Eng. Refresher Parts, 159, Sept. 1971.

4. Ashworth, V. Boden, P.J., and Leach, J.S. On the Cl^- breakdown of passive film on mild steel. Corrosion Sci. 10, 481 - 488, 1970.

5. Fontana, M.G. and Greene, N.D. Corrosion Engineering. Pub. McGraw-Hill N.Y. 1967.

6. Scully, J.C. Fundamentals of Corrosion, Pub.Pergamon 2nd Ed. Oxford, UK. 1975.

7. Shrier, L.L. Corrosion Vol.I, Metal/Environment Reaction Pub. Newness Butter worths, 2nd Ed. London, 1978.

8. Hoar, T.P. The Production and Breakdown of the passivity of metals. Corr. Sci. 7, 381 & 481, 1967.

9. West, J.M. Electrodeposition and corrosion processes Pub. Van Nostrand. NY 81, 1961.

10. Wagner,C and Grunewald, K. Z Phys. Chem. 40, 455, 1938.

11. Butlin, T., Vernon and Whiskin, L. Symposium on corrosion of buried metals iron and steel Inst. P.29, London, 1951.

12. Farrer, T., Bick,L., and Wormwell, F., J. Appl. Chem. 3, Part 2, 80, 1953.

13. Stern, M. Corrosion polarisation studies, J. Elechem. Soc. 102, 609 and 663, 1955 with Greasy bid 104, 56, 1957.

14. Pourbaix, M. Atlas of Electrochemical Equilibria in Aqueous Solutions, Pub. Pergamon Press, N.Y. 1966.

15. Pourbaix, M. Corr. 25, 6No., 267, 1969.

16 Passive Film breakdown due to chloride ion, J. Electrochem. Soc. 119, 572, 1972.

17. Schroeder, W.E., Berk,A.A. and O'Brian, R.A. Effect of oxidizing agents. Metal and alloys 8, 320, 1937.

18. Agard: Stress Corrosion Cracking (SCC) in Aircraft Structural Material, Conference Procs. Series No. 18, 1967.

19. Rhodin, thor.ed. Phys. metallurgical of stress corrosion fracture, Interscience, N.Y. 1959.

20. Logan, H., Stress corrosion of metals, Pub. John Weley & Sons, London, 1967, and (ii) J. Research N.B.S. 61, 503, 1958.

21. Brown, B.F. Stress corrosion cracking controll measures, Pub. USA Dept. of Commerce, Wash. D.C. June, 1977.

22. Greenfield, P. Mechanical Engineering: Stress Corrosion failure M & B Monograph, London, 1971.

23. Scully, J.C. Ed. "The theory of stress corrosion cracking in alloys" Procs. of NATO Science Committee Conference, Brussel, December 1971.

24. Smith, H.R., Piper, D.E., Stress corrosion cracking in high strength steels and Titanium and aluminium alloys and (ii) Brown, B.F., Ed. Naval Research Laboratory, Wash.D.C. 18, 17, 1972.

25. Pascoe, K.J. An introduction to the properties of engineering material, Chapters 11 & 12. Pub. Blackie, Glasgow, 1963.

26. Stress corrosion cracking of metals, A state of the art, ASTM special tech. Publication No. 518, Phil Pa Metal Conference 18th October, 1971.

27. (i) West, J.M. Metal Science Journal 7, 169, 1973.
(ii) or Parkins, R.N. British Corrosion Journal 7, 15, 1972.

28. Hoar, T.P. "Proc. of the 2nd International Congress on metallic corr." P.14, Houston, Texas, 1966.

29. Irwin, G.R. and Wells, A.A. Met. Review 10, 223, 1965.

30. Nielsen, N.A. A study of crack propagation in S.C.C. Corrosion 20, 105t, 1964.

31. Hoar, T.P., and Hines, J.G. J. Iron Steel Inst. 182, 124, 1956.

32. Parkins, R.N., Proc. Conference of SCC and Hydrogen Embrittlement of iron base alloys. NACE, 1971.

33. Harston, J.D.and Scully, J.C. Corr. 26, 387, 1971.

34. Hoar, T.P. and Hines, J.G. International Committee for Electro-chem. Thermodynamics and Kinetics (C.I.T.C.E.), Proc. of 18th meeting, Madrid, 1956, Pub. Butterworth, London, P.273, 1958.

35. Hoar, T.P. and West, J.M. Nature 181, 835, 1958.

36. Tysack, C. British Corrosion Journal, 6, 124, 1971.

37. Knott, J.F. Fundamental of fracture mechanics, Pub. Butterworth, London, 1973.

38. Wells, A.A. The application of fracture mechanics to SCC Testing. Spring meeting on fracture mechanics. Metals and material 3, 173, 1969. (ii) Scully, J.C. 1bid p.174.

39. Mostovoy, S., Crosley, P.B. and Ripling, E.J. Use of crack-live-headed specimen for measuring plain fracture toughness, J. Material 2, 661, 1967.

40(i) American Society for Testing and Material (ASTM) Stress Corrosion testing, special technical Publication No. 425, 1965.

(ii) British Standard Inst. - method for plane strain fracture toughness K_{1c} Testing. Pub. London, 1971.

41. Brown, B.F. The application of fracture mechanics to stress corrosion cracking metallurgical review 2, 171, 1968.

42. Fracture toughness testing and its application (ASTM) special publication No. 381, Phild. Pa 1967.

43. West, J.M. A general model for stress corrosion crack propagation, Metal Science Journal 7, 169, 1973.

44. Parkins, R.N. Metallurgical Review 9, No. 35, 201, 1964.

45. Cater, C.S. Engineering Fracture Mechanics No.1, 3, 1-13, July, 1971.

46. McIntyre,P., Proc. Institute of metallurgists. The practical implications of fracture mechanisms, P88, March, 1973.

47. Peisl, H. Topics in applied physics: Hydrogen In Metals Vol.I. Ed. G. Alafeld and Völkl Series 28, Pub. Berlin Heidelberg, N.Y. 1978.

48. Ubbelohde, A.R. Proc. Roy. Soc. 159A, 295, 1973, and in J. Chem. Soc. 1143, 1950.

49. Isenberg, I. Phys. Review 79, 736, 1950.

50. Wiswall,R. Hydrogen storage in metals, Vol.II. "Application - orientated properties" Ed. Alefeld G and Völkl,J. Pub. Springer - Verlag, N.Y. 1978.

51. Davanathan, M.A. Starchurski,Z. and Becks, W. A technique for the Evaluation of Hydrogen embrittlement characteristic of electroplating Baths. J. Electrochem Soc. 8 No. 110, 886, 1963.

52. Barrer, R.M. Trans Faraday Soc. 36, 1235, 1940.

53. McBreen, J., Nanis, L. and Beck, W. A method for determination of the permeation rate of H through metal membrane. J. Electrochem Soc. 113, 1218, 1966.

54. Bockris, J. O'M.; McBreen,J., and Nanis, L. The hydrogen evaluation kinetics and hydrogen entry into α - iron. J. Electrochem Soc. 112, 1025, 1965.

55. Glass, A.L., Taylor, E., and Beck, W. The role of adsorbed CN^- groups in the hydrogen embrittlement of steel. J. Electrochem Soc. 112, 53, 1965.

56. Kabozev, W.and Montblanova, V.
Zhur, Fiz. Kim, 6, 38t, 1952.

57. Montblanova, V. and Kabozev, W.
Acta Physiochim. U.S.S.R. 1, 611t, 1936.

58. Vaughan, D.A. and Phalen, D.I.
Reaction contributing to the formation of susceptible paths for stress corrosion cracking, stress corrosion testing, ASTM special tech. paper No. 425, 209, 1967.

59. Becks, W., Bockris, J.O'M, McBreen, J and Nanis, L.
Hydrogen permeation in metals as a function of stress, temperature and dissolved hydrogen concentration. Proc. Roy. Soc. 290, 220, 1966.

60. Heyrovsky, Horiuti and Okamoto, sited in Bockris, J.O'M. Kick, D.F.A. J. Phys. Chem. 65, 1941, 1961.

61.(i) Brown, D.B., Ericeira, Conference 186, 1971.
(ii) Snape, E. British Corrosion Journal 4, 253, 1969.
(iii) Kennedy and Whittaker, J.A. Corr. Sci. 13, 513, 1973.

62. Dawson, J.L. Paper presented at the Hot Riser Corrosion Symposium, CEGB Sudbury House, 19th Feb. 1979.

63. Tomashov, N.D. Corrosion Science 1, 77, 1961.

64. Bockris, J.O'M., Damjanovic, A. and Mannam, R.
J. Electroanal. Interfacial Electrochem. 18, 349, 1968.

65. Mills, M.H. and Thomason, A.M. J. Electrochem. Soc. 123, 1459, 1976.

66. Tseung, A.C.C. and Man, H. British Patent Application No. 44362/77, 25th October, 1977.

67. Man, M. "High performance hydrogen evolution electrocatalyst in alkaline media". PhD thesis, The City University, London, May, 1978.

68. Rogers, T.H. An introduction to marine corrosion, Pergamon 2nd Ed. London, 1975.

69. Laque, F.L. Marine corrosion, Pub. John Wiley and Inc. Canada, 1975.

70. Devin, M.T. and Wells, L. Anodic polarisation behaviour of an Amorphous metal sricpta metallurgica, 10, 309, 1976.

71. Vogel, A.I. A Text Book of Quantitative Inorganic Analysis, Including Instrumental Analysis, Pub. Longmans, 3rd Edition P917 London, 1961.

72. Luther, R.G. and Williams. Changes in static yielding of a ferritic steel during fatigue cycle. J. of Metals 11, 164, 1977.

73. Everett, K.G., Drem, L.A. and Ericson, S.J. The FeII/FeIII and quinone-hydroquinone reaction on oxygen covered rhodium electrode. J. Electrochem. Soc. 125, 3 No. 289, 1978.

74. Damaskin, B.B. "The Principles of Current Methods for the Study of Electrochemical Reactions,Scripta Technical, Inc. Special paper, Pub. McGraw-Hill, N.Y. London, 1968.

75. Bockris, J.O'M. and Reddy, A.K.N. Modern Electrochemistry Vol. 2. A plenum/Rosetta, 2nd Ed. N.Y. 1976.

76. Delahay, P. Double Layer Electrode Kinetics, Pub. Interscience, New York, Chapter 7, P153, London.

77. Onuchukwu, A.I., Chan, H.C. and Tseung, A.C.C. An Electrochemical Method for Detecting Threshold Corrosion Science 19, 209, 1979.

78. Onuchukwu,A.I. 'A study of stress corrosion of steel in sea water', M.Sc desertation, The City University, Northampton Square, London, EC1. 1977.

79. Onuchukwu, A.I., Chan, H.C. and Tseung, A.C.C. The application of potentiostatic pulse method for the determination of critical stress intensity factor for stress corrosion. Electrochem. Soc.,Spring Meeting, Extended Abstract Vol. 79-1, P140, May 6th, 1979.

80. Bockris, J.O'M, McBreen, J and Nanis, L. The hydrogen evolution kinetics and hydrogen entry into - iron. J. Electrochem. Soc. 112, 1025, 1965.

81. Davanathan, M.A.V. O.N.R. Technical Report No. 4, 1961, and Trans Faraday Sec. 56, 1820, 1960.

82. Troiano, A.R., Berth, C.F. and Steigerwald, E.A. Corrosion 25, 353, 1969.

83. Davanathan, M.A.V. and Stachurski, Z. The mechanism of hydrogen evolution on iron in acid solution by determination of permeation rate. J. Electrochem. Soc. 111, 619, 1964.

84. Davanathan, M.A.V. and Stachurski, Z. Proc. Roy. Soc. A270, 90, 1962.

85. Moffatt, W.G., Pearsall, G.W. and Wulff, J. The structure and properties of material Vol. 1, Structure Pub. Wiley, N.Y. 2nd Ed. 1966.

86.(i) Kabozev, W. and Montblanova, V. Acta Physiochim. U.S.S.R. 1, 611, 1936.
(ii) Zhur, Fiz. Khim 6, 38, 1952.

87. Bockris, J.O'M "Modern aspects of electrochemistry" chapter 4. Pub. Butterworth, London, 1972.

88. Wood, G. Private Communication Reported in J. Electrochem. 110, 886, 1963.

89. Stross, T.M. and Tompkins, F.C. 49, The diffusion coefficient of hydrogen in iron. J. Electrochem. P230, 1956.

90. Heinrich, R.R., Johnson, C.E. and Gronthamel, C.E. Hydrogen permeation studies. J. Electrochem. Soc. 112, 1067, 1965.

91. Smithels, C.J. and Ransley, C.E. Proc. Roy. Soc. A152, 706, London, 1935.

92. Vaughan, D.A., and Phalen, D.I. The effect of hydrogen on the structural properties of stainless steel as related to its corrosion behaviour. Metals Engineering Quarterly 3, 5 No., 39, Aug. 1965.

93. Phalen, D.I. and Vaughan, D.A.
The role of surface stress on hydrogen absorption by 4340 steel. Corrosion - Nacl 24, 8No., 243, 1968.

94. Coutts, J.A. and Coombs, A.J. "Preparing a metal specimen for the installation of a bonded resistance strain gauge". Strain Vol 5 3No., 1969 and (ii) "A method of installing a strain gauge" Strain Vol. 5 2No. 1969.

95. Flinn, R.A. and Trojan, P.K. Engineering materials and their applications, chapter 11, P378, Publ Houghton & Mifflin Hopewell, N.J. London, 1975.

96. Van Vlack. Elements of material science, an introduction text for engineering students. Chapter I, P2, Pub. Addison-Wesley, Inc. Sydney, London, 2nd Ed. 1973.

97. Design Engineering. Material selector and design guides. Material special publication, No. 74, London, 1972.

98. Mills, R.L. and Edeskuty, F.S.
Test for hydrogen embrittlement of steels used in tank farm cylinders. Loss Alamos Sci. Laboratory. U.S.A.E.C. Report LA - 3602, October, 1966.

99. Morlett, J.G., Johnson, H.H. and Troiano, A.R.
J. Iron and Steel, 189, 27, 1958.

100. William, L.O. Electrolysis of sea water special paper. Martin Marietta Aerospace. Denver, Colorado, and Design News, 25 No. 1, 74, 1970.

101. Gregory, D.P., NG, D.Y.C. and Long, G.M.
The electrochemistry of cleaner environments (Ed. J.O'M Bockris), Pub. Plenum Press, N.Y. 1971.

102. Bockris, J.O'M. and Wroblowa, H. J. Electroanal. Chemistry 7, 428, 1964 and J. Phys. Chem. 26, 532, 1957.

103. Parsons, R. Discussion Faraday Soc. 45, 40, 1968 and (ii) Breiter, M.W. and Clamroth, R.
Z. Electrochem. 58, 493, 1954.

104. Mills, M.H. and Thomason, M.A.
J. Electrochem. Soc. 123, 1459, 1976.
(ii) Trasatti, S. J. Electroanal. Chem. 39, 163, 1954,

105. Greeness, M., Thompson, M.W. and Cohn, R.W.
J. Appli. Electrochem. 4, 211, 1974.
(ii) Balej, J and Vondrak, T.P. Electrochim. Acta 20, 283, 1975.

106. Kerovin, N.V., Kicheev, A.G. and Schmachkova, I.G.
Proc. Symp. Electrolysis, Ed. M.W. Breiter, P156, Electrochem. Soc. 1974.

107. Tseung, A.C.C. and Man, M. British Patent Application No. 44362/77, 25th March 1977.

108. Man, M. High performance hydrogen evolution electrocatalyst in alkaline media. PhD thesis, The City University, London, EC1. May, 1978.

109. Heyrovsky, Horriuti and Okomato sited in Bockris, J.O'M. and Koch,D.F.A. J. Phydical Chem. 65, P1941, 1961.

110. Tseung, A.C.C. and Bevan, H.L.
J. Material Science, 5, 604, 1970.

111. Alen, T. Powder Technology Series. Particle size measurement,chapter 16, P.355-392. Pub. Chapman and Hall, 2nd Ed. London, 1975.

112. Reiff, N.M., Grey, I.E. and Fan, A.
J. Solid State Chemistry, 13, 32, 1975.

113. Shoesmith, D.W., Rummery, T.E. Bailey, M.G. and Owen, D.G. Electrocrystallization of pyrite and marcesite on stainless steel surface. J. Electrochem. Soc. 126, 911, 1979.

114. Bockris, J.O'M., Damjanovic, A., Mannan, R.
J. Electroanal. Interfacial Electrochem. 18, 349, 1968.

115. Smith, J.A., Peterson, M.H. and Brown, B.F.
Corrosion, 26, 12No., 539, December, 1970.

APPENDIX I

X-RAY ANALYSIS OF PREPARED IRON OXIDES AND JCPDS X-RAY POWDER INDEX EXPOSED IN MOLYBDENUM REDIATION

PREPARED IRON OXIDES						J.C.P.D.S. POWDER DIFFRACTION INDEX					
Iron Rust		Oxide from FeII/FeIII Chlorides		Oxide from FeIII Nitrate		19-629		4-0755		5-0499	
						Fe_3O_4		α-Fe_2O_3		α-FeO(OH)	
dA°	I	dA°	I	dA°	I	dA°	I/I_1	dA°	I/I_1	dA°	I/I_1
6.74	f	2.92	m	4.82	m	4.85	40	4.82	5	7.30	90
4.80	m	2.49	s	2.94	vf	2.97	70	2.95	35	3.27	100
3.55	vf	2.15	vs	2.55	vs	2.53	100	2.52	100	2.56	80
2.55	f	1.69	f	2.34	s	2.09	70	2.08	25	2.34	30
2.05	vs	1.60	vf	1.75	f	1.71	60	1.70	10	1.93	65
1.55	f	1.38	f	1.58	vf	1.61	85	1.61	35	1.73	30
1.375	f	-	-	1.46	f	1.48	85	1.48	55	1.38	15

I = Intensity estimated visually

where vs = very strong s = strong vf = very faint f = faint m = medium

APPENDIX II

X-RAY ANALYSIS OF PREPARED IRON SULPHIDES AND JCPDS POWDER INDEX EXPOSED IN MOLYBDENUM RADIATION

PREPARED GRADES OF IRON SULPHIDES						J.C.P.D.S. POWDER DIFFRACTION INDEX							
Sulphide from rust		Sulphide from FeII/FeIII chloride		Sulphide from FeIII nitrate		H-0832		1-1247		6-0710		11-334	
						FeS		FeS(troilite)		FeS_2		FeSx.H_2O	
dA°	I	dA°	I	dA°	I	dA°	I/I_1	dA°	I/I_1	dA°	I/I_1	dA°	I/I_1
2.70	f	6.20	m	3.00	vf	2.98	90	2.97	33	2.71	84	2.96	90
2.35	vf	5.10	f	2.75	s	2.67	90	2.65	33	2.42	66	2.46	90
1.95	s	4.50	f	2.05	vs	2.09	100	2.06	100	1.63	100	1.74	100
1.72	vs	2.65	f	1.80	f	-	-	-	-	-	-	-	-
1.45	s	2.05	vs	1.45	f	-	-	-	-	-	-	-	-
-	-	1.75	vf	-	-	-	-	-	-	-	-	-	-

I = Intensity estimated visually

where vs = very strong, s = strong, f = faint, vf = very faint, m = medium.

PUBLICATIONS

1. A.C.C. Tseung, H.C. Chan and A.I. Onuchukwu.
An electrochemical method for detecting threshold stress intensity in stress corrosion.
Corrosion Science, Vol. 19, P209, 1979.

2. H.C. Chan, A.C.C. Tseung, A.I. Onuchukwu.
The Electrochem. Soc. Inc. Spring Meeting, Boston, Massachusetts. Extended Abstract No.53, Vol. 79-1, P140, 6th May, 1979.

3. A.C.C. Tseung, A.I. Onuchukwu, H.C. Chan, British Patent Application No. , 1979.